

ARTICLE



<https://doi.org/10.1038/s41467-022-30722-9>

OPEN

# The drug-induced phenotypic landscape of colorectal cancer organoids

Johannes Betge<sup>1,2,3,4,5,10</sup>, Niklas Rindtorff<sup>1,10</sup>, Jan Sauer<sup>1,6,10</sup>, Benedikt Rauscher<sup>1,10</sup>, Clara Dingert<sup>1</sup>, Haristi Gaitantzi<sup>2,5</sup>, Frank Herweck<sup>2,5</sup>, Kauthar Srour-Mhanna<sup>2,3,4</sup>, Thilo Miersch<sup>1</sup>, Erica Valentini<sup>1</sup>, Kim E. Boonekamp<sup>1</sup>, Veronika Hauber<sup>2,5</sup>, Tobias Gutting<sup>2,5,9</sup>, Larissa Frank<sup>1</sup>, Sebastian Belle<sup>2,5</sup>, Timo Gaiser<sup>5,7</sup>, Inga Buchholz<sup>2,5</sup>, Ralf Jesenofsky<sup>2,5</sup>, Nicolai Härtel<sup>2,5</sup>, Tianzuo Zhan<sup>1,2,5</sup>, Bernd Fischer<sup>1,6</sup>, Katja Breitkopf-Heinlein<sup>1,2,5</sup>, Elke Burgermeister<sup>1,2,5</sup>, Matthias P. Ebert<sup>1,2,4,5,✉</sup> & Michael Boutros<sup>1,8,✉</sup>

Patient-derived organoids resemble the biology of tissues and tumors, enabling ex vivo modeling of human diseases. They have heterogeneous morphologies with unclear biological causes and relationship to treatment response. Here, we use high-throughput, image-based profiling to quantify phenotypes of over 5 million individual colorectal cancer organoids after treatment with >500 small molecules. Integration of data using multi-omics modeling identifies axes of morphological variation across organoids: Organoid size is linked to IGF1 receptor signaling, and cystic vs. solid organoid architecture is associated with LGR5 + stemness. Treatment-induced organoid morphology reflects organoid viability, drug mechanism of action, and is biologically interpretable. Inhibition of MEK leads to cystic reorganization of organoids and increases expression of *LGR5*, while inhibition of mTOR induces IGF1 receptor signaling. In conclusion, we identify shared axes of variation for colorectal cancer organoid morphology, their underlying biological mechanisms, and pharmacological interventions with the ability to move organoids along them.

<sup>1</sup>German Cancer Research Center (DKFZ), Division Signaling and Functional Genomics, and Heidelberg University, Medical Faculty Mannheim, Department of Cell and Molecular Biology, Heidelberg, Germany. <sup>2</sup>Heidelberg University, Department of Medicine II, University Medical Center Mannheim, Medical Faculty Mannheim, Mannheim, Germany. <sup>3</sup>German Cancer Research Center (DKFZ), Junior Clinical Cooperation Unit Translational Gastrointestinal Oncology and Preclinical Models, Heidelberg, Germany. <sup>4</sup>DKFZ-Hector Cancer Institute at University Medical Center Mannheim, Mannheim, Germany. <sup>5</sup>Mannheim Cancer Center, Mannheim, Germany. <sup>6</sup>German Cancer Research Center (DKFZ), Computational Genome Biology Group, Heidelberg, Germany. <sup>7</sup>Heidelberg University, Institute of Pathology, University Medical Center Mannheim, Medical Faculty Mannheim, Mannheim, Germany. <sup>8</sup>German Cancer Consortium (DKTK), Heidelberg, Germany. <sup>9</sup>Present address: Department of Internal Medicine IV, Heidelberg University, Heidelberg, Germany. <sup>10</sup>These authors contributed equally: Johannes Betge, Niklas Rindtorff, Jan Sauer, Benedikt Rauscher. ✉email: matthias.ebert@medma.uni-heidelberg.de; m.boutros@dkfz.de

**C**olorectal cancer is globally the third most common cancer and the second leading cause of cancer related death<sup>1</sup>. Patients with advanced disease are usually treated with chemotherapy and antibody therapies, however, with current treatment, tumors may continue to progress and prognosis remains poor<sup>2</sup>. Tumor plasticity, as well as the stemness of neoplastic cells have been proposed as major factors in treatment resistance and tumor progression under antineoplastic therapies<sup>3,4</sup>. However, mechanisms behind these tumor cell states and drugs modulating or targeting them are not well understood.

Patient-derived organoids are stem cell derived 3D tumor models that can be efficiently established from (colorectal-)cancer and normal tissues<sup>5–7</sup>. Organoid isolation from human primary tumors and metastases<sup>5,8</sup> has enabled the establishment of living biobanks<sup>6,7,9</sup>. Notably, patient-derived organoids have been shown to represent their origin's molecular features and morphology<sup>6–8,10</sup>, enabling functional experiments such as drug testing *ex vivo*<sup>7,9,11–16</sup>. As a consequence, organoids are an attractive model system, as they combine the modeling capacity of patient-derived xenografts with the scalability of adherent *in vitro* cell lines.

Image-based profiling is a high-throughput microscopy-based methodology to systematically measure phenotypes of *in vitro* models. When combined with chemical or genetic perturbations, image-based profiling is a powerful approach to gain systematic insights into biological processes, for instance in drug discovery and functional genomics research<sup>17–19</sup>. Image-based assays have been used to screen large libraries of small molecules to identify potential drug candidates, to analyze a drug's mode-of-action, or to classify drug-gene interactions by cell-morphology<sup>20–23</sup>. Performing large image-based profiling experiments of organoids has been, however, a biological, technical and computational challenge<sup>24–26</sup>. As a consequence, the morphological heterogeneity of patient-derived cancer organoids between and within patient donors, their diverging behaviors upon pharmacological perturbation as well as the underlying mechanisms of cancer organoid morphology are not yet systematically understood.

Here we report a large scale image-based phenotyping study of patient-derived cancer organoids to understand underlying factors governing organoid morphology. Colorectal cancer organoids from 11 patients were treated with more than 500 experimental and clinically used small molecules at different concentrations. We systematically mapped the morphological heterogeneity of patient-derived organoids and their response to compound perturbations from more than 3,700,000 confocal microscopy images. We found that the resulting landscape of organoid phenotypes was mainly driven by differences in organoid size, viability and cystic vs. solid organoid architecture. Using multi-omics factor analysis for integrating organoid morphology, size, gene expression, somatic mutations and drug activity, we identified biological programs underlying these phenotypes and small molecules that modulate them.

## Results

**Image-based profiling captures the morphological diversity of patient-derived cancer organoids.** To better understand the diversity of organoid phenotypes, drug-induced phenotypic changes and the underlying factors driving them, we generated patient-derived organoids from 13 colorectal cancer patients representing different clinical stages and genotypes (Supplementary Fig. S1a–d, Supplementary Tables 1 and 2). We performed image-based profiling at single organoid resolution with 11 organoid lines (Fig. 1a) using small molecules targeting developmental pathways, protein kinases (464 compounds at a single 7.5 µM concentration), as well as small molecules in clinical use

(63 compounds in 5 concentrations, Supplementary Fig. S2a–c). After three days of culture and four days of pharmacological perturbation in 384-well plates, organoids were subsequently stained with fluorescent markers for actin (Phalloidin), DNA (DAPI), and cell permeability (DeadGreen) to capture their morphology with high-throughput confocal microscopy. We projected the 3D image data onto a 2D plane, segmented organoids and calculated morphological profiles for each organoid spanning 528 phenotypic features (such as dye intensity, texture, and shape) that were subsequently reduced into 25 principal components representing 81% of morphological variance (Supplementary Fig. S2c).

To visualize the heterogeneity of colorectal cancer organoids and treatment induced changes across and within organoid lines, we embedded features of approximately 5.5 million profiled organoids using uniform manifold approximation and projection (UMAP, Fig. 1b, Supplementary Fig. S2d–f). Within most organoid lines there was a characteristic two-component log-normal mixture distribution of organoid size with one component containing small organoids and another component containing larger organoids with varying, organoid line specific, reproducible average size (Fig. 1c, Supplementary Fig. S2g, h). The log-normal-like size distribution likely resulted from intrinsic differences in cellular size and growth rate accumulating throughout the course of the experiment in multicellular organoids. Next, we performed graph-based clustering on this embedding to describe the landscape, resulting in 12 clusters (Fig. 1d). Organoid lines within the embedding were located in characteristic clusters, with organoid size and organoid architecture as primary organizing factors (Fig. 1e). For example, organoid line D018T had the largest median organoid size within the dataset and a cystic organoid architecture with a single central hollow lumen and monolayer of surrounding cells. In contrast, D020T organoids had a solid architecture and smaller median size. In most cases, organoid lines had two areas of main density, with one of them in clusters 2, 3 or 4, reflecting the previously mentioned bimodal size distribution. When comparing drug-treated organoids to baseline organoids treated with the solvent control (DMSO), no clear separation of groups was apparent, suggesting that organoid morphology was distributed on a continuum of phenotypes spanning perturbed and unperturbed conditions of our experiment (Supplementary Fig. S2i). In summary, image-based profiling of patient-derived colorectal cancer organoids showed strong morphological heterogeneity with donor dependent differences in size and organoid architecture.

**Organoid phenotype-profiles capture organoid viability.** Drug-induced changes in cell viability are a fundamental readout in cancer drug discovery. Prompted by the observation that organoid size was a major factor determining the phenotype embedding, we hypothesized that small organoid size, which was seen across all donors, was at least partially the result of cell death within the organoid and, more broadly, that phenotype data could be used to estimate organoid viability. To test this hypothesis, we chose bortezomib, a small molecule proteasome inhibitor with high *in vitro* toxicity, as well as SN-38 (active metabolite of irinotecan). Both small molecules led to dose dependent organoid death in all organoid lines (Fig. 2a). Analogous to pseudotime in single-cell gene expression analysis<sup>27</sup>, we fitted dose-dependent trajectories of bortezomib (Fig. 2b) and SN-38 (Supplementary Fig. S3a). Starting from diverse baseline morphologies, increasing doses of these compounds led to a step-wise convergence on a final death-related phenotype, which corresponded to the areas with enrichment of small objects

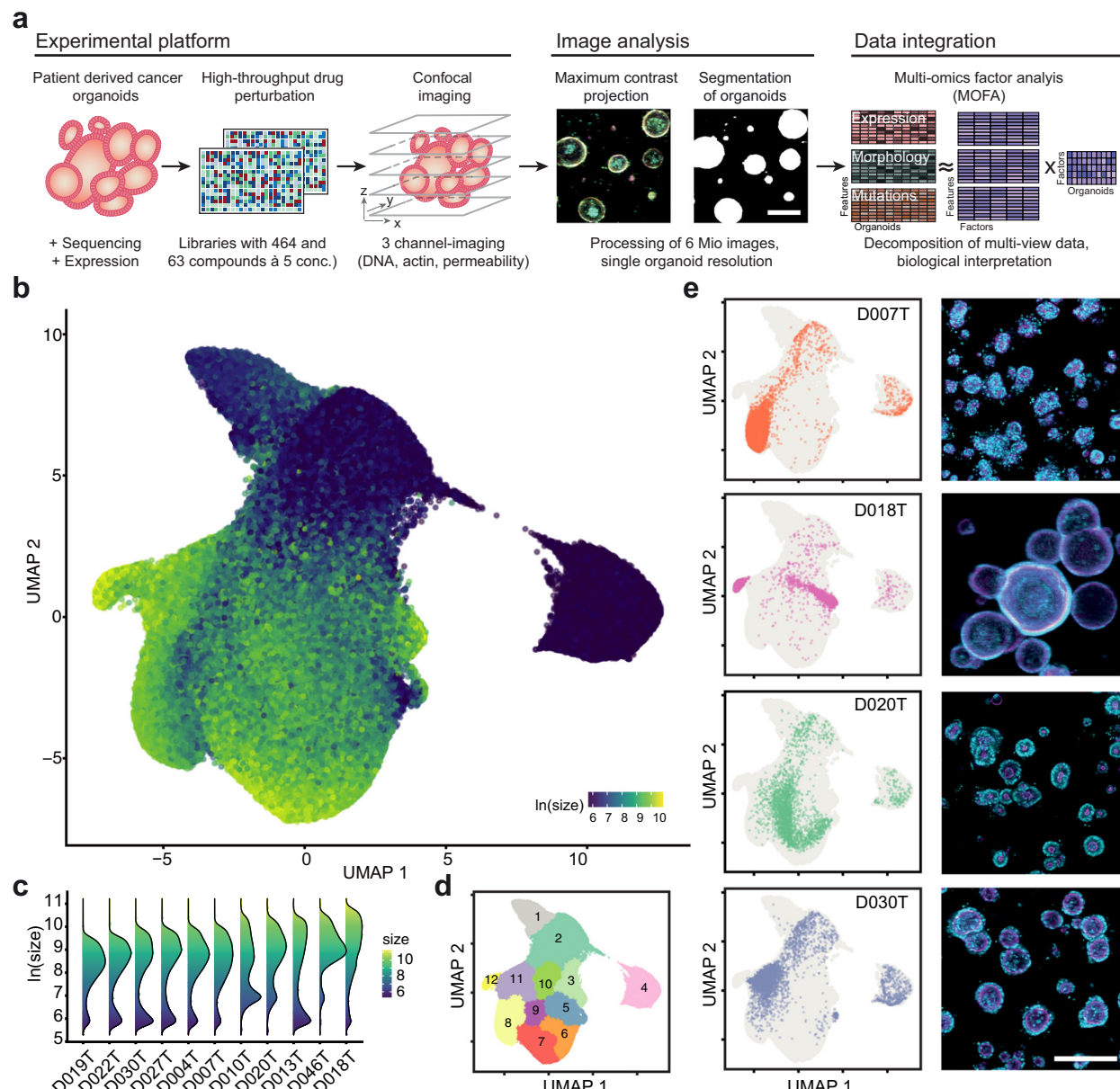
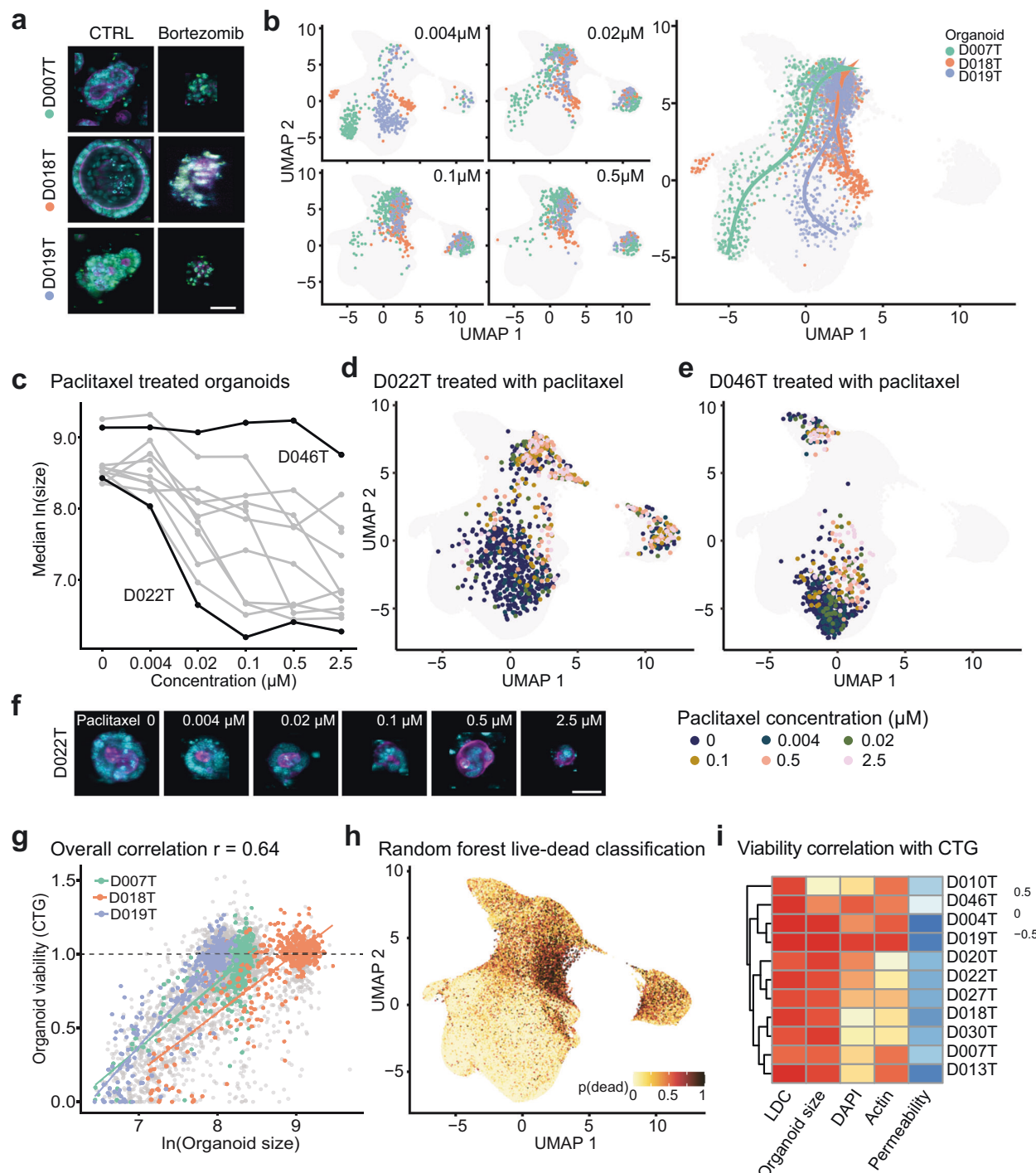


**Fig. 1 Image-based profiling captures the phenotype diversity of patient-derived cancer organoids.** **a** Schematic overview of experiments: Organoids were isolated from endoscopic biopsies from patients with colorectal cancer. Organoids were dissociated and evenly seeded in 384-well plates before perturbation with an experimental (464 compounds) and a clinical compound library (63 compounds at 5 concentrations each, 842 perturbations across both libraries). After treatment, high-throughput fluorescence microscopy was used to capture the morphology of organoids. The multi-channel (DNA, beta-actin, cell permeability) 3D imaging data was projected, segmented, and phenotype features were extracted to quantify potential drug-induced phenotypes. Untreated organoid morphology, organoid size and drug activity scores were integrated with mRNA expression and mutation data in a Multi-Omics Factor Analysis (MOFA). **b** Uniform Manifold Approximation and Projection (UMAP) of organoid-level features for a random 5% sample out of approximately 5.5 million organoids. The same sample is used for visualizations throughout the figure. Color corresponds to the log-scaled organoid area (dark blue: minimum size, yellow: maximum size). **c** Organoid size distribution across organoid lines. **d** UMAP representation of DMSO treated and drug treated organoids. Graph-based clustering of organoids by morphology with 12 resulting clusters. **e** UMAP embeddings of selected organoid lines (baseline state = 0.1% DMSO control-treated organoids) representing different morphological subsets, grey background consists of randomly sampled points. Depicted are representative example images for each organoid line (right, cyan = DNA, magenta = actin, scale bar: 200 μm).

(clusters 2, 3 and 4 shown in Fig. 1d). Similarly, paclitaxel, a microtubule disassembly inhibitor, shifted the bimodal size distribution of organoids in a dose-dependent fashion (Supplementary Fig. S3b), while organoid count remained largely unchanged (Supplementary Fig. S3c). This effect, however, was organoid line-specific, as we observed a dose-dependent decrease in median organoid size in paclitaxel “responder” lines (e.g.

D022T), while the size of other organoids remained unaffected (e.g. D046T, Fig. 2c-f). These observations suggested a link between organoid morphology, especially organoid size, with a loss of cell viability. To test the ability of organoid morphology to predict cell viability, we performed a luminescence-based, ATP dependent, cell viability assay (CTG) in parallel with imaging as a benchmark for drugs within the clinical cancer library. We saw a



strong association of CTG viability with organoid size (Fig. 2g), prompting us to test whether a more accurate prediction of organoid viability was possible by using all available imaging data including organoid size. To this end, we trained random forest classifiers (live/dead classifiers, LDC) on individual organoid phenotype profiles to distinguish between negative and positive control treatments (DMSO, bortezomib and SN-38, Supplementary Fig. S3d, e). We observed robust classification performance when applied to sets of the same or unseen organoid lines (Supplementary Fig. S3f). As expected, when applying the classifier to the whole imaging dataset and visualizing predictions via

UMAP, small organoids within previously identified clusters 2, 3 and 4 had the highest probabilities for death (Fig. 2h). The LDC predictions had the highest correlation with CTG based viability data (Fig. 2i), however, the association with organoid size was almost as strong in the majority of organoid lines (Fig. 2i, Supplementary Fig. S3g), while other simple features, such as DNA (DAPI), actin (phalloidin), and especially permeability (Dead-Green) intensity in isolation were less suitable to predict viability of organoids (Fig. 2i). We also noticed in ablation experiments that LDCs with incomplete access to channel information (i.e. only DAPI and phalloidin staining derived features were available

**Fig. 2 Organoid phenotype-profiles capture organoid viability.** **a** Representative example images of negative (0.1% DMSO) and positive control treated organoids (2.5  $\mu$ M bortezomib, cyan = DNA, magenta = actin, yellow = cell permeability; representative images were selected and embedded in black background; scale bar: 50  $\mu$ m). **b** Dose-dependent-trajectory of bortezomib drug effect. UMAP of organoid morphology at different bortezomib doses and (right panel) dose-dependent trajectory for three representative organoid lines. During the principle curve fitting, trajectory inference excluded cluster 4, a set of measurements representing mostly dead organoid particles comprising ca. 5% of all imaging data. **c** Dose-response relationship of organoid size and paclitaxel dose. D022T and D046T are highlighted as examples for responder/non-responder lines. Source data are provided as a Source Data file. **d** UMAP of organoid morphology highlighting D022T organoids treated at different concentrations of paclitaxel. **e** D046T organoids treated at different concentrations of paclitaxel. cyan = DNA, magenta = actin, representative images of organoids were selected and embedded in black background; scale bar: 50  $\mu$ m). **g** Association of organoid size of selected example organoid lines with viability determined by luminescence-based, ATP-dependent viability profiling with CellTiter-Glo (CTG), which was performed in parallel with imaging on a subset of drug treatments for benchmarking. **h** UMAP visualization of viability predictions for organoids within our dataset, based on supervised machine learning of organoid viability using classifiers trained on positive (high-dose bortezomib and SN-38) and negative (DMSO) controls (live-dead classifiers, LDC). **i** Association of LDC and example organoid features (size, DAPI, actin and permeability dye intensities) with benchmark CTG viability read out. Source data are provided as a Source Data file.

for training and inference) showed, in some instances, classification accuracies almost as high as classifiers with access to complete data (Supplementary Fig. S3h). Finally, we observed examples of diverging results between LDC predictions and CTG read-outs. These included (1) the antifolate drug methotrexate and (2) a doxorubicin-induced artifact due to the strong red color of the compound. Methotrexate showed strong toxicity in almost all organoid lines in CTG based experiments but had no visible effect on organoid viability based on the LDC (Supplementary Fig. S3i–l). This discordance may be explained by non-lethal metabolic effects of methotrexate. In conclusion, basic features, such as median organoid size, as well as classification of texture and shape information from basic DNA and actin stainings can predict organoid viability.

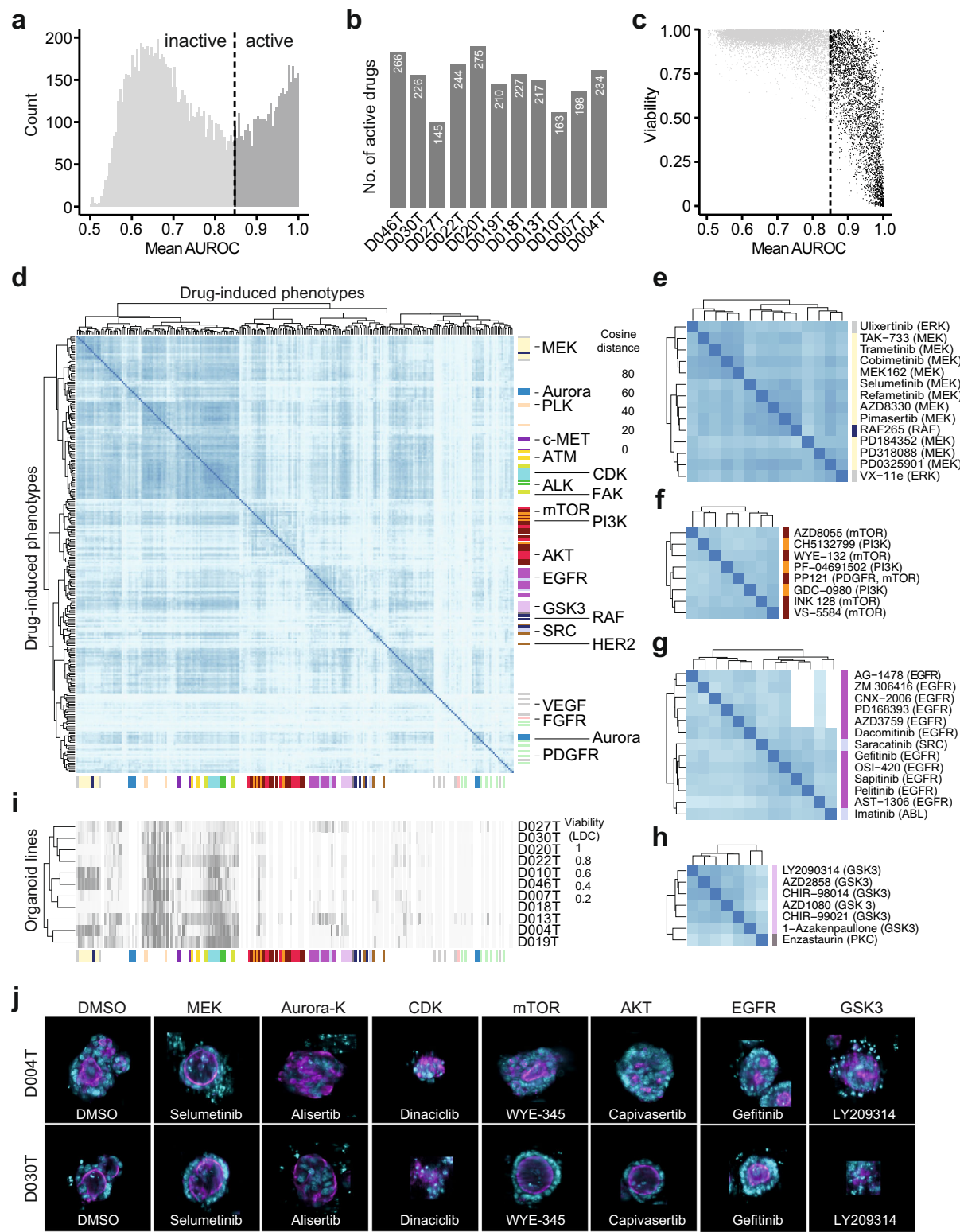
**Drug-induced organoid phenotypes correspond to drug mechanism of action.** An advantage of image-based profiling over cell viability measurements in drug discovery is the ability to use the high dimensional drug-induced phenotype profiles to identify active but not necessarily lethal small molecules and estimate their mechanism of action by similarity-based clustering. To test whether this approach could be used in patient-derived cancer organoids, we used a supervised learning approach for drugs within the KiStem library to identify drug effect profiles and group them by similarity. First, we trained logistic regression models to distinguish individual compound-treated organoids from unperturbed controls and defined the resulting normal vector between control- and treated organoid phenotypes as the drug effect profile. Next we scored every logistic regression model's ability to separate treated and untreated organoids to identify active treatments that induce a robust change in organoid morphology (area under the receiver operating characteristic, AUROC, ranging from 0.5 to 1). We considered treatments active when their classifiers' performance exceeded an AUROC of 0.85 (Fig. 3a, b). Based on our observations, drug activity was necessary but not sufficient for a viability effect (Fig. 3c) as a fraction of drugs led to identifiable changes in organoid morphology (they were considered active drugs) but were not classified as lethal by our live/dead classifier (LDC) models.

To test whether active drugs systematically induced organoid phenotypes that were informative of mechanism of action, we assessed similarity by two different methods, (1) the cosine distance between concatenated drug effect profiles and (2) the euclidean distance of averaged treatment-induced phenotypes (Fig. 3d–h, Supplementary Figs. S4a–c, S5a–c). While both methods were similar in terms of their ability to cluster drugs by mechanism of action, we proceeded with cosine distance clustering, as drug effect profiles did not only capture the direction of phenotype change, but were also linked to AUROC as

a metric of drug activity that was scaled between 0.5 and 1. We observed a clustering of drugs by their specific mode-of-action, including inhibitors of MEK, aurora kinase, CDK, mTOR, AKT, EGFR or GSK3 (Fig. 3d). Small molecules with targets within the same signaling pathway also induced related morphologies, for example MEK inhibitors clustered with specific RAF- and ERK inhibitors (Fig. 3e) and AKT/ PI3K inhibitors were part of a cluster mainly containing mTOR targeting small molecules (part of the cluster is shown in Fig. 3f, whole cluster in Supplementary Fig. S5a). The clustering also suggested additional mode-of-actions or off-target effects for well-described small molecules (Fig. 3g–h). For example, the PKC inhibitor enzastaurin was clustered with GSK3 inhibitors, substantiating a previously described interaction of enzastaurin with the alpha and beta subunits of GSK3<sup>28,29</sup> (Fig. 3h). Of note, several drug-induced phenotypes were observable across most or all tested organoid lines, but the majority of compound classes led to significant enrichments in drug profile vector clustering only in subsets or individual organoid lines (Supplementary Fig. S5d).

To assess whether morphological profiles of active drug treatments were primarily driven by differences in organoid viability, we compared LDC predictions with the phenotypic clustering (Fig. 3i). We observed a larger cluster of lethal treatments (including molecules targeting ATM, JAK, PLK, CDK). However, the majority of clusters were caused by non-lethal phenotypes, including those induced by inhibitors of AKT, mTOR, EGFR or GSK3. Visual inspection of several phenotypes (Fig. 3j) revealed recurring drug target dependent morphologies. Most notably, MEK inhibitors led to reorganization towards a more cystic organoid architecture. Altogether, drug-induced phenotypes were capturing drug mode-of-action and were visible across most tested organoids lines.

**Multi-omics factor analysis identifies shared factors linking morphology, genomic data and drug activity.** A limitation of image-based profiling experiments is that both unperturbed and drug-induced morphologies are challenging to interpret in terms of their underlying biology. Theoretically, in the presence of multiple *in vitro* models with both phenotype and genomic measurements, links between the two data modalities can be learned. Based on the observation that organoid morphology was distributed in a continuous space, we hypothesized that variation in organoid baseline morphology could be associated with differences in gene expression, mutations, as well as drug activity for the 11 cancer organoid lines in our sample (2 biological replicates each, 22 observations in total). To factorize the joint distribution of unperturbed organoid morphology, unperturbed organoid size, gene expression, selected somatic mutations, and drug activity, we performed multi-omics factor analysis (MOFA)<sup>30</sup>. MOFA is a



matrix factorization method that decomposes a set of different measurements into a shared table of factors scoring each observed sample and a set of corresponding loading tables linking each factor to features in the set of original measurements<sup>30</sup>. When trained with  $k=3$  factors, MOFA recovered factors explaining approximately 24–41% of variance across the different data

modalities (Fig. 4a, b, Supplementary Fig. S6a–c). While gene expression, mutations and drug activity profiles for organoid lines contributed to all factors, factor 1 captured most variation in median organoid size (ca. 39%). In contrast, factor 2 was primarily capturing variation within untreated organoid morphology (ca. 16%) (Fig. 4a). Organoid lines D046T and D004T stood

**Fig. 3 Drug-induced organoid phenotypes correspond to drug mechanism of action.** **a** Histogram of average model performance for each tested drug. For every tested drug and organoid line, logistic regression models were trained to distinguish negative control-treated organoids from drug treated organoids. A drug was considered “active” when it induced a phenotype that could be separated from DMSO control-phenotypes with a mean classification performance of  $>0.85$  area under the receiver operating characteristic curve (AUROC). **b** Number of active drugs per organoid line. **c** Relationship between drug-induced viability change (predicted by LDC, compare Fig. 2) and general compound activity. **d** Unsupervised clustering of drug effect profiles for active drugs. Distance between drug effect profiles was calculated using cosine similarity. Drug effect profiles were determined by fitting logistic regression models between treated and untreated organoids for each drug and line. PCA transformed morphology information was used as input features. Fisher’s exact test was used to identify enrichments of drugs annotated with the same drug target within the hierarchical clustering. Tested clusters had a minimum cluster size of 3 and were evaluated iteratively from the tree bottom to top. Colors on the side of the heatmap represent drug mechanisms of action. **e–h** Zoom-ins of **(d)** showing clusters enriched for MEK (**e**), PI3K/mTOR (**f**), EGFR (**g**) and GSK-3 (**h**). **i** Viability of drug-induced phenotypes in individual organoid lines as determined by supervised machine learning. The drugs were arranged on the x axis in the same order as in **(d)**. **j** Organoids representative of selected drug-induced phenotypes. Images from organoid lines D004T and D030T were selected for each organoid phenotype, automatically cropped and embedded in black background. Cyan = DNA, magenta = actin; scale bar: 50  $\mu$ m.

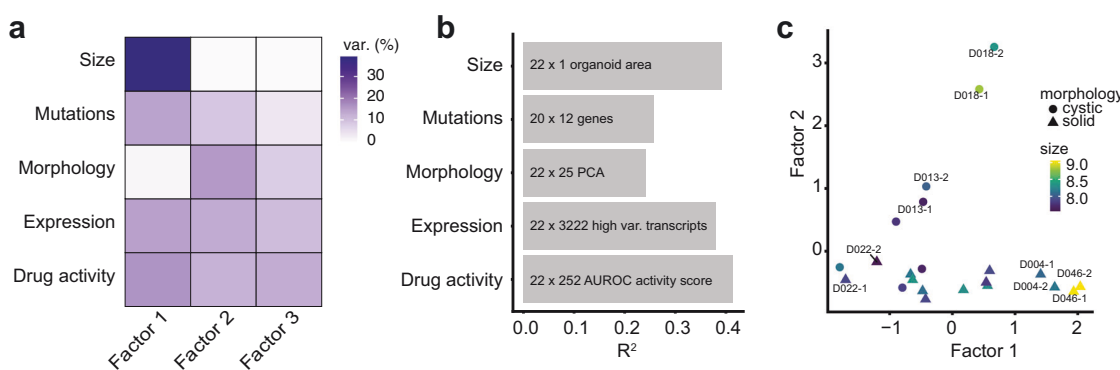


**Fig. 4 Multi-omics factor analysis identifies shared factors linking morphology, gene expression and drug activity.** **a, b** Variance decomposition of the MOFA model. Untreated organoid morphology, organoid size and drug activity scores were integrated with DNA sequencing and mRNA expression data. Source data are provided as a Source Data file. **a** Percentage of variance explained by each factor in each data modality. **b** Cumulative proportion of total variance explained by each experimental data modality within the MOFA model. **c** Visualization of samples in factor space showing factors 1 and 2. Shown are two independent replicates for each organoid line. Organoid morphology (cystic vs. solid) as determined by visual inspection of DMSO phenotypes and organoid size (log-scaled organoid area) are represented by symbol shape and color, respectively.

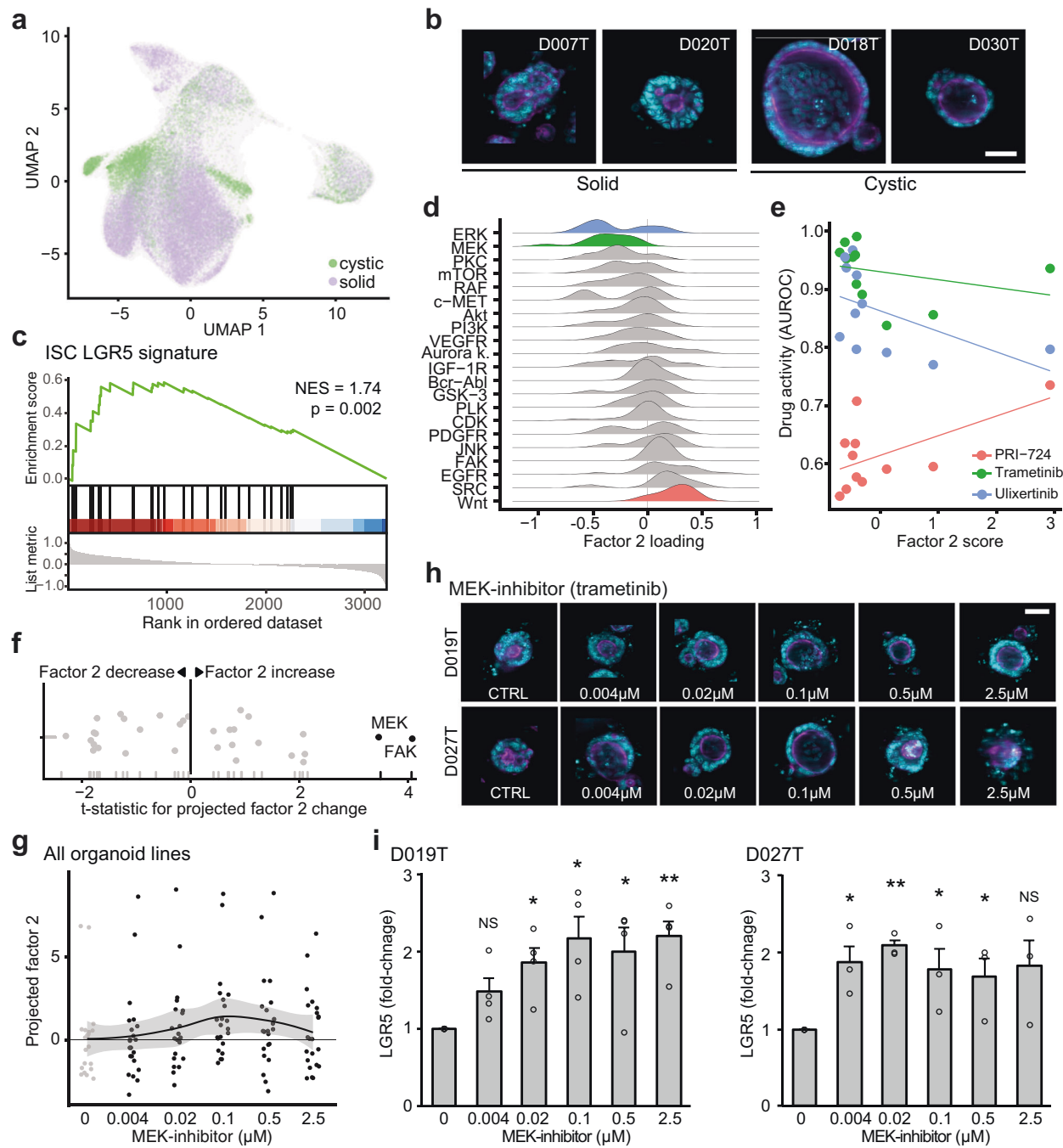
out as lines with the strongest score for factor 1, while organoid lines D018T and D013T had the strongest score in factor 2 (Fig. 4c). Organoids with high factor scores were located in characteristic regions of the previously defined UMAP embedding (Supplementary Fig. S6d). Visual inspection of organoids revealed that organoid lines with a higher factor 1 score tended to be larger in size and organoids with high factor 2 score tended to have a more cystic organoid architecture based on manual classification. Analysis of gene expression data alone recovered patterns analogous to factor 1 and factor 2 (Supplementary Fig. S6e, f). We could not identify interpretable morphological differences between factor 3 low and high organoids and focused our subsequent analysis on the first two interpretable factors generated by MOFA. In summary, MOFA identified factors within the dataset that explained variation between organoid lines across different data modalities, including organoid morphology and median size.

**An LGR5+ stemness program is associated with cystic organoid architecture and can be induced by inhibition of MEK.** A particularly strong recurring organoid phenotype was the presence of a cystic organoid architecture, seen in untreated D018T or D013T organoids and organoids treated with MEK inhibitors (Figs. 1e, 3f and 5a). MOFA showed that factor 2 represented this cystic organoid state. In the cystic state, organoids consisted of a monolayer of uniform cells lining a central spherical lumen with a pronounced actin cytoskeleton (Fig. 5b). We considered this phenotype related to organoid morphologies previously described in genetically engineered APC<sup>−/−</sup> or Wnt ligand treated intestinal organoids<sup>31–33</sup>. To test if factor 2 in fact captured Wnt

signaling and intestinal stem cell identity related gene expression programs, we performed gene set enrichment analyses (GSEA) for cell identity signatures previously identified in intestinal crypts and colorectal cancer<sup>34</sup>. GSEA revealed an enrichment of Lgr5+ stem cell signature-related genes for the factor 2 loadings (Fig. 5c) (FDR = 0.002, NES = 1.74) among other biological processes (Supplementary Fig. S7a). In terms of genetic mutations, ERBB2 mutation status had the strongest positive contribution to factor 2 loadings (Supplementary Fig. 6c).

Next, we asked if factor 2 was associated with particular drug activity or inactivity patterns. As previously described, we used the performance of a logistic regression model as drug activity score (AUROC) (Fig. 3a). Activity of Wnt signaling inhibitors and EGFR inhibitors were the strongest average contributors to a positive factor 2 score ( $t$  statistic = 3.02, FDR = 0.046 and  $t$  statistic = 3.08, FDR = 0.046, respectively), while activity of ERK and MEK inhibitors were associated with a low factor 2 score (Fig. 5d), albeit not significantly. To summarize, factor 2 high organoid lines showed an increased expression of LGR5 and were more sensitive to Wnt signaling inhibitors, such as the CBP/beta-catenin inhibitor PRI-724 (Fig. 5e and Supplementary Fig. S7b) overall suggesting increased dependency on Wnt signaling in the factor 2 high organoid state.

Prompted by the visual observation that MEK inhibitor treatment led to a related cystic architecture in organoids (Fig. 3j), we hypothesized that compound treatments could influence the plasticity between the observed organoid states. Thus we tested whether drug treatments shifted organoid phenotype profiles in the previously defined factor space. To test for shifts in factor



space, we used the previously estimated factor loading matrix for unperturbed organoid morphology, which was generated during MOFA training, as a starting point. By projecting the average phenotypic profiles of drug-treated organoids onto the factors learnt by MOFA, we were able to approximate the influence various drug treatments had on biological programs previously identified in unperturbed organoids. We observed MEK and focal adhesion kinase inhibitors significantly shifted tested organoid lines towards higher factor 2 scores (Fig. 5f and Supplementary Fig. S7c). This change in factor 2 scores was concentration dependent for MEK inhibitors (Fig. 5g and Supplementary Fig. S7d, e) and corresponded to a visual shift in organoid morphology (Fig. 5h) which was most noticeable at concentrations of 100 nM ( $p = 0.017$ , Fig. 5h, Supplementary Fig. S7e).

Given the observation that factor 2 was enriched for an LGR5 + stem cell signature (Fig. 5c), we measured the expression of *LGR5* transcripts at different concentrations of MEK inhibitor treatment for two organoid lines with representative factor scores (D019T and D027T). We observed analogous dose-dependent increases in transcript abundance (Fig. 5i). These findings were in concordance with the observation that MEK inhibitor activity had a negative contribution to factor 2 (Fig. 5d): While organoids are shifted to a factor 2 high state via MEK inhibition, within the factor 2 high state itself, organoids are relatively insensitive to this class of inhibitors. In summary, we observed an organoid state with cystic architecture, increased expression of LGR5 + stem cell related genes and increased sensitivity to Wnt signaling inhibitors that could be induced by MEK inhibition.

**Fig. 5 An LGR5+ stemness program is associated with cystic organoid architecture and can be induced by inhibition of MEK.** **a** UMAP visualization of cystic and solid organoid morphology in baseline state (DMSO-treated) as defined by factor 2 scores. **b** Example images of cystic (right) and solid organoid lines. Images were automatically cropped and embedded in black background. Cyan = DNA, magenta = actin; scale bar: 50  $\mu$ m. **c** Gene set enrichment analysis of the LGR5+ intestinal stem cell signature<sup>34</sup> over ranked factor 2 gene expression loadings (ranking from high factor 2 loading to low factor 2 loading), NES = normalized enrichment score, statistics were calculated with GSEA using 100.000 permutations. **d** Distributions of drug activity loadings for factor 2 grouped by drug targets. **e** Relationship of representative drugs' activity with factor 2 score. Source data are provided as a Source Data file. Further samples can be found in Fig. S7. **f** Projection of factor 2 scores for drug-induced phenotypes. Highlighted are drug targets leading to a significant change in projected factor scores across all organoid lines (ANOVA). Source data are provided as a Source Data file. **g** Projected dose-dependent changes in factor 2 scores after treatment with the MEK inhibitor binimetinib across organoid lines. The black line indicates median factor 2 values of 2 replicates from  $N=11$  organoids treated with binimetinib, grey shading indicates the 95% confidence intervals based on the loess regression with default parameters<sup>94</sup>. Source data are provided as a Source Data file. **h** Dose-dependent changes in organoid morphology after treatment with the MEK inhibitor trametinib. Shown are images of organoid lines D019T and D027T (cyan = DNA, magenta = actin; sampled images were cropped and embedded in black background; scale bar: 50  $\mu$ m) (**i**). Dose-dependent changes in LGR5 transcript abundance after treatment with the MEK inhibitor trametinib, as assessed by qPCR, data from 3 (D027T) and 4 (D019T) independent replicates are presented as mean + s.e.m. \* $p < 0.05$ , \*\* $p < 0.005$ , NS = not significant, two-sided Student's t test.  $p$  values: D019T:  $p = 0.061$  (0.004  $\mu$ M),  $p = 0.0196$ , (0.02  $\mu$ M),  $p = 0.0187$  (0.1  $\mu$ M),  $p = 0.024$  (0.5  $\mu$ M),  $P = 0.0024$  (2.5  $\mu$ M), D027T:  $p = 0.0051$  (0.004  $\mu$ M),  $p = 0.00038$ , (0.02  $\mu$ M),  $p = 0.045$  (0.1  $\mu$ M),  $p = 0.048$  (0.5  $\mu$ M),  $P = 0.090$  (2.5  $\mu$ M). Source data are provided as a Source Data file.

**An IGF1R signaling program is associated with increased organoid size, decreased EGFR inhibitor activity and can be induced by mTOR inhibition.** Next, we set out to identify the mechanisms underlying and modulating factor 1. We had previously observed that organoid size was influenced by both organoid line and drug treatments and was associated with factor 1 scores (Fig. 6a). An unsupervised gene set enrichment analysis (GSEA) for reactome pathways across factor 1 loadings showed an enrichment for IGF1R signaling and mitogen-activated protein kinase signaling related genes. In fact, transcripts belonging to the *IGF* imprinting control region, *H19* (rank 1) and *IGF2* (rank 13), were among the strongest contributors to factor 1 (Supplementary Fig. S8a). This increase in proliferative signaling was confirmed by GSEA of a previously identified intestinal proliferation signature<sup>34</sup>. To better understand clinical correlates to the identified gene expression patterns, we tested for molecular subtypes stemming from an analysis of cancer-cell intrinsic gene expression profiles<sup>35</sup>. Factor 1 showed an enrichment for CRIS D, a molecular subtype linked to *IGF2* overexpressing tumors with resistance to EGFR inhibitor therapy (Fig. 6c), and a depletion for CRIS C, which has been linked to EGFR dependency (Supplementary Fig. S8b). In fact, activity of EGFR inhibitors was the strongest contributor to a negative factor 1 score while IGF1R and MEK inhibitor activity contributed to a positive factor 1 score (Fig. 6d, e and Supplementary Fig. S8c–e). When assessing the contribution of somatic mutations, activating mutations of *NRAS* had the strongest contribution to a high factor 1 score (Supplementary Fig. S6c).

Next, we again used phenotype profiles of drug treated organoids and approximated how drug treatment shifted organoids along the factor 1 program. We observed a group of cell cycle related kinase inhibitors targeting polo like kinases, Aurora kinases and cyclin dependent kinases that shifted organoids to a low factor 1 score. In contrast, mTOR inhibitor treatment increased factor 1 scores in cancer organoids (Fig. 6f and Supplementary Fig. S8f). Given the observation that factor 1 was associated with IGF1R signaling and mTOR inhibitor treatment led to an increase in factor 1 scores, we hypothesized that mTOR inhibition leads to a reactive upregulation of IGF1R signaling in cancer organoids. In fact, inhibition of mTOR signaling had previously been linked to transcriptional disinhibition of *IRS1* in a negative feedback loop<sup>36</sup> and reactive induction of IGF1R signaling had previously been described as a resistance mechanism to small molecule mTOR inhibitors in cancer<sup>37</sup>. When testing this hypothesis in patient-derived organoids, we observed a dose-dependent increase of IRS-1 protein abundance

in organoids treated with the ATP competitive mTOR inhibitor WYE-132 (Fig. 6g). In accordance with our previous findings, visual inspection of organoids treated with different mTOR inhibitors in our screen revealed increased size compared to negative controls (Supplementary Fig. S8g). To summarize our findings, we observed an organoid state marked by large organoid size, elevated IGF1R dependent mitogenic signaling and relative inactivity of EGFR inhibitors. This state was inducible by inhibition of a mTOR dependent negative feedback loop in patient-derived cancer organoids (Fig. 6h).

## Discussion

Organoids are in vitro cancer models with high morphological and molecular similarity to their origin that can be established from a wide variety of tumors and normal tissue<sup>6,7,10,14,38–40</sup>. Given the benefits in culture efficiency and high model representativeness in comparison to conventional cell lines, they are used for preclinical functional analyses of cancer<sup>41,42</sup>, and are evaluated in functional precision medicine projects amongst other models, such as tumor explants or fragments<sup>43,44</sup>. Tumor organoids are still far away from being a predictive tool for clinical decision making, as recent clinical studies have failed to show a clear benefit of organoid-based treatment allocation or consistent predictive value<sup>16,45,46</sup>. However, previous studies have successfully used patient-derived organoids to perform small- and medium-scale drug testing using ATP based cell viability readouts and have described clinically relevant predictive molecular features<sup>7,9–15,47–49</sup>. Additionally, imaging studies with organoids have been used to characterize developmental processes such as the self-organization of intestinal cells<sup>25,50</sup> or the morphological response to individual drugs<sup>24,51</sup>.

While image-based profiling of in vitro models has become an important tool for the analysis of biological processes, particularly in drug discovery and functional genomics<sup>17–19</sup>, performing such high-content experiments in disease models that cannot be cultured and perturbed in 2D, has been a technological challenge. In this study, we used image-based profiling to systematically map heterogeneous phenotypes of patient-derived cancer organoids and their response to small-molecule perturbations. We collected data on approximately 5.5 million single organoids from 11 different colon cancer patients with >500 different small molecule perturbations. The morphology of untreated patient-derived cancer organoids varied extensively within and between organoid donors. Despite the heterogeneity, organoids from different patients and perturbations showed overlapping morphological distributions, which shifted as a response to perturbation.

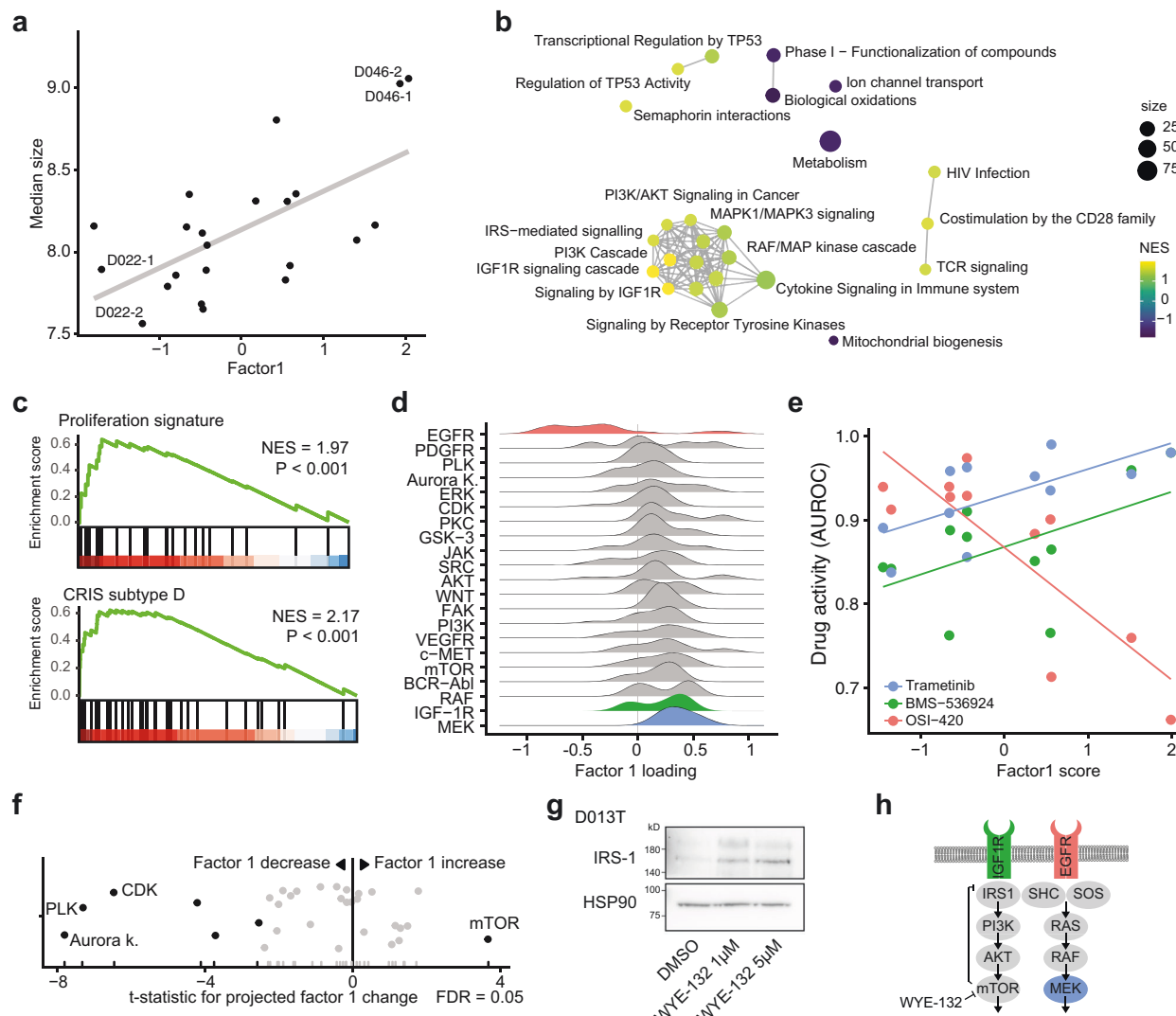


**Fig. 6 An IGF1R signaling program is associated with increased organoid size, EGFR inhibitor resistance and can be induced by mTOR inhibition.**

**a** Association of factor 1 with organoid size. Source data are provided as a Source Data file.

**b** Gene-set enrichment network of factor 1 gene expression loadings. An edge connects Reactome pathways with more than 20% overlap.

**c** Gene set enrichment results of the "proliferation" intestinal signature and the colorectal cancer CRIS-D subtype over ranked factor 1 gene expression loadings (ranking from high factor 1 loading to low factor 1 loading), NES = normalized enrichment score, statistics were calculated with GSEA using 100,000 permutations.

**d** Distributions of drug activity loadings grouped by drug targets for factor 1.

**e** Relationship of selected drugs' activity (AUROC) with factor 1 score. Source data are provided as a Source Data file.

**f** Projection of factor 1 scores for drug-induced phenotypes. Highlighted are drug targets leading to a significant change in projected factor 1 scores across all organoid lines (ANOVA). Source data are provided as a Source Data file.

**g** Western blot of IRS-1 protein abundance under mTOR inhibition. A representative blot of three biological replicates with organoid line D013T is shown. Scans of complete membranes are shown in Supplementary Fig. S9. Source data are provided as a Source Data file.

**h** Illustration of IGF1R signaling pathway with highlighted drug targets. Shown is the disinhibition of mTOR mediated IRS-1 repression by mTOR inhibitors.

Organoid morphology revealed compound mode-of-action and when integrated with additional biological measurements gave insight into the first set of principles governing cancer organoid architecture and plasticity. As a result, we identified two shared axes of variation for colorectal cancer organoid morphology (organoid size and cystic vs. solid architecture), their underlying biological mechanisms (IGF1R signaling and Wnt signaling), and pharmacological interventions able to move organoids along them (mTOR inhibition and MEK inhibition).

Cancer stem cells play a central role in cancer recurrence and metastasis<sup>52</sup>. In colorectal cancer, cells with cancer stem cell

identity are LGR5 positive<sup>53</sup>. Organoid models enriched for an LGR5+ stem cell signature presented with a characteristic cystic architecture and were sensitive to inhibitors of Wnt signaling. This LGR5+ organoid state was also linked to a reduced sensitivity towards MEK inhibitors, a potential consequence of the already suppressed ERK signaling activity that has been linked to Wnt signaling in colorectal cancer<sup>54</sup>. In fact, pharmacological MEK inhibition led to a shift in organoids towards a LGR5+ state, an effect that we have previously described<sup>33</sup>. The use of MEK inhibitors together with Wnt signaling activating GSK3 inhibitors is an established method to maintain embryonic stem

cells in vitro<sup>55</sup>. A related MEK inhibitor dependent modulation of stemness in Wnt signaling dependent colon tissue may in part explain the limited success of using MEK inhibitors as monotherapy in colorectal cancer.

Insulin-like growth factors are central and conserved regulators promoting cell size, organ size and organism growth<sup>56,57</sup>. The IGF1 receptor (IGF1R) signaling cascade is activated in around 20% of colorectal cancer patients and leads to downstream mitotic stimuli via mitogen activated kinase signaling and mTOR<sup>58</sup>. In patient-derived cancer organoids, we observed that organoid size was positively correlated with elevated IGF1R signaling activity. In accordance with previous observations<sup>35</sup>, colorectal cancer organoids in a high IGF1R signaling state were less responsive to EGFR inhibitors and more responsive to IGF1R and MEK blockade, demonstrating the central role of IGF1R mediated mitogen activated protein kinase (IGFR1-MAPK) signaling. In fact, combined blockade of MEK and IGF1R has recently been demonstrated to be a synergistic drug combination across colorectal cancer cell lines<sup>59</sup> and reciprocal resistance between IGF1R and EGFR signaling inhibitors has been described in multiple cancer types<sup>60</sup>. Also, organoids could be moved into a state of increased IGF1R-MAPK signaling by inhibition of mTOR, a downstream mediator of IGF1R activity. In line with this observation, a reactive induction of IGF1R signaling has been previously described as a resistance mechanism to small molecule mTOR inhibitors in cancer<sup>37,61</sup>. The emerging role of IGF1R signaling in organoid culture was recently emphasized by the observation that addition of the IGF-1 ligand, relative to EGF, increased culture efficiency of organoids from healthy human intestinal tissue<sup>62</sup>.

Statistical representation learning methods such as MOFA factorize a distribution of observations spanning multiple data modalities. In other words, MOFA learns factors that capture correlations between diverse biological features and scores observations along these factors. Learning factors helped identify relationships between biological processes, such as the link between organoid size, IGF1R signaling and sensitivity to IGF1R inhibitors. In search for treatments that led to drug-induced phenotype change along factors, we extended the application of factor-learning to factor-projection. This enabled us to identify mTOR and MEK inhibitors as modulators of factor 1 and factor 2, respectively. Given the fact that observations during factor-learning were sampled from a distribution of unperturbed organoids while factor-projection was done on observations from a overlapping, but distinct, distribution of perturbed organoids, our projections of perturbed organoid profiles are limited to the axes of variation defined during factor-learning. As a consequence, we are unable to observe causal relationships between factors and interventions, but only generate hypotheses based on observational data. For example, CDK inhibitor treatment reduced the score of factor 1 across all organoid models. It is, however, unlikely the reduction in factor 1 was due to CDK being an upstream regulator of IGF1R signaling. Instead CDK might serve as the dependent, mediating variable (IGF1R signaling -> CDK signaling -> organoid size) or an independent contributor to organoid size (IGFR1 signaling-> organoid size and CDK signaling -> organoid size). Despite limitations, we believe that the approach of interpreting drug-induced phenotypes using a multi-omics representation of untreated in vitro models is applicable to other large image-based profiling data of multiple heterogeneous in vitro models. This approach could potentially be further extended using causal representation learning methods that increase the understanding of cellular signaling mechanisms, the way they shape cellular morphology and how they change under various treatments during drug discovery.

The clinical translatability of drug screenings with preclinical models, such as organoids, always has to be cautiously interpreted, since these models lack *in vivo* pharmacodynamics and kinetics, microenvironmental factors or microbiota modulating drug response, (dose-limiting) healthy tissues and organs and uncertainty of “correct” drug concentrations compared to *in vivo* situations. Therefore, direct clinical application of organoid-based treatment predictions are difficult and negative results have been published recently<sup>45,46</sup>. Nevertheless, organoids provide a high model representativeness and associations between morphology, molecular features and drug response within organoid cohorts may well be representative of specific biological features of cancer. Additionally, while our image-based profiling study is limited by the number of studied organoid lines and organoid-level imaging resolution, our work is a comprehensive mapping of patient-derived cancer organoid morphologies across 11 organoid donors and >500 small molecule perturbations at single organoid resolution. We identified two key axes of morphological variation in cancer organoids, their underlying biological processes and pharmacological perturbations that move organoids along these axes. Previously, primary cells of monogenic diseases have been intensively studied using image based profiling for drug discovery<sup>63</sup>. Our work opens up new directions for image-based profiling of complex *in vitro* disease models, as we believe this work could be expanded to search for therapeutics in somatic multigenic disease models, for example stepwise genetically edited organoid models of early colorectal cancer<sup>31,32</sup>, or larger cohorts of patient-derived cancer organoids. In addition, more complex cellular interactions such as interactions of immune cells with solid tumors could be explored with refined image based drug screening protocols based on our method<sup>64–66</sup>. A better understanding of organoid phenotypes and the ability to use multi-omics data to annotate organoid states and their plasticity have the potential to further accelerate image-based drug discovery for complex multigenic diseases such as colorectal cancer.

## Methods

**Patients.** All patients were recruited at University Hospital Mannheim, Heidelberg University, Mannheim, Germany. We included untreated patients with a new diagnosis of colon or rectal cancer in this study and obtained biopsies from their primary tumors via endoscopy. Exclusion criteria were active HIV, HBV or HCV infections. Biopsies were transported in phosphate buffered saline (PBS) on ice for subsequent organoid extraction. Clinical data, tumor characteristics and molecular tumor data were pseudonymized and collected in a database. The study was approved by the Medical Ethics Committee II of the Medical Faculty Mannheim, Heidelberg University (Reference no. 2014-633N-MA and 2016-607N-MA). All patients gave written informed consent before tumor biopsy was performed. In total, we extracted organoids from 13 patients with colorectal cancer for this study. Patient characteristics including sex, tumor location and stage can be found in Supplementary Table 1. Participants were not compensated.

**Organoid culture.** Organoid cultures were extracted from tumor biopsies as reported by Sato et al.<sup>5</sup> with slight modifications. In short, tissue fragments were washed in DPBS (Life technologies) and digested with Liberase TH (Roche) before embedding into Matrigel (Corning) or BME R1 (Trevigen). Advanced DMEM/F12 (Life technologies) medium with Pen/Strep, Glutamax and HEPES (basal medium) was supplemented with 100 ng/ml Noggin (Peprotech), 1 x B27 (Life technologies), 1,25 mM n-Acetyl Cysteine (Sigma), 10 mM Nicotinamide (Sigma), 50 ng/ml human EGF (Peprotech), 10 nM Gastrin (Peprotech), 500 nM A83-01 (Biocat), 10 nM Prostaglandin E2 (Santa Cruz Biotechnology), 10 µM Y-27632 (Selleck chemicals) and 100 mg/ml Primocin (Invivogen). Initially, cells were kept in 4 conditions including medium as described (ENA), or supplemented with additional 3 µM SB202190 (Biomol) (ENAS), 50% Wnt-conditioned medium and 20% R-Spondin conditioned medium (WENRA) or both (WENRAS), as described by Fujii et al.<sup>6</sup>. The tumor niche was determined after 7–14 days and cells were subsequently cultured in the condition with best visible growth. Organoids were passaged every 7–10 days and medium was refreshed every 2–3 days. 13 organoid lines were analyzed within this study, data of all organoid lines including niche and growth rate are denoted in Supplementary Table 1.

**Amplicon sequencing.** DNA was isolated with the DNA blood and tissue kit (Qiagen). Sequencing libraries were prepared with a custom panel (Tru-Seq custom library kit, Illumina) according to the manufacturer's protocol and sequenced on a MiSeq (Illumina) as reported previously<sup>67</sup>. Targeted regions included the most commonly mutated hot spots in colorectal cancer in 46 genes captured with 157 amplicons of approximately 250 bp length. Sequencing reads were first evaluated using FastQC v.0.11.5<sup>68</sup> and the low quality reads together with the adapters were trimmed using TrimGalore v.0.4.3<sup>69</sup>. After mapping the reads to the GRC38 reference genome using Burrows-Wheeler Aligner (BWA) v.0.7.16, the resulting aligned reads were first compressed to BAM files using samtools v.1.3.1<sup>70</sup> and then sorted and indexed using the Picard tools v.1.138. The resulting bam files were analyzed using the Genome Analysis Toolkit (GATK) v. 3.8<sup>71</sup>. Base recalibration was performed and variants were called using the MuTect2 pipeline. Variants with a variant frequency below 10%, with less than 10 reads, or with high strand bias ( $FS < 60$ ) were filtered out. Variants were annotated with Ensembl variant effect predictor<sup>72</sup> and manually checked and curated using integrative genomics viewer, if necessary<sup>73</sup>. Only non-synonymous variants present in COSMIC<sup>74</sup> were considered true somatic cancer mutations. Also, all variants annotated "benign" according to PolyPhen database and "tolerated" in SIFT database were excluded, as well as variants with a high frequency in the general population as determined by a GnomAD<sup>75</sup> frequency of >0.001.

**Expression profiling.** Organoid RNA was isolated with the RNeasy mini kit after snap freezing organoids on dry ice. Samples were hybridized on Affymetrix U133 plus 2.0 arrays. Raw microarray data were normalized using the robust multi-array average (RMA) method<sup>76</sup> followed by quantile normalization as implemented in the "affy"<sup>77</sup> R/Bioconductor package. In order to exclude the presence of batch effects in the data, principal component analysis and hierarchical clustering were applied. Consensus molecular subtypes were determined as described previously<sup>78</sup> using the single sample CMS classification algorithm with default parameters as implemented in the R package "CMSclassifier". In all cases, differential gene expression analyses were performed using a moderated *t* test as implemented in the R/Bioconductor package "limma"<sup>79</sup>. Gene set enrichment analyses were performed using ConsensusPathDB<sup>80</sup> for discrete gene sets or GSEA as implemented in the "gsea"<sup>81,82</sup> R/Bioconductor package for ranked gene lists. Wikipathways<sup>83</sup> or Reactome<sup>84</sup> were used for pathway analysis. Gene expression analysis was done in R version 4.0.0. When possible, packages were installed via bioconductor.

### Compound profiling

**Cell seeding.** Organoid drug profiling followed a standardized protocol with comprehensive documentation of all procedures. Organoids were collected and digested in TrypLE Express (Life technologies). Fragments were collected in basal medium with 300 U/ml DNase (Sigma) and strained through a 40  $\mu$ m filter to achieve a homogeneous cell suspension with single cells and small clusters of cells, but without large organoid fragments. 384 well uclear assay plates (Greiner) were coated with 10  $\mu$ L BME V2 (Trevigen) at a concentration of 6.3 mg/ml in basal medium, centrifuged and incubated for >20 min at 37 °C to allow solidification of the gel. Organoid cell clusters together with culture medium (ENa) and 0.8 mg/ml BME V2 were added in a volume of 50  $\mu$ L per well using a Multidrop dispenser (Thermo Fisher Scientific). Plates were sealed with a plate-loc (Agilent) and centrifuged for an additional 20 min allowing cells to settle on the pre-dispersed gel. Cell number was normalized before seeding by measuring ATP levels in a 1:2 dilution series of digested organoids with CellTiter-Glo (Promega). The number of cells matching 10,000 photons (Berthold Technologies) was seeded in each well. After seeding of organoid fragments, plates were incubated for three days at 37 °C to allow organoid formation before addition of small molecules. Two biological replicates (defined as an independent passage) of each organoid line were profiled. Mean passage number of the organoid lines by the time of profiling of the first replicate was 9 (median 9) and organoids were passaged up to two more times before the second replicate. In total, 13 organoid lines underwent profiling with the clinical cancer library and the KiStem library with high throughput imaging. Data from two organoid lines (D015T, D021T) later had to be excluded due to too many out-of-focus organoids (more details below). One line, D020T, was profiled twice within different experimental batches (D020T01 and D020T02). If not shown otherwise, data from D020T01 was used.

**Compound libraries.** Two compound libraries were used for screening: A library containing 63 clinically relevant small molecules (clinical cancer library, Supplementary Table 3) and a library of 464 compounds targeting kinases and stem cell or developmental pathways associated genes (KiStem library, Supplementary Table 4). The clinical cancer library was manually curated by relevance for current (color-coded) cancer therapy, mechanism of action and potential clinical applicability. Small molecules of this library were mainly in clinical use or in phase I/II clinical trials. Five concentrations per compound were screened (five-fold dilutions). The concentrations were determined by analysis of literature data from previous 3D and 2D drug screens and own experiments. All small molecules within the KiStem library were used in a concentration of 7.5  $\mu$ M. All small molecules were obtained from Selleck chemicals. Libraries were arranged in an optimized random layout. We stored compound libraries in DMSO at -80 °C.

**Compound treatment.** 30  $\mu$ L medium was aspirated from all screening plates and replaced with fresh ENa medium devoid of Y-27632, resulting in 45  $\mu$ L volume per well. Drug libraries were diluted in basal medium and subsequently 5  $\mu$ L of each small molecule was distributed to screening plates. All liquid handling steps were performed using a Biomek FX robotic system (Beckmann Coulter). Plates were sealed and incubated with small molecules for four days.

**Luminescence viability read out.** Plates undergoing viability screening were treated with 30  $\mu$ L CellTiter-Glo reagent after medium aspiration with a Biomek FX (Beckmann Coulter). After incubation for 30 min, luminescence levels were measured with a Mithras reader (Berthold technologies).

**Image-based phenotyping.** Image-IT DeadGreen (Thermo Fisher) was added to the cultures with a Multidrop dispenser (Thermo Fisher) in 100 nM final concentration and incubated for 4 h. Afterwards, medium was removed and organoid cultures were fixed with 3% PFA in PBS with 1% BSA. Fixed plates were stored at 4 °C for up to 3 days before permeabilization and staining. On the day of imaging, organoids were permeabilized with 0.3% Triton-X-100 and 0.05% Tween in PBS with 1% BSA and stained with 0.1  $\mu$ g/ml TRITC-Phalloidin (Sigma) and 2  $\mu$ g/ml DAPI (Sigma). All liquid handling steps were performed with BiomekFX (Beckmann Coulter). Screening plates were imaged with an Incell Analyzer 6000 (GE Healthcare) line-scanning confocal fluorescent microscope. We acquired 4 fields per well with z-stacks of 16 slices at 10x magnification. The z-steps between the 16 slices had a distance of 5  $\mu$ m, the depth of field of each slice was 3.9  $\mu$ m.

**Immunohistochemistry.** Organoids were fixed for 20 min in 4% (v/v) Roti Histofix (Carl Roth) followed by embedding into MicroTissues 3D Petri Dish micromolds (Sigma-Aldrich) using 2% (w/v) Agarose LE (Sigma) in PBS supplemented with 0.5 mM DTT. Thereafter, organoids were subjected to dehydration steps and embedding in paraffin. Formalin-fixed agarose/paraffin-embedded sections (3–5  $\mu$ m) were manually cut from blocks with a microtome (Leica RM 2145) and transferred to glass slides (Superfrost, Thermo Fisher Scientific) before H&E staining using automated staining devices.

**Real time quantitative PCR.** Total RNA was isolated from organoids with the RNeasy Mini kit (Qiagen), cDNA synthesis was done with Verso cDNA kit (Thermo Fisher Scientific), and RT-PCR was performed using the SYBR Green Mix (Roche, Nutley, NJ, USA) on LightCycler480 system (Roche). The following primers for LGR5 were used: 5'-TTC CCA GGG AGT GGA TTC TAT-3' (forward) and 5'-ACC AGA CTA TGC CTT TGG AAA C-3' (reverse). Results were normalized to UBC mRNA using 5'-CTG ATC AGC AGA GGT TGA TCT TT-3' forward and 5'-TCT GGA TGT TGT AGT CAG ACA GG-3' reverse primers.

**Western blot.** Organoids seeded in 6-well plates were harvested after 3-days incubation with WYE-132 in RIPA buffer (Thermo Scientific) supplemented with protease inhibitors (Complete Mini, Roche) and phosphatase inhibitors (Phosphatase Inhibitor 1 and 2, Sigma), followed by sonication (Branson Sonifier, Heinemann). Protein concentrations of supernatants were measured using a BCA assay kit (Thermo Fisher Scientific). Lysates were mixed with an SDS-loading buffer and heated to 99 °C for 5 min. Proteins were separated by SDS-PAGE in MOPS running buffer and transferred to a nitrocellulose membrane. Membranes were blocked with 5% (w/v) skim milk in PBS containing 0.1% (v/v) Triton X-100 (PBS-T). Antibodies against IRS1 (06-248, Sigma-Aldrich) and HSP-90 (sc-13119, Santa Cruz) as loading control were used in 1:1000 dilution in 5% milk in PBS-T, secondary antibodies (Mouse IgG HRP ECL, Sigma-Aldrich) were used in 1:10000. ECL Western Blotting W1001 (Promega) was used for visualization of bands.

### Image analysis

**Image processing.** Microscopic image z-stacks were illumination corrected using a prospective method, compressed to HDF5 format and underwent maximum contrast projection using the MaxContrastProjection package for further processing of the images. This algorithm projects the multi-channel 3D image stack onto a plane by retaining the pixel information with the strongest contrast to its neighboring pixels. We used a two-step procedure to establish segmentation: First, organoids were segmented using a model based on fluorescence channel intensity. The intensity segmentation was then used to perform weakly supervised learning with a deep convolutional neural network (CNN) for object identification on the partially correct intensity segmentation, leveraging the robustness of CNNs with regard to mislabeled training data and eliminating the need for expensive manual annotations. For further analysis, we used a model-free outlier detection to remove segmented objects with a particle size of 300 pixels and lower to remove non-organoid objects. Standard image features, including shape, moment, intensity, and Haralick texture features<sup>85</sup> on multiple scales, were extracted using the R/Bioconductor package EBImage<sup>86</sup>. Initially, we extracted a total of 1572 features for each individual organoid image. However, texture features were meaningless for scales larger than the actual organoid size. To simplify the analysis, we thus only retained texture features that were well defined for all organoids and on a scale smaller than the smallest organoids in the image dataset. This ensured that the dataset contained no NA-values requiring imputation. A feature was considered

“well-defined” if the median absolute deviation across the entire dataset was strictly greater than 0. In other words, if more than half of all organoids exhibited an identical value for a feature, then that feature was discarded for further analysis. This resulted in 528 well-defined features. We did not perform feature selection based on between-replicate correlation of well-averaged features as we used single-organoid features for further analysis and selected downstream methods used (Random-Forest) did not require pre-selection of features or were based on principal components across the complete dataset (logistic regression). To allow comparison between various organoid lines and drug perturbations, the distributions of features describing organoids from different batches were adjusted by centering. Out-of-focus objects were programmatically removed from the dataset using a feature based random forest classifier. Data from two organoid lines (D015T, D021T) had to be excluded from image analysis due to too many out of focus objects, resulting in 11 analyzed organoid lines. In addition, data from three individual plates (D027T01P906L03, D020T01P906L03, D013T01P001L02) were excluded from further analysis due to out-of-focus artifacts. Images were processed with R 3.6.0 and packages were downloaded from bioconductor.

**Analysis of unperturbed organoid phenotypes.** Principal components were calculated for the entire dataset using incremental principal component analysis. A set of 25 principal components were selected, explaining approx. 81% of the total variance within the dataset. We chose 25 principal components because the next PCs only added up minimal more information, i.e. we would have to include a large number of more PCs to increase the covered variance by only a few percent. 25 therefore seemed a reasonable cut-off. Next we embedded the first 25 principal components using uniform manifold approximation and projection (UMAP) with min\_distance of 0.1, 15 nearest neighbors and otherwise default monocle3 parameters<sup>27</sup>. Embedded objects were clustered using the leiden graph based clustering algorithm with a resolution parameter of 10E-7<sup>87</sup>. For the illustration of dose-dependent changes in organoid morphology we fitted principal curves through downsampled UMAP observations using the princcurve R package<sup>88</sup>.

**Live-dead classification.** A random forest classifier (scikit-learn v1.0) with 10 trees was trained on the original 1572 single organoid features to differentiate living from dead organoids. Organoids treated with DMSO were used as negative (i.e. living) controls while organoids treated with Bortezomib and SN-38 at the two highest concentrations were used as positive (i.e. dead) controls. Visual inspection of the projected images confirmed our choice of positive controls. Models were trained and validated using only observations from the clinical cancer panel with a 60–40 train-validation split. Initial classification performance metrics were estimated using the validation dataset. A separate classifier was trained for each individual line to ensure inter-line independence, however individual classifiers were evaluated on validation data from foreign organoid lines to assess generalizability. Classifiers relying on less information (i.e. a combination of actin/TRITC or DNA/DAPI staining alone, compared to all three fluorescence channels) were tested by masking of input features. Binary classification results were averaged within wells to obtain viability scores ranging from 0 to 1, indicating how lethal a treatment was. This procedure was applied to the complete imaging data.

**Analysis of drug activity and drug-induced phenotypes.** A logistic regression model (scikit-learn) was trained per line and treatment (and per concentration where applicable) to differentiate treated organoids from negative controls based on the PCA-transformed features<sup>89</sup>. For model training, organoid observations were separated into training and validation data with a 50–50 split. A hyperparameter grid search for L2 regularization strength was performed on the training set using 5-fold cross validation. Selected models were then trained on the validation set and model performance, expressed in the area under the receiver operating characteristic curve (AUROC), was estimated using 10-fold cross validation. Next, we selected active compound treatments in which robust morphological changes were observed in at least one line. Treatments were categorized as either active or inactive based on the performance of the logistic regression classifier. We defined a compound treatment as “active” when treated and untreated organoids in the validation dataset could be correctly identified by their corresponding classifier with an average area under the receiver operating characteristic curve (AUROC) of 0.85 or greater. The model coefficients, which can be understood as the direction of the normal vector perpendicular to the separating hyperplane in organoid feature space, was interpreted as the drug-induced effect. We chose this approach to account for the high intra- and inter-sample heterogeneity of primary patient-derived organoids. We accepted the strong reference to DMSO treated organoids in order to describe compound treatments. Drugs were clustered based on the cosine similarity. We compared this approach to a model-free Pearson correlation based clustering. We then aggregated compound induced phenotypic profiles across all organoid lines and applied contingency testing<sup>90</sup>. Fisher’s exact test was used to identify enrichments of compounds with the same mode-of-action.

**Analysis of dose-response relationships for organoid viability measurements.** Cell Titer Glo raw data of each plate were first normalized using the Loess-fit method<sup>91</sup> in order to correct for edge effects. Subsequently, each plate was normalized by division with the median viability score of the DMSO controls. For drugs tested in multiple concentrations, drug response Hill curves (DRC) were fitted and area

under the curve values were calculated for each DRC using the “PharmacoGx” R/Bioconductor package<sup>92</sup>. The same method was used for predictions by the Live-dead classifier in cases where multiple concentrations were available.

### Multi-omics factor analysis

**Model training.** A multi-omics factor analysis model was trained based on a set of five modalities describing unperturbed organoid lines:

- organoid size estimated based on log-normal model fit of all DMSO treated organoids [22 replicates, 1 feature]
- organoid somatic mutations as determined by amplicon sequencing [20 replicates, 12 features]
- organoid gene expression including the top 10% genes with the highest coefficient of variance after robust multi-array average normalization [22 replicates, 3222 features]
- organoid morphology as determined by averaging DMSO treated morphological profiles [22 replicates, 25 features]
- organoid drug activity as determined by AUROC score of logistic regression models for drugs that were defined as active in at least one observation [22 replicates, 252 features]

Input data was scaled and the MOFA model was trained with default MOFA2 training parameters and a number of 3 factors<sup>30</sup>. The number of factors was chosen given the limited number of observations in our training data. The further analysis focused on the first two factors, which correlated with prominent visible organoid phenotypes. Gene set enrichment analysis and Reactome pathway enrichment of factor loadings was performed using the clusterprofiler R package (v4.2)<sup>93</sup>. Enrichment of drug targets within factor loadings was tested using ANOVA by fitting a linear model, lm(factor loading ~ target). Drug targets that were represented with at least three small molecule inhibitors were included in this analysis. The analysis was run using the MOFA docker container available from <https://hub.docker.com/r/gtca/mofa2>.

**Model projection.** To estimate the factor scores for drug-induced organoid morphologies, the morphology profiles of organoids treated with the same drug were averaged. The resulting average profile matrix was multiplied with the pseudoinverse of the previously learnt model loading matrix for organoid morphology data. The resulting projected factor score matrix was used to estimate the drug-induced biological changes in cancer organoids. Associations between drug targets and projected factor scores of drug treated organoids were identified via ANOVA by fitting a linear model, lm(projected factor score ~ target). Drug targets that were represented with at least three small molecule inhibitors were included in this analysis.

**Statistics and reproducibility.** If not otherwise stated, drug screening experiments were performed in two biological replicates. A total of 5.5 Mio organoids were analyzed after perturbation with 842 conditions, so that on average, more than 6000 organoids were analyzed per condition. When example images of phenotypes are shown, we selected representative organoids from the images taken in screening experiments and embedded them in black background for better visualization of phenotypes.

**Reporting summary.** Further information on research design is available in the Nature Research Reporting Summary linked to this article.

### Data availability

Microarray data are available in Gene Expression Omnibus (GEO) under accession no. GSE117548 and under [https://github.com/boutroslab/Supp\\_BetgeRindtorff\\_2021/tree/master/data/](https://github.com/boutroslab/Supp_BetgeRindtorff_2021/tree/master/data/). Raw Amplicon sequencing data are available through controlled access in the European Genome Phenome Archive (EGA, <https://www.ebi.ac.uk/ega/home>, accession no. EGAD00001004313) to adhere with donating patient’s data security and informed consent. Data access requests for sequence data will be evaluated and transferred upon completion of a data transfer agreement and authorization by the data access committee of Division Signaling and Functional Genomics, DKFZ and Department of Medicine II, Medical Faculty Mannheim. Processed sequencing results are available in Supplementary Table S2. Imaging data can be made available upon request to the corresponding authors after completion of a data transfer agreement and under the premise of adhering to EU General Data Protection Regulation. Pre-processed, PCA-transformed feature data and all other data to reproduce the analyses for the figures are available under [https://github.com/boutroslab/Supp\\_BetgeRindtorff\\_2021](https://github.com/boutroslab/Supp_BetgeRindtorff_2021). Source data are provided with this paper.

### Code availability

Software for organoid image analysis (including projection, segmentation, feature extraction, analysis of drug-induced phenotypes, live-dead-classification), the scripts for analysis of luminescence data, dose response relationships, expression, amplicon sequencing and multi-omics factor analysis are available at: [https://github.com/boutroslab/Supp\\_BetgeRindtorff\\_2021](https://github.com/boutroslab/Supp_BetgeRindtorff_2021).

Received: 12 December 2021; Accepted: 12 May 2022;

Published online: 06 June 2022

## References

- Sung, H. et al. Global cancer statistics 2020: GLOBOCAN estimates of incidence and mortality worldwide for 36 cancers in 185 countries. *Ca Cancer J. Clin.* **71**, 209–249 (2021).
- Piawah, S. & Venook, A. P. Targeted therapy for colorectal cancer metastases: a review of current methods of molecularly targeted therapy and the use of tumor biomarkers in the treatment of metastatic colorectal cancer. *Cancer* **125**, 4139–4147 (2019).
- Hervieu, C., Christou, N., Battu, S. & Mathonnet, M. The role of cancer stem cells in colorectal cancer: from the basics to novel clinical trials. *Cancers* **13**, 1092 (2021).
- Gupta, P. B., Pastushenko, I., Skibinski, A., Blanpain, C. & Kuperwasser, C. Phenotypic plasticity: driver of cancer initiation, progression, and therapy resistance. *Cell Stem Cell* **24**, 65–78 (2019).
- Sato, T. et al. Long-term expansion of epithelial organoids from human colon, adenoma, adenocarcinoma, and Barrett's Epithelium. *Gastroenterology* **141**, 1762–1772 (2011).
- Fujii, M. et al. A Colorectal Tumor Organoid Library Demonstrates progressive loss of niche factor requirements during tumorigenesis. *Cell Stem Cell* **18**, 827–838 (2016).
- van de Wetering, M. et al. Prospective derivation of a living organoid biobank of colorectal cancer patients. *Cell* **161**, 933–945 (2015).
- Weeber, F. et al. Preserved genetic diversity in organoids cultured from biopsies of human colorectal cancer metastases. *Proc. Natl Acad. Sci. USA* **112**, 13308–13311 (2015).
- Schütte, M. et al. Molecular dissection of colorectal cancer in pre-clinical models identifies biomarkers predicting sensitivity to EGFR inhibitors. *Nat. Commun.* **8**, 14262 (2017).
- Vlachogiannis, G. et al. Patient-derived organoids model treatment response of metastatic gastrointestinal cancers. *Science* **359**, 920–926 (2018).
- Driehuis, E., Kretzschmar, K. & Clevers, H. Establishment of patient-derived cancer organoids for drug-screening applications. *Nat. Protoc.* **15**, 3380–3409 (2020).
- Yan, H. H. N. et al. A comprehensive human gastric cancer organoid biobank captures tumor subtype heterogeneity and enables therapeutic screening. *Cell Stem Cell* **23**, 882–897.e11 (2018).
- Lee, S. H. et al. Tumor evolution and drug response in patient-derived organoid models of bladder. *Cancer Cell* **173**, 515–528.e17 (2018).
- Broutier, L. et al. Human primary liver cancer-derived organoid cultures for disease modeling and drug screening. *Nat. Med.* **23**, 1424–1435 (2017).
- Brandenberg, N. et al. High-throughput automated organoid culture via stem-cell aggregation in microcavity arrays. *Nat. Biomed. Eng.* **4**, 863–874 (2020).
- Ooft, S. N. et al. Patient-derived organoids can predict response to chemotherapy in metastatic colorectal cancer patients. *Sci. Transl. Med.* **11**, eaay2574 (2019).
- Boutros, M., Heigwer, F. & Laufer, C. Microscopy-based high-content screening. *Cell* **163**, 1314–1325 (2015).
- Pegoraro, G. & Misteli, T. High-throughput imaging for the discovery of cellular mechanisms of disease. *Trends Genet.* **33**, 604–615 (2017).
- Carpenter, A. E. Image-based chemical screening. *Nat. Chem. Biol.* **3**, 461–465 (2007).
- Perlman, Z. E. et al. Multidimensional drug profiling by automated microscopy. *Science* **306**, 1194–1198 (2004).
- Breining, M., Klein, F. A., Huber, W. & Boutros, M. A chemical–genetic interaction map of small molecules using high-throughput imaging in cancer cells. *Mol. Syst. Biol.* **11**, 846 (2015).
- Kraus, O. Z. et al. Automated analysis of high-content microscopy data with deep learning. *Mol. Syst. Biol.* **13**, 924 (2017).
- Styles, E. B., Friesen, H., Boone, C. & Andrews, B. J. High-throughput microscopy-based screening in *Saccharomyces cerevisiae*. *Cold Spring Harb. Protoc.* **2016**, pdb.top087593–pdb.top087593 (2016).
- Baddar, L. M. et al. 3D imaging of colorectal cancer organoids identifies responses to Tankyrase inhibitors. *Plos ONE* **15**, e0235319 (2020).
- Lukonin, I. et al. Phenotypic landscape of intestinal organoid regeneration. *Nature* **586**, 275–280 (2020).
- Bock, C. et al. The organoid cell atlas. *Nat. Biotechnol.* **39**, 13–17 (2021).
- Trapnell, C. et al. The dynamics and regulators of cell fate decisions are revealed by pseudotemporal ordering of single cells. *Nat. Biotechnol.* **32**, 381–386 (2014).
- Kotliarova, S. et al. Glycogen synthase kinase-3 inhibition induces glioma cell death through c-MYC, nuclear factor- $\kappa$ B, and glucose regulation. *Cancer Res.* **68**, 6643–6651 (2008).
- Klaeger, S. et al. The target landscape of clinical kinase drugs. *Science* **358**, eaan4368 (2017).
- Argelaguet, R. et al. Multi-Omics Factor Analysis—a framework for unsupervised integration of multi-omics data sets. *Mol. Syst. Biol.* **14**, e8124 (2018).
- Drost, J. et al. Sequential cancer mutations in cultured human intestinal stem cells. *Nature* **521**, 43–47 (2015).
- Matano, M. et al. Modeling colorectal cancer using CRISPR-Cas9-mediated engineering of human intestinal organoids. *Nat. Med.* **21**, 256–262 (2015).
- Zhan, T. et al. MEK inhibitors activate Wnt signalling and induce stem cell plasticity in colorectal cancer. *Nat. Commun.* **10**, 2197 (2019).
- Merlos-Suárez, A. et al. The intestinal stem cell signature identifies colorectal cancer stem cells and predicts disease relapse. *Cell Stem Cell* **8**, 511–524 (2011).
- Isella, C. et al. Selective analysis of cancer-cell intrinsic transcriptional traits defines novel clinically relevant subtypes of colorectal cancer. *Nat. Commun.* **8**, 15107 (2017).
- O'Reilly, K. E. et al. mTOR inhibition induces upstream receptor tyrosine kinase signaling and activates Akt. *Cancer Res.* **66**, 1500–1508 (2006).
- Sharma, S. V. et al. A chromatin-mediated reversible drug-tolerant state in cancer cell subpopulations. *Cell* **141**, 69–80 (2010).
- Boj, S. F. et al. Organoid models of human and mouse ductal pancreatic. *Cancer Cell* **160**, 324–338 (2015).
- Sachs, N. et al. A living biobank of breast cancer organoids captures disease heterogeneity. *Cell* **172**, 373–386.e10 (2018).
- Pasch, C. A. et al. Patient-derived cancer organoid cultures to predict sensitivity to chemotherapy and radiation. *Clin. Cancer Res.* **25**, 5376–5387 (2019).
- Larsen, B. M. et al. A pan-cancer organoid platform for precision medicine. *Cell Rep.* **36**, 109429 (2021).
- Ledford, H. Global initiative seeks 1,000 new cancer models. *Nature* <https://doi.org/10.1038/nature.2016.20242> (2016).
- Letai, A., Bhola, P. & Welm, A. L. Functional precision oncology: testing tumors with drugs to identify vulnerabilities and novel combinations. *Cancer Cell* **40**, 26–35 (2021).
- Voabil, P. et al. An ex vivo tumor fragment platform to dissect response to PD-1 blockade in cancer. *Nat. Med.* **27**, 1250–1261 (2021).
- Ooft, S. N. et al. Prospective experimental treatment of colorectal cancer patients based on organoid drug responses. *Esco Open* **6**, 100103 (2021).
- Veninga, V. & Voest, E. E. Tumor organoids: opportunities and challenges to guide precision medicine. *Cancer Cell* **39**, 1190–1201 (2021).
- Pauli, C. et al. Personalized and cancer models to guide precision medicine. *Cancer Discov.* **7**, 462–477 (2017).
- Jabs, J. et al. Screening drug effects in patient-derived cancer cells links organoid responses to genome alterations. *Mol. Syst. Biol.* **13**, 955 (2017).
- Boehnke, K. et al. Assay establishment and validation of a high-throughput screening platform for three-dimensional patient-derived colon cancer organoid cultures. *Slas Disco.* **21**, 931–941 (2016).
- Serra, D. et al. Self-organization and symmetry breaking in intestinal organoid development. *Nature* **569**, 66–72 (2019).
- Verissimo, C. S. et al. Targeting mutant RAS in patient-derived colorectal cancer organoids by combinatorial drug screening. *Elife* **5**, e18489 (2016).
- Battle, E. & Clevers, H. Cancer stem cells revisited. *Nat. Med.* **23**, 1124–1134 (2017).
- Shimokawa, M. et al. Visualization and targeting of LGR5+ human colon cancer stem cells. *Nature* **545**, 187–192 (2017).
- Harmston, N. et al. Widespread repression of gene expression in cancer by a Wnt/ $\beta$ -Catenin/MAPK pathway. *Cancer Res.* **81**, 464–475 (2021).
- Nichols, J. & Jones, K. Derivation of mouse embryonic stem (ES) cell lines using small-molecule inhibitors of Erk and Gsk3 signaling (2i). *Cold Spring Harb. Protoc.* **2017**, pdb.prot094086 (2017).
- Puche, J. E. & Castilla-Cortázar, I. Human conditions of insulin-like growth factor-I (IGF-I) deficiency. *J. Transl. Med.* **10**, 224–224 (2012).
- Sun, H., Tu, X. & Baserga, R. A mechanism for cell size regulation by the insulin and insulin-like growth factor-i receptors. *Cancer Res.* **66**, 11106–11109 (2006).
- Zhong, H. et al. Overproduction of IGF-2 drives a subset of colorectal cancer cells, which specifically respond to an anti-IGF therapeutic antibody and combination therapies. *Oncogene* **36**, 797 EP- (2017).
- Flanigan, S. A. et al. Overcoming IGF1R/IR resistance through inhibition of MEK Signaling in Colorectal Cancer Models. *Clin. Cancer Res.* **19**, 6219–6229 (2013).
- Hua, H., Kong, Q., Yin, J., Zhang, J. & Jiang, Y. Insulin-like growth factor receptor signaling in tumorigenesis and drug resistance: a challenge for cancer therapy. *J. Hematol. Oncol.* **13**, 64 (2020).
- Yoon, S.-O. et al. Focal Adhesion- and IGF1R-dependent survival and migratory pathways mediate tumor resistance to mTORC1/2 Inhibition. *Mol. Cell* **67**, 512–527.e4 (2017).

62. Fujii, M. et al. Human intestinal organoids maintain self-renewal capacity and cellular diversity in niche-inspired culture condition. *Cell Stem Cell* **23**, 787–793.e6 (2018).
63. Gibson, C. C. et al. Strategy for identifying repurposed drugs for the treatment of cerebral cavernous malformation. *Circulation* **131**, 289–299 (2015).
64. Rios, A. C. & Clevers, H. Imaging organoids: a bright future ahead. *Nat. Methods* **15**, 24–26 (2018).
65. Yuki, K., Cheng, N., Nakano, M. & Kuo, C. J. Organoid models of tumor immunology. *Trends Immunol.* **41**, 652–664 (2020).
66. Dijkstra, K. K. et al. Generation of Tumor-Reactive T cells by co-culture of peripheral blood lymphocytes and tumor organoids. *Cell* **174**, 1586–1598.e12 (2018).
67. Zhan, T. et al. Cancer-associated mutations in normal colorectal mucosa adjacent to sporadic neoplasia. *Clin. Transl. Gastroen.* **11**, e00212 (2020).
68. Wingett, S. W. & Andrews, S. FastQ Screen: a tool for multi-genome mapping and quality control. *F1000research* **7**, 1338 (2018).
69. Martin, M. Cutadapt removes adapter sequences from high-throughput sequencing reads. *Embeit J.* **17**, 10–12 (2011).
70. Li, H. et al. The Sequence Alignment/Map format and SAMtools. *Bioinformatics* **25**, 2078–2079 (2009).
71. McKenna, A. et al. The Genome Analysis Toolkit: A MapReduce framework for analyzing next-generation DNA sequencing data. *Genome Res.* **20**, 1297–1303 (2010).
72. McLaren, W. et al. The ensembl variant effect predictor. *Genome Biol.* **17**, 122 (2016).
73. Thorvaldsdóttir, H., Robinson, J. T. & Mesirov, J. P. Integrative Genomics Viewer (IGV): high-performance genomics data visualization and exploration. *Brief. Bioinform* **14**, 178–192 (2013).
74. Forbes, S. A. et al. COSMIC: exploring the world's knowledge of somatic mutations in human cancer. *Nucleic Acids Res.* **43**, D805–D811 (2015).
75. Consortium, E. A. et al. Analysis of protein-coding genetic variation in 60,706 humans. *Nature* **536**, 285–291 (2016).
76. Irizarry, R. A. et al. Exploration, normalization, and summaries of high density oligonucleotide array probe level data. *Biostatistics* **4**, 249–264 (2003).
77. Gautier, L., Cope, L., Bolstad, B. M. & Irizarry, R. A. affy—analysis of Affymetrix GeneChip data at the probe level. *Bioinformatics* **20**, 307–315 (2004).
78. Guinney, J. et al. The consensus molecular subtypes of colorectal cancer. *Nat. Med.* **21**, 1350–1356 (2015).
79. Ritchie, M. E. et al. limma powers differential expression analyses for RNA-seq and microarray studies. *Nucleic Acids Res.* **43**, e47–e47 (2015).
80. Kamburov, A., Stelzl, U., Lehrach, H. & Herwig, R. The ConsensusPathDB interaction database: 2013 update. *Nucleic Acids Res.* **41**, D793–D800 (2013).
81. Subramanian, A. et al. Gene set enrichment analysis: knowledge-based approach for interpreting genome-wide expression profiles. *Proc. Natl Acad. Sci. USA* **102**, 15545–15550 (2005).
82. Korotkevich, G. et al. Fast gene set enrichment analysis. *Biorxiv* 060012. <https://doi.org/10.1101/060012> (2021).
83. Slenter, D. N. et al. WikiPathways: a multifaceted pathway database bridging metabolomics to other omics research. *Nucleic Acids Res.* **46**, D661–D667 (2018).
84. Croft, D. et al. The Reactome pathway knowledgebase. *Nucleic Acids Res.* **42**, D472–D477 (2014).
85. Haralick, R. M., Shanmugam, K. & Dinstein, I. Textural features for image classification. *Ieee Trans. Syst. Man Cyber. SMC* **3**, 610–621 (1973).
86. Pau, G., Fuchs, F., Sklyar, O., Boutros, M. & Huber, W. EBImage—an R package for image processing with applications to cellular phenotypes. *Bioinformatics* **26**, 979–981 (2010).
87. Traag, V. A., Waltman, L. & Eck, N. J. van. From Louvain to Leiden: guaranteeing well-connected communities. *Sci. Rep.* **9**, 5233 (2019).
88. Hastie, T. & Stuetzle, W. Principal curves. *J. Am. Stat. Assoc.* **84**, 502 (1989).
89. Loo, L.-H., Wu, L. F. & Altschuler, S. J. Image-based multivariate profiling of drug responses from single cells. *Nat. Methods* **4**, 445–453 (2007).
90. Freudenberg, J. M., Joshi, V. K., Hu, Z. & Medvedovic, M. CLEAN: clustering enrichment analysis. *Bmc Bioinforma.* **10**, 234 (2009).
91. Mpindi, J.-P. et al. Impact of normalization methods on high-throughput screening data with high hit rates and drug testing with dose-response data. *Bioinformatics* **31**, 3815–3821 (2015).
92. Smirnov, P. et al. PharmacogenomicX: an R package for analysis of large pharmacogenomic datasets. *Bioinformatics* **32**, 1244–1246 (2016).
93. Yu, G., Wang, L.-G., Han, Y. & He, Q.-Y. clusterProfiler: an R Package for comparing biological themes among gene clusters. *Omics J. Integr. Biol.* **16**, 284–287 (2012).
94. Wickham, H. ggplot2, Elegant Graphics for Data Analysis. (Springer-Verlag New York, 2016). [https://doi.org/10.1007/978-3-319-24277-4\\_2](https://doi.org/10.1007/978-3-319-24277-4_2).

## Acknowledgements

We thank all patients participating in this study as well as the teams approaching patients for consent. We thank A. Falzone, A. Kerner and K. Kaiser for excellent technical assistance, B. Velten, C. Scheeder and F. Heigwer for helpful discussions on the manuscript and C. Cai for help with immunohistochemical stainings. We are grateful to H. Farin for helpful discussions. We are grateful to J. Hodzic, B. Huber, M. Hirth, G. Kähler, M. Sold and the Central Endoscopy Unit (ZIE) of the University Hospital Mannheim for inclusion of patients and asservation of biopsies. We thank the DKFZ Genomics and Proteomics Core Facility and the Center for Medical Research (ZMF) Mannheim for assistance with Microarrays and H/E stainings, respectively. This work was supported by the Hector Stiftung II, Germany. J.B. was supported by the “Translational Physician Scientist (TraPS)” program of the Medical Faculty Mannheim, Heidelberg University, by the Dr. Hans und Lore Graf Stiftung, Germany and by the Hector II Foundation, Weinheim, Germany. T.Z. was supported by the Clinician Scientist program “Interfaces and Interventions in Chronic Complex Conditions” (DFG EB 187/8-1). M.P.E. is supported by the DFG (GRK2727) and the Land Baden-Württemberg (BW-ZDFP). Research in the lab of MB was in part supported by an ERC Advanced Grant and the German Network for Bioinformatics Infrastructure (de.NBI).

## Author contributions

Conceptualization: J.B., N.R., J.S., M.E. and M.B. Methodology: J.B., N.R., T.M. Formal Analysis: N.R., J.S., B.R., E.V. Software: J.S., N.R. and B.F. Investigation: J.B., N.R., C.D., H.G., F.H., K.S.-M., K.E.B., V.H., T.Gu., L.F., S.B., T.Ga., I.B., R.J., N.H. and T.Z. Writing – Original Draft: J.B. and N.R. Writing – Review & Editing: J.B., N.R., M.E. and M.B. Data curation: J.B., N.R., J.S. and B.R. Visualization: J.B., N.R., J.S. and B.R. Funding Acquisition: M.E., M.B. and J.B. Resources: M.E. and M.B. Supervision: J.B., K.B-H., E.B., M.E. and M.B.

## Funding

Open Access funding enabled and organized by Projekt DEAL.

## Competing interests

M.B. and M.E. received a research grant within the Merck Heidelberg Innovation Program which did not support this study. The remaining authors declare no competing interests.

## Additional information

**Supplementary information** The online version contains supplementary material available at <https://doi.org/10.1038/s41467-022-30722-9>.

**Correspondence** and requests for materials should be addressed to Matthias P. Ebert or Michael Boutros.

**Peer review information** *Nature Communications* thanks Kevin Myant and the other anonymous reviewer(s) for their contribution to the peer review of this work.

**Reprints and permission information** is available at <http://www.nature.com/reprints>

**Publisher's note** Springer Nature remains neutral with regard to jurisdictional claims in published maps and institutional affiliations.



**Open Access** This article is licensed under a Creative Commons Attribution 4.0 International License, which permits use, sharing, adaptation, distribution and reproduction in any medium or format, as long as you give appropriate credit to the original author(s) and the source, provide a link to the Creative Commons license, and indicate if changes were made. The images or other third party material in this article are included in the article's Creative Commons license, unless indicated otherwise in a credit line to the material. If material is not included in the article's Creative Commons license and your intended use is not permitted by statutory regulation or exceeds the permitted use, you will need to obtain permission directly from the copyright holder. To view a copy of this license, visit <http://creativecommons.org/licenses/by/4.0/>.

© The Author(s) 2022

---

# A Biologically Plausible Benchmark for Contextual Bandit Algorithms in Precision Oncology Using *in vitro* Data

---

**Niklas T. Rindtorff\***

Department of Signaling & Functional Genomics  
German Cancer Research Center  
INF 280, Heidelberg, 69120 Germany  
n.rindtorff@dkfz.de

**MingYu Lu**

Laboratory for Computational Physiology  
Massachusetts Institute of Technology

**Nisarg A. Patel**

Department of Oral and Maxillofacial Surgery  
University of California, San Francisco

**Huahua Zheng**

Department of Biostatistics  
Harvard T.H. Chan School of Public Health

**Alexander D'Amour**

Google Research  
355 Main Street, Cambridge, MA 02138 USA

## Abstract

Precision oncology, the genetic sequencing of tumors to identify druggable targets, has emerged as the standard of care in the treatment of many cancers. Nonetheless, due to the pace of therapy development and variability in patient information, designing effective protocols for individual treatment assignment in a sample-efficient way remains a major challenge. One promising approach to this problem is to frame precision oncology treatment as a contextual bandit problem and to apply sequential decision-making algorithms designed to minimize regret in this setting. However, a clear prerequisite for considering this methodology in high-stakes clinical decisions is careful benchmarking to understand realistic costs and benefits. Here, we propose a benchmark dataset to evaluate contextual bandit algorithms based on real *in vitro* drug response of approximately 900 cancer cell lines. Specifically, we curated a dataset of complete treatment responses for a subset of 7 treatments from prior *in vitro* studies. This allows us to compute the regret of proposed decision policies using biologically plausible counterfactuals. We ran a suite of Bayesian bandit algorithms on our benchmark, and found that the methods accumulate less regret over a sequence of treatment assignment tasks than a rule-based baseline derived from current clinical practice. This effect was more pronounced when genomic information was included as context. We expect this work to be a starting point for evaluation of both the unique structural requirements and ethical implications for real-world testing of bandit based clinical decision support.

---

\* Additional affiliation of Niklas Rindtorff, Nisarg Patel and MingYu Lu: Department of Biomedical informatics, Harvard Medical School, 10 Shattuck Street Boston, MA 02115

## 1 Introduction

Precision oncology, the genetic sequencing of tumors to identify druggable targets, has quickly progressed as the standard of care in the treatment of many cancers [7]. Here, targeted treatments show therapeutic activity in subsets of patients defined by tumor-specific genetic alterations, such as imatinib for chronic myelogenous leukemia. [1] However, assigning patients to adequate treatments remains challenging. Current practice applies published and approved therapeutic protocols that consider the patient’s clinical characteristics, including the presence of (most often one) particular genetic mutation, to choose a therapeutic. For example, based on the presence of a single genetic variant, such as a BRAF V600E mutation (a gene involved in cell growth), a treatment decision can be made [2]. However, this limits the ability to make high-confidence clinical decisions in a real-world scenario with a large number of both observable genetic data and treatment options to choose from. The implications for the practice of precision oncology are (I) a high selectivity: only 4.9% of oncology patients are eligible for genome-targeted therapies with robust clinical evidence [9], and subsequently (II) high compassionate use: the majority of oncology patients are left with limited treatment options outside of existing therapeutic protocols, of which off-label use does not contribute systematically to the development of new clinical evidence.

Given the nature of precision oncology, treatment assignment can be modeled as a contextual bandit problem with a patient’s information informing the choice of treatment. In contrast to supervised learning on the one end and reinforcement learning on the other end, contextual bandit problems, especially when based on Thompson sampling, are a well-suited method for this task as it allow agents to explore new treatment options while ensuring that every action has a non-zero chance of being optimal [10]. Put differently, Thompson sampling based agents would never make choices for a patient that are certainly non-optimal in order to improve decision making at a later time point, something that can not be excluded for more most full reinforcement learning algorithms. While contextual bandit applications in oncology have been previously proposed [3, 8], there are no established benchmarks to evaluate different algorithms, objectives, and state representations, due to a lack of biologically interpretable and complete observations of drug response in cancer. This is especially relevant as major ethical questions of how to balance the competing directives of individual utility and population utility remain.

Here we propose a benchmark for contextual bandits in precision oncology based on real *in vitro* drug response of approximately 900 cancer cell lines [6]. For each cell line, mutation, copy number variation, and gene expression data is available to represent the sample’s state. After defining rewards based on treatment response, we used all available algorithms implemented in the Bayesian bandit showdown project [5, 10] to subsequently choose the best treatments for randomly selected cell lines. In addition, we defined a rule-based agent based on a set of current evidence-based therapeutic protocols to evaluate bandit performance and to include prior knowledge into the available state information during selected experiments.

## 2 Methods

### 2.1 Benchmark Construction

We derived all molecular and drug sensitivity data from the Genomics of Drug Sensitivity in Cancer database, a public research repository described by Iorio et al [6] and available at <https://www.cancerrxgene.org>. In a first pre-processing step we focused on a subset of 7 drugs that are currently used in clinical practice. We log transformed the  $IC_{50}$  values and normalized them relative to the median  $\ln(IC_{50})$  across cell-lines for each drug. We used the resulting score to quantify drug response and calculate response-based rewards (Figure 1A).

In order to reduce the dimensionality of the state representation, we reduced 18523 cell-line specific features including scaled gene expression data, and binarized mutation and copy-number variant information into 20 dimensions by uniform manifold approximation and projection (UMAP) using default parameters. UMAP projected features recovered tissue types (Figure 1B) while not directly recovering overall drug sensitivities (Figure 1C).

Next we manually curated therapeutic protocols based on **current clinical evidence, established** and **recent** databases, as well as **trial protocols** with selected simplifications: (I) we excluded any protocols involving combination treatments, (II) we excluded any protocols that are based on the presence of

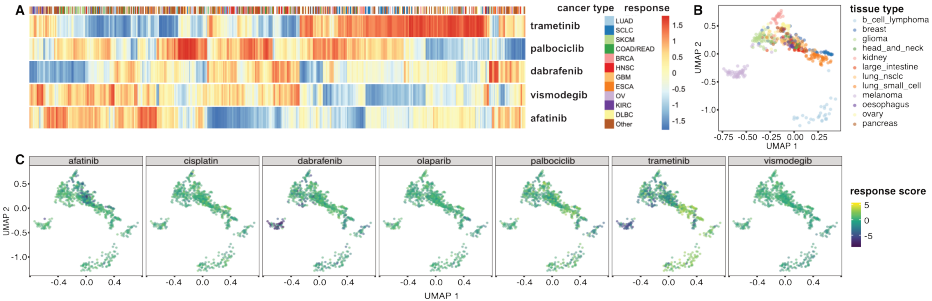


Figure 1: Benchmark Construction. **A** Drug vulnerability data for 896 cell lines and 5 drugs. Blue color corresponds to high drug sensitivity. Only 5 of 7 treatment choices are shown. **B** 20-dimensional embedding of genomic information for all cancer cell lines included in the study. The first two dimensions of the UMAP embedding recovered tissue type differences between cancer cell lines. **C** The first two dimensions of the UMAP embedding did not completely recover differences in drug sensitivity

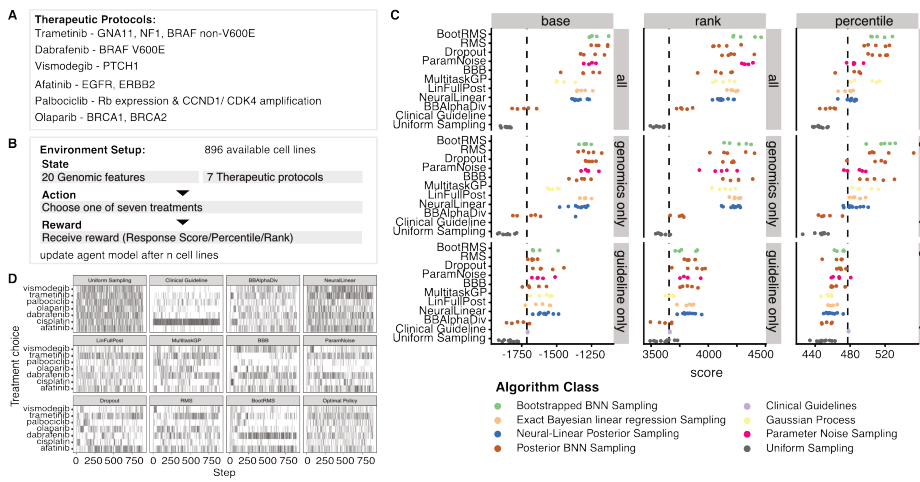


Figure 2: Contextual bandit experimental results. **A** Rules derived from current therapeutic protocols which are used by the reference "Clinical Guideline" agent. **B** Overview of the experimental setup. Both state representation and reward function are varied between experiments. **C** Overview of model performance across reward metrics and state definitions. Dashed line represents the performance of the rule-based agent. A higher score indicates lower regret and better performance. **D** Agent activity over time for different posterior distribution approximations. In this example, state was represented by both genetic information and clinical guidelines. In this instance, RMS was the most successful model.

oncogenic gene-fusions as they were not included in our dataset, (III) in analogy to a basket trials, we did not include tissue type restrictions into any protocols. Cell lines that did not qualify for any of the curated treatments were assigned to be treated with Cisplatin, an established chemotherapeutic used, among others, for treatment of cancers of unknown progeny (Figure 2A).

## 2.2 Contextual Bandit Formulation

We followed the definition of the contextual bandit problem as described in [10]. The algorithm assigns treatments to units sequentially. At a time  $t = 1, \dots, n$  the algorithm takes as input a context corresponding to the next unit  $X_t$  (e.g., a cell line's projected genetic data). The algorithm selects one of  $k$  actions  $a_t$  (e.g., one of 7 available treatments). A reward  $r_t = r_t(X_t, a_t)$  is then generated and returned. At the end, the cumulative reward for the algorithm is defined as  $r = \sum_{t=1}^n r^t$ . The goal is to maximize cumulative reward, and thus minimize the cumulative regret, defined as  $R_A = E[r - r^*]$ ,

where  $r^*$  is the cumulative reward of the optimal policy (i.e., the policy that always selects the ideal treatment given the context).

Similar to the study in [10], we exclusively examined the performance of decision making via Thompson sampling. In each round of Thompson Sampling, parameters,  $\theta_t$ , are sampled from the posterior distribution  $\pi_{t-1}$  given all previous observations. Using these parameters and the current context  $X_t$ , an action  $a_t$  is chosen to optimize the expected regret  $E[r_t|\theta_t, a_t, x_t]$  according to an internal model.

In this study, we examined the effect of (I) different state representations (II) different reward functions and (III) different posterior distribution approximations [10] on performance. We evaluated three different state representations by including only genetic features, only rule-based recommendations or both datatypes in the state. Thus, in total, the state was represented by up to 27 features (20 UMAP + 7 recommendations). Further we defined three different reward metrics:

- subtract the lowest drug response score (the strongest response) from the response score of the selected drug.
- rank the drugs by drug response score in ascending order. The best drug will be ranked 7, while the least active drug will be ranked 1.
- for each drug, we map its response score to its distribution over cell lines and use the percentile as reward.

For posterior approximation, we consider all of the Bayesian bandit algorithms included in [10] with default parameters. These included uniform sampling, Bayesian linear regression, Gaussian Processes, stochastic variational inference, and several neural-network based approximations. A full listing of methods and their hyperparameters are included in the appendix.

For each state representation, reward function and all posterior approximators, we ran 100 epochs with 512 as the batch size for deep Bayesian network training to obtain the final results. We repeated each experiment with 5 independent random seeds, thus generating 5 random patient sequences to go through. We did not define a separate validation dataset to measure agent performance, as commonly done in methods such as cross-validation, because the UMAP representation was learned on the complete dataset, leading to an overestimation of agent performance.

All experiments were run in python 3.6 using modified code from the **Deep Bayesian Bandits Library**, including an additional rule-based "Clinical Guideline" agent that followed current therapeutic protocols and a logging function to export an agent's actions over all experiment steps.

### 3 Results

Overall, our results suggest that contextual bandit algorithms show promise in the precision oncology setting. In our experiments, contextual bandits methods were able to leverage genomic information to consistently achieve substantially lower regret than both uniform random allocation and rule-based clinical guidelines 2B. This main result is shown in Figure 2C with an exemplary plot visualising agent activity 2D. Specifically, in a baseline experiment where each algorithm was only given the information needed to implement clinical guidelines, all agents out-performed uniform random allocation, and had comparable performance to the rule-based reference agent (bottom row). This was to be expected, as clinical guidelines have already been tuned to take advantage of this information. However, when genomic information was available, most of the contextual bandit algorithms were able to improve on the rule-based protocol significantly (top and middle rows). Providing both genomic information and guideline input in the state information did not further improve model performance in most cases (top row vs middle row).

These results were generally robust across reward definitions (columns), although the percentile-based reward showed the weakest results. Of note, three Neural Network based algorithms, bootstrapped-, greedy and Dropout, consistently scored higher rewards compared to linear methods or Gaussian Processes.

## 4 Discussion

In summary, we state that genomics based assignment mechanisms in precision oncology programs can be framed as a contextual bandit problem. When provided with a representation of genomic information, contextual bandit agents can outperform simplified abstractions of current clinical standards based on *in vitro* drug response data. Among the most successful agents were bootstrapped or dropout-based dense neural networks.

This study has several limitations including: (I) *In vitro* drug response data of cancer models has limited transferability into a clinical context although recovering a considerable portion of clinically established genetic predictors of drug response [6], (II) The response scores are on average lower in treatments vs. reference agents, (III) We reduced the dimensionality of available genomic data without dedicated learning of a shared multi-omics embedding, for example as described in [11] (IV) Cisplatin is a limited reference treatment for all considered cancer types.

We decided to reduce the dimensionality of the available feature space in order to reduce model complexity and increase training efficiency. We chose UMAP for this purpose as it recovers both global- and local structure of the dataset. As mentioned before, we believe that this dataset does not only offer a benchmark for machine learning based treatment assignment for cancer, but also action-oriented multomic feature representation of this disease.

In the future, we plan to address the limitations above and validate our findings in alternative *in vitro* and *in vivo* drug response datasets [4], which were measured by perturbing cancer cell lines, patient-derived organoids or xenografts. Clinical outcome data, although valuable, does not lend itself directly for benchmarking, as not all available treatments have been observed for every patient and thus no ideal policy beyond the standard of care is known. Nevertheless, we plan to validate our finding by analyzing agent behaviour for action-patterns that correspond to current clinical best practices. In addition, we plan to measure the impact of certain genomic information types on model performance, for example by using only the available information provided by current genetic testing services.

We would like to stimulate an open discussion about the limitations and potential benefits of bandit-guided treatment assignments in precision oncology programs to minimize collective treatment regret.

## 5 Code and Data availability

All code and data can be accessed in this [repository](#) or the following [directory](#).

## References

- [1] David Blumenthal and Marilyn Tavenner. “A New Initiative on Precision Medicine”. In: *The New England journal of medicine* 363.1 (2010), pp. 1–3. ISSN: 15334406. DOI: [10.1056/NEJMmp1002530](https://doi.org/10.1056/NEJMmp1002530). arXiv: [arXiv:1011.1669v3](https://arxiv.org/abs/1011.1669v3). URL: <http://scholar.google.com/scholar?hl=en%7B%5C%7DbtnG=Search%7B%5C%7Dq=intitle:New+engla+nd+journal%7B%5C%7D0>.
- [2] Jeannie Hou et al. “Improved Survival with Vemurafenib in Melanoma with BRAF V600E Mutation”. In: *New England Journal of Medicine* 364.26 (2011), pp. 2507–2516. ISSN: 0028-4793. DOI: [10.1056/nejmoa1103782](https://doi.org/10.1056/nejmoa1103782).
- [3] Audrey Durand and Joelle Pineau. “Treatment Allocation as Contextual Bandit”. In: Dec. 2015.
- [4] Hui Gao et al. “High-throughput screening using patient-derived tumor xenografts to predict clinical trial drug response”. In: *Nature Medicine* 21 (Oct. 2015), p. 1318. URL: <https://doi.org/10.1038/nm.3954%20http://10.0.4.14/nm.3954%20https://www.nature.com/articles/nm.3954%7B%5C%7Dsupplementary-information>.
- [5] Jasper Snoek et al. “Scalable Bayesian Optimization Using Deep Neural Networks”. In: (2015). ISSN: 1938-7228. DOI: [10.1002/j.2161-1912.1997.tb00313.x](https://doi.org/10.1002/j.2161-1912.1997.tb00313.x). arXiv: [1502.05700](https://arxiv.org/abs/1502.05700). URL: [http://arxiv.org/abs/1502.05700](https://arxiv.org/abs/1502.05700).
- [6] Francesco Iorio et al. “A Landscape of Pharmacogenomic Interactions in Cancer”. In: *Cell* 166.3 (2016), pp. 740–754. ISSN: 10974172. DOI: [10.1016/j.cell.2016.06.017](https://doi.org/10.1016/j.cell.2016.06.017). arXiv: [NIHMS150003](https://arxiv.org/abs/1500.003).
- [7] Lee Schwartzberg. “Precision oncology: who, how, what, when, and when not?” In: *American Society of Clinical Oncology Educational Book* 37 (2017), pp. 160–169.
- [8] Audrey Durand et al. “Contextual Bandits for Adapting Treatment in a Mouse Model of de Novo Carcinogenesis”. In: *MLHC*. 2018.
- [9] John Marquart, Emerson Y. Chen, and Vinay K. Prasad. “Estimation of the Percentage of US Patients With Cancer Who Benefit From Genome-Driven Oncology”. In: *JAMA Oncology* 4.8 (2018), pp. 1093–1098. DOI: [10.1001/jamaoncol.2018.1660](https://doi.org/10.1001/jamaoncol.2018.1660).
- [10] Carlos Riquelme, George Tucker, and Jasper Snoek. “Deep Bayesian Bandits Showdown: An Empirical Comparison of Bayesian Deep Networks for Thompson Sampling”. In: (2018). arXiv: [1802.09127](https://arxiv.org/abs/1802.09127). URL: [http://arxiv.org/abs/1802.09127](https://arxiv.org/abs/1802.09127).
- [11] Nikola Simidjievski et al. “Variational Autoencoders for Cancer Data Integration: Design Principles and Computational Practice”. In: *bioRxiv* (2019). DOI: [10.1101/719542](https://doi.org/10.1101/719542). eprint: <https://www.biorxiv.org/content/early/2019/07/30/719542.full.pdf>. URL: <https://www.biorxiv.org/content/early/2019/07/30/719542>.

## A Full Listing of Bayesian Bandit Algorithms

Here we list the full suite of Bayesian bandit algorithms that we evaluated with our benchmark.

- Uniform Sampling (Takes each action at random with equal probability)
- Bayesian linear (Noise prior  $a_0 = 6, b_0 = 6$ . Ridge prior  $\lambda = 0.25$ )
- Neural Linear (Noise prior  $a_0 = 3, b_0 = 3$ . Ridge prior  $\lambda = 0.25$ . Based on RMS2 net)
- Neural Greedy (Greedy NN approach with fixed learning rate ( $\gamma = 0.01$ ))
- Dropout (Dropout with probability  $p = 0.8$ . Based on RMS3 net)
- Parameter-Noise (Initial noise  $\sigma = 0.01$ , and level  $\epsilon = 0.01$ . Based on RMS2 net)
- Bootstrapped Networks (Bootstrapped with  $q = 5$  models, and  $p = 0.85$ . Based on RMS3 net)
- Stochastic Variational Inference (BayesByBackprop with noise  $\sigma = 0.1$ )
- Expectation-Propagation (Alpha Divergences BB  $\alpha$ -divergence with  $\alpha = 0.1$ , noise  $\sigma = 0.1$ ,  $K = 10$ , prior var  $\sigma_0^2 = 0.1$ .)
- RMS2 net (Learning rate decays, and it is reset every training period)
- RMS3 net (Learning rate decays, and it is not reset at all. Starts at  $\gamma = 1$ )

## REVIEW

## Wnt signaling in cancer

T Zhan<sup>1,2,4</sup>, N Rindtorff<sup>1,4</sup> and M Boutros<sup>1,3</sup>

Wnt signaling is one of the key cascades regulating development and stemness, and has also been tightly associated with cancer. The role of Wnt signaling in carcinogenesis has most prominently been described for colorectal cancer, but aberrant Wnt signaling is observed in many more cancer entities. Here, we review current insights into novel components of Wnt pathways and describe their impact on cancer development. Furthermore, we highlight expanding functions of Wnt signaling for both solid and liquid tumors. We also describe current findings how Wnt signaling affects maintenance of cancer stem cells, metastasis and immune control. Finally, we provide an overview of current strategies to antagonize Wnt signaling in cancer and challenges that are associated with such approaches.

*Oncogene* (2017) **36**, 1461–1473; doi:10.1038/onc.2016.304; published online 12 September 2016

## INTRODUCTION

More than 40 years ago, the *wingless* gene was discovered in a mutagenesis screen for visual phenotypes, affecting various developmental patterning processes in *Drosophila melanogaster*.<sup>1</sup> Subsequently, further genetic screens identified many components of the Wnt family of signaling proteins as key mediators of patterning decisions during embryonic development.<sup>2</sup> A connection of the Wnt pathway to cancer was implicated by the discovery that activation of int1 (Wnt1), which, either by proviral insertion into the Wnt1 locus or transgenic overexpression in mice, resulted in mammary hyperplasia and tumors.<sup>3–5</sup> It was also shown that the *Drosophila* gene *wingless* and the murine proto-oncogene Wnt1 are orthologous.<sup>6</sup> Furthermore, injection of murine Wnt1 mRNA into embryos of *Xenopus* could induce axis duplication.<sup>7</sup> These observations suggested that genes involved in Wnt signaling are highly conserved through evolution. In 1991, mutations of the adenomatous polyposis coli (APC) gene were discovered as the underlying cause of the hereditary colon cancer syndrome termed familial adenomatous polyposis.<sup>8,9</sup> The APC gene was found to interact with β-catenin<sup>10,11</sup> and loss of function of APC resulted in overactive T-cell factor (TCF)4/β-catenin signaling.<sup>12</sup> These findings established a direct link between Wnt signaling and human colorectal cancer.

In the past years, many genetic and biochemical studies have sought to identify novel Wnt pathway components and their functions. Identified components and processes include the Wnt secretory machinery, Wnt co-receptors, components of the β-catenin destruction complex and nuclear co-factors. With the advance in sequencing technology and the comprehensive structural characterization of cancer genomes,<sup>13,14</sup> it became evident that mutations in the Wnt pathway occur frequently in human cancers.<sup>15–18</sup> Despite the fact that major pathway components have been characterized, the function of Wnt signaling within the context of cancer biology is intriguingly complex and remains only partially understood.

In this review we focus on novel insights into Wnt signaling in cancer, gained from studies published within the past 5 years. We describe recently discovered Wnt pathway components and novel functions of the Wnt pathway for cancer stemness, metastasis and immune surveillance. Furthermore, we review the current progress on targeting the Wnt pathway.

## CANONICAL AND NON-CANONICAL WNT SIGNALING

The Wnt pathway is commonly divided into β-catenin dependent (canonical) and independent (non-canonical) signaling. Both the canonical and non-canonical pathway are outlined in detail in Figure 1.

In recent years, novel insights into multiple levels of canonical Wnt signaling were obtained, refining the model of how the pathway is regulated. Production of Wnt ligands in secreting cells is an important and surprisingly complex step in Wnt signaling. The ER resident acyl-transferase Porcupine is required for the attachment of palmitoleic acid to Wnt ligands.<sup>19</sup> Thereafter, lipid-modified Wnt ligands bind to the transmembrane protein Evi/Wls and are shuttled to the plasma membrane via the Golgi apparatus.<sup>20–22</sup> The transport of Wnts from the ER to the Golgi is assisted by p24 proteins.<sup>23,24</sup> After secretion of Wnt ligands, Evi/Wls is undergoing clathrin based endocytosis and is recycled to the Golgi apparatus by the retromer complex.<sup>25,26</sup> Finally, Evi/Wls is transported back to the ER to re-engage in Wnt secretion.<sup>22</sup>

Wnt proteins can either be tethered to the plasma membrane or exit the cell via multiple routes, including direct release from the plasma membrane by solubilization,<sup>27</sup> the formation of exosomes<sup>28</sup> or on lipid protein particles.<sup>29</sup> The variety of mechanisms by which Wnt ligands are released may correspond to their diverse roles during development and organismal maintenance. For example, although membrane-bound Wnt3 ligands retain a short range, but high level of Wnt signaling in intestinal organoids,<sup>30,31</sup> exosome-bound Wnt2b in the

<sup>1</sup>German Cancer Research Center (DKFZ), Division Signaling and Functional Genomics, Heidelberg University, Department Cell and Molecular Biology, Faculty of Medicine Mannheim, Heidelberg, Germany; <sup>2</sup>Heidelberg University, Department of Internal Medicine II, Medical Faculty Mannheim, Mannheim, Germany and <sup>3</sup>German Cancer Consortium (DKTK), Heidelberg, Germany. Correspondence: Professor M Boutros, German Cancer Research Center (DKFZ), Division Signaling and Functional Genomics, Im Neuenheimer Feld 580, Heidelberg, Germany.

E-mail: m.boutros@dkfz.de

<sup>4</sup>These authors contributed equally to this work.

Received 29 May 2016; revised 7 July 2016; accepted 17 July 2016; published online 12 September 2016

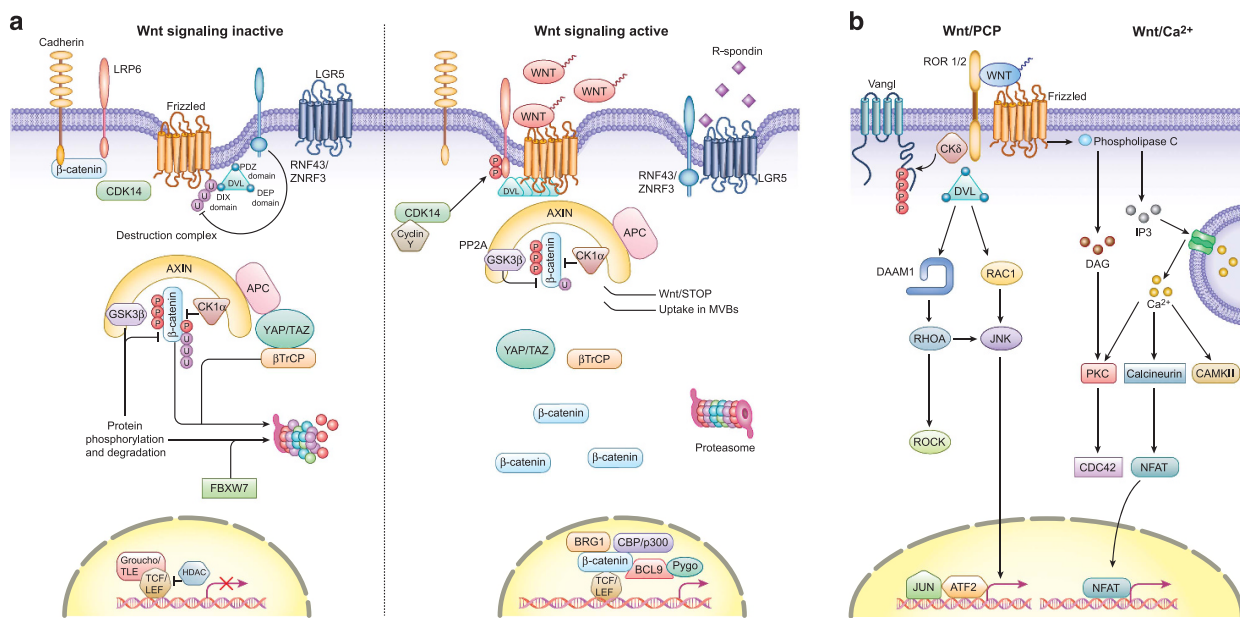


**Figure 1.** Overview of canonical and non-canonical Wnt signaling. (a) In canonical Wnt signaling, absence of Wnt ligands (Wnt signaling inactive state, left) leads to phosphorylation of  $\beta$ -catenin by the destruction complex, which contains the scaffold protein Axin, APC and the kinases GSK3 $\beta$  and casein kinase (CK1 $\alpha$ ). In this state,  $\beta$ -catenin is phosphorylated by GSK3 $\beta$ , ubiquitinated by  $\beta$ -TrCP<sup>200</sup> and targeted for proteasomal degradation. In the absence of nuclear  $\beta$ -catenin, a repressive complex containing TCF/LEF and transducing-like enhancer protein (TLE/Groucho) recruits HDACs to repress target genes. The canonical pathway is activated upon binding of secreted Wnt ligands (for example, Wnt3a and Wnt1) to Fzd receptors and LRP co-receptors (Wnt signaling active, right). LRP receptors are then phosphorylated by CK1 $\alpha$  and GSK3 $\beta$ , which recruits Dishevelled (Dvl) proteins to the plasma membrane where they polymerize and are activated.<sup>201</sup> The Dvl polymers inactivate the destruction complex, for example, by sequestration in multivesicular bodies. This results in stabilization and accumulation of  $\beta$ -catenin which then translocates into the nucleus. There,  $\beta$ -catenin forms an active complex with LEF (lymphoid enhancer factor) and TCF (T-cell factor) proteins by displacing TLE/Groucho complexes and recruitment of histone modifying co-activators such as CBP/p300, BRG1, BCL9 and Pygo (reviewed in Lien and Fuchs<sup>48</sup>). This transcriptional switch leads to a change of multiple cellular processes.<sup>49,202</sup> (b) Non-canonical Wnt signaling is defined by  $\beta$ -catenin-independent mechanisms of signal transduction. During Wnt/PCP signaling, Wnt ligands bind to the ROR-Frizzled receptor complex to recruit and activate Dvl.<sup>203</sup> Dvl binds to the small GTPase Rho by de-inhibition of the cytoplasmic protein DAAM1 (Dvl associated activator of morphogenesis 1).<sup>204</sup> The small GTPase Rac1 and Rho together trigger ROCK (Rho kinase) and JNK. This leads to rearrangements of the cytoskeleton and/or transcriptional responses via for example, ATF2 (activating transcription factor 2).<sup>205</sup> Next to Dvl, Vangl, a key member of Wnt/PCP signaling is activated by phosphorylation in a Wnt5a-dependent manner.<sup>206</sup> Wnt/Ca $^{2+}$  signaling is initiated by G-protein triggered phospholipase C activity<sup>207</sup> leading to intracellular calcium fluxes and downstream calcium dependent cytoskeletal and/or transcriptional responses.<sup>208</sup>

epididymal lumen ensures long-range effects needed for sperm maturation.<sup>32</sup> It is unclear which release mechanism of Wnt ligands is most prevalent in cancer. However, the presence of exosome-based Wnt signaling in the breast cancer microenvironment<sup>33</sup> as well as short range Wnt signaling in RNF43/ZNRF3 double mutant intestinal organoids<sup>31</sup> suggest that tissue-specific mechanisms exist.

Beyond secreted Wnts, members of the R-spondin ligand family were discovered as positive effectors of Wnt signaling.<sup>34–36</sup> R-spondins bind to leucine-rich repeat containing G-protein-coupled receptors (Lgr) 4-6.<sup>37</sup> In the absence of R-spondin binding, the two homologues E3 ubiquitin ligases ZNRF3/RNF43 target the Frizzled (Fzd) receptor for lysosomal degradation.<sup>37,38</sup> Binding of R-spondins to Lgr4-6 inhibits the activity of ZNRF3/RNF43 and leads to the accumulation of Fzd receptors on the cell surface.<sup>36,39</sup> Being transcriptional targets of Wnt signaling, ZNRF3 and RNF43 function as negative feedback regulators in Lgr5-positive cells.<sup>37,38</sup> The interaction of ZNRF3 and RNF43 with the Fzd receptor was found to be dependent on Dishevelled (Dsh).<sup>40</sup> The important role of the R-spondin/Lgr5/RNF43 module in cancer has been demonstrated in several tumor subtypes of colorectal cancer (CRC), pancreatic ductal adenocarcinoma (PDAC) and endometrial cancer which all harbor inactivating mutations of RNF43<sup>41,42</sup> (Figure 2).

At the level of the destruction complex, YAP/TAZ, two transcriptional regulators of the Hippo pathway were recently identified as novel Wnt regulators.<sup>43</sup> Complementing previous evidence for a negative effect of YAP/TAZ on Wnt signaling,<sup>44–46</sup> Azzolin *et al.* proposed a double role for these factors: in the absence of Wnt ligands, YAP/TAZ are part of the destruction complex and recruit  $\beta$ -TrCP, thereby acting as negative regulators of Wnt signaling. However, in an activated pathway state, YAP/TAZ and bound  $\beta$ -TrCP are displaced from Axin1 by LRP during sequestration of the destruction complex. Free YAP/TAZ can subsequently act as positive transcriptional effectors of Wnt signaling.<sup>43,47</sup> The dual role of YAP/TAZ in the Wnt pathway underlines the close connection of Wnt and Hippo signaling.

The transcriptional response to Wnt signaling activation is orchestrated by a complex network of  $\beta$ -catenin binding factors in the nucleus (reviewed in Lien and Fuchs<sup>48</sup> and MacDonald *et al.*<sup>49</sup>), of which novel cancer related components were recently identified. LATS2 kinase, a repressor of YAP/TAZ activity, was found to downregulate Wnt signaling by competing with BCL9,<sup>50</sup> a co-activator of the TCF/LEF transcriptional complex which is highly expressed in human tumors.<sup>51</sup> Furthermore, the DNA-repair gene PAF (PCNA-associated factor) was found to be specifically overexpressed in colon cancer and intestinal stem cells.<sup>52</sup> Overexpression of PAF induced intestinal neoplasia in a mouse model. Mechanistically, PAF enhances Wnt signaling by recruiting the

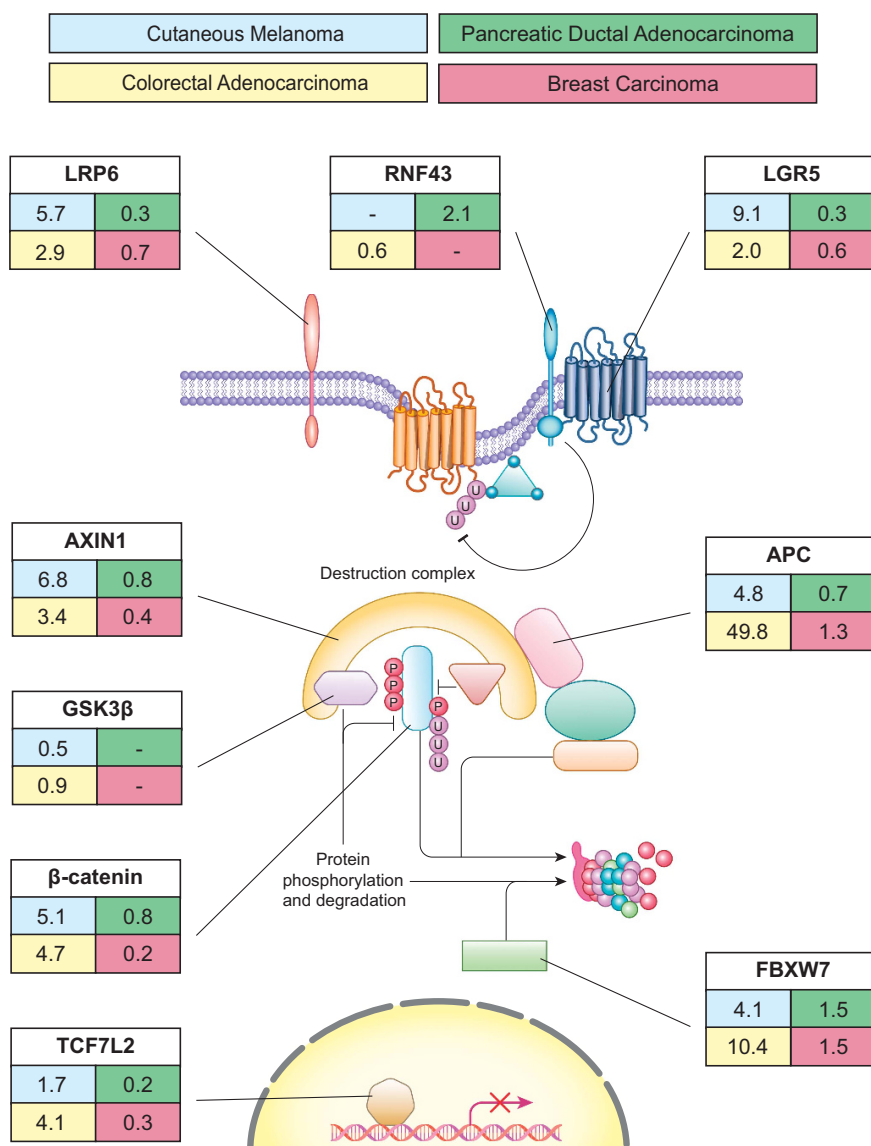


**Figure 2.** Mutation rates of Wnt pathway components in selected cancer entities. Percentage of cancer patients with mutations of selected canonical Wnt pathway related genes. Information was retrieved from the ICGC data portal (accessed 5/2016). The frequency of exonic mutations was determined based on cases with single nucleotide variant data in the MELA-AU, SKCA-BR, SKCM-US, PACA-US, PACA-CA, COAD-US, COCA-CN, READ-US, BRCA-UK and BRCA-US studies.

histone methyltransferase EZH2 to the TCF transcriptional complex (Figure 1).

Beyond the transcriptional response of canonical Wnt signaling, Wnt-dependent stabilization of proteins (Wnt/STOP) has been introduced as a novel β-catenin-independent mechanism. Canonical Wnt signaling, which peaks during G2/M phase due to priming of LRP6 by Cyclin Y/CDK14,<sup>53</sup> was shown to promote β-catenin-independent stabilization of proteins.<sup>54</sup> Activation of this β-catenin-independent Wnt cascade leads to inhibition of GSK3β and the subsequent blockade of poly-phosphorylation and poly-ubiquitination of target proteins, which were predicted to comprise 20% of the proteome.<sup>55,56</sup> These targets include prominent oncogenes such as c-Myc,<sup>54</sup> which is degraded by the E3 ubiquitin ligase FBXW7 (Figure 1). Wnt/STOP has also been proposed to affect chromosomal stability, cell division and endolysosomal biogenesis.<sup>57–59</sup> It remains to be further elucidated whether tissue- and time-dependent preferences for Wnt/STOP or

transcriptional Wnt responses exist and can be exploited for cancer therapy.

Although the canonical pathway is comparatively well understood, the non-canonical Wnt pathways are more diverse and less well characterized (reviewed in Anastas and Moon<sup>60</sup>). The Wnt ligands Wnt5a and Wnt11 can bind to a panel of different receptors to preferentially activate non-canonical Wnt signaling, including receptors of the Fzd family and other receptors such as ROR2, ROR1 or RYK (reviewed in Wang<sup>61</sup> and Katoh<sup>62</sup>). Binding of these non-canonical Wnt ligands can activate multiple intracellular pathways, of which the planar cell polarity (PCP) and calcium signaling pathways are most extensively studied (Figure 1b). The PCP pathway is implicated in cell orientation during development, but also has a role in metastasis formation, whereas the calcium signaling pathway controls intracellular influx of calcium which can activate various downstream kinases including PKC and CaM kinase II (reviewed in De<sup>63</sup> and Yang and Mlodzik,<sup>64</sup> see Figure 2c).

The most prominent ligand receptor pair in non-canonical Wnt signaling is the Wnt5a-ROR2 module. Binding of Wnt5a leads to the formation of the ROR2 receptor complex (Figure 1b). In addition to Wnt/PCP and Wnt/Casignaling, further cascades can be triggered by ROR2. By binding of Filamin A to its prolin-rich domain (PRD), ROR2 can directly cause the formation of filopodia and subsequent cell migration.<sup>65</sup> Of note, although related, ROR2 and ROR1 show a relatively low homology in their PRD, indicating differing functions of these receptors in cell migration.<sup>66</sup> Although non-canonical Wnt signaling plays an undisputed—but understudied—role in most cancer types, our review will primarily focus on canonical Wnt signaling.

## EMERGING ROLES OF WNT IN CANCER

### Gastrointestinal cancers

The impact of Wnt signaling on carcinogenesis of colorectal cancer is well-studied (reviewed in Polakis<sup>67</sup>). Loss of APC is the main driver of Wnt signaling in colorectal cancer and its important role was further highlighted by several recent studies. By genome editing of APC using the CRISPR/Cas9 technology, the carcinogenesis of CRC could be modeled *ex vivo* in human intestinal organoids.<sup>68,69</sup> Furthermore, studies of human CRC samples and tumors from mouse models revealed that different mutations of APC result in distinct levels of canonical Wnt pathway activity and are associated with characteristic tumor locations within the large intestine.<sup>70,71</sup> Using a mouse model with reversible knockdown of APC via shRNA, it was demonstrated that adenomas could regress to normal tissue if APC function is restored, underlining the importance of continuous Wnt signaling for tumor maintenance.<sup>72</sup> Moreover, it was also shown that in spite of truncated APC, Wnt pathway activity can still be modulated by interference with Wnt secretion.<sup>73</sup> Interestingly, a molecular classification of colorectal cancers based on expression and mutation data demonstrates that despite comparable frequencies of APC mutations between subtypes, Wnt target genes can be differentially expressed. Molecular subtypes with high expression levels of Wnt target genes were associated with better overall survival rate after relapse compared to subtypes with low expression levels of the respective genes.<sup>74</sup>

Besides APC, mutations in the R-spondin/Lgr5/RNF43 module were implicated as drivers of Wnt-dependent tumor growth. Deleterious RNF43 mutations have been described in ~19% of CRC cases and are mutually exclusive to APC mutations.<sup>41</sup> In addition, R-spondin3 mutations and fusion proteins expressed at a high level have been described in 10% of CRC cases.<sup>75</sup> RNF43 mutant CRC are strongly dependent on Wnt secretion, rendering them highly susceptible to Wnt secretion targeted therapy.<sup>76</sup>

Chromosomal instability (CIN) is frequently observed in CRC and associated with poor prognosis. Loss of function of Wnt pathway components, particularly APC, have been linked to CIN by multiple mechanisms.<sup>77–79</sup> Although direct interactions of APC with the cytoskeleton and the transcriptional Wnt response via β-catenin are known routes to CIN, Wnt/STOP was introduced as new mechanism: Erych *et al.* recently showed that loss of basal Wnt/STOP leads to increased microtubule assembly rates and subsequent CIN in HCT116 cells,<sup>57,80</sup> while reconstitution of normal assembly rates could reverse the CIN phenotype.<sup>57</sup>

Development of PDAC is mainly driven by oncogenic Ras signaling and the impact of Wnt signaling has not been fully understood. Unlike CRC, mutations of key Wnt pathway components are rare in PDAC (Figure 2), but nuclear localization of β-catenin is regularly found.<sup>81</sup> Results from mouse models indicate that Wnt signaling can initiate tumor formation when activated at distinct tumor stages (reviewed in White *et al.*<sup>82</sup>). However, stabilized β-catenin can also inhibit reprogramming of acini into preneoplastic lesions in the presence of mutated KRAS,<sup>83</sup>

indicating a more complex role of Wnt signaling during tumor development. Recent studies show that PDAC relies on Wnt ligand stimulation, as PDAC cell lines carrying a mutation in RNF43 are particularly sensitive towards treatment with the Porcupine inhibitor LGK974.<sup>42</sup> Furthermore, induction of the Wnt antagonist DKK1 as well as treatment with the anti-Fzd antibody OMP18R5 delays PDAC formation.<sup>84,85</sup> Autocrine Wnt7b was found to increase Wnt signaling in pancreatic cell lines and to promote anchorage-independent cell growth.<sup>85</sup>

Wnt signaling is also activated in cholangiocarcinoma, but genomic alterations of major Wnt pathway components are rare, with the exception of RNF43.<sup>76</sup> Pharmacological inhibition of Wnt signaling, both at the level of β-catenin and Wnt secretion, reduces proliferation of cholangiocarcinoma cells in a mouse model.<sup>86</sup> Interestingly, Wnt secreting inflammatory macrophages in the microenvironment are required to maintain high Wnt signaling in the tumor.<sup>86,87</sup> Furthermore, secreted inhibitors of Wnt signaling such as SFRP2 are frequently silenced by hypermethylation in cholangiocarcinoma.<sup>88,89</sup> Taken together, novel findings reinforce the view that dependence on Wnt signaling of gastrointestinal cancers can be mediated by different, tissue-specific routes.

### Leukemia

In recent years, knowledge about the role of Wnt signaling in hematopoiesis and leukemia has increased.<sup>90</sup> Normal hematopoietic stem cells (HSC) depend on a finely controlled level of Wnt signaling for long-term maintenance, whereas Wnt activity is substantially increased in most leukemias.<sup>91</sup> Acute myelogenous leukemia (AML) is the most common type of acute leukemia in adults and characterized by frequent chromosomal translocations. In MLL-fusion positive AML mouse models, leukemia initiating cells (LIC) can arise from HSC as well as myeloid progenitor cells after progression through a pre-LIC state.<sup>92,93</sup> β-catenin appears to be essential for the progression of pre-LICs to the LIC state and for LIC self-renewal.<sup>94,95</sup> Frequent translocation products found in AML, such as AML1-ETO, MLL-AF9 and PML-RARα positively affect canonical Wnt signaling in patient samples and derived cell lines.<sup>93,96,97</sup>

The most common leukemia in childhood is acute lymphoblastic leukemia (ALL). The majority of LICs in T-cell ALL (T-ALL) harbor activating mutations of the Notch signal pathway (reviewed in Ferrando<sup>98</sup>). However, canonical Wnt signaling in HSC and thymocytes synergizes with PTEN loss and c-Myc amplification to generate a β-catenin dependent and Notch independent T-ALL subset in mouse studies and human T-ALL patients.<sup>99,100</sup> Besides the driving role of canonical Wnt signaling during tumorigenesis of specific T-ALL subsets, active β-catenin appears to play an important role during LIC self-renewal in a broader context. Giambra and colleagues showed that LICs in bulk NOTCH1 driven T-ALL mouse models are marked by high Wnt activity.<sup>101</sup> Inactivation of β-catenin in these tumors eliminated LICs without affecting the short-term viability of the bulk tumor.

Chronic lymphocytic leukemia (CLL) is the most prevalent form of adult leukemia in western countries. Canonical Wnt signaling is active in CLL cells and its inhibition increases apoptosis *in vitro*.<sup>102</sup> Next to frequent silencing of Wnt inhibiting factors such as DKK1/2,<sup>103</sup> somatic mutations in Wnt pathway related genes (for example, FZD5, BCL9) were found in 14% of studied cases.<sup>104</sup> Knockdown of mutated Wnt pathway members reduced cell viability in CLL cells carrying the targeted Wnt pathway alteration, while those without Wnt pathway mutations remained unaffected.<sup>104</sup> These findings demonstrate that a subset of CLL is dependent on active Wnt signaling for survival. In summary, canonical Wnt signaling is able to drive tumor development in major leukemia subtypes and is required for maintenance of leukemia initiating cells.

### Melanoma

About 25% of melanomas arise from benign nevi (commonly known as moles) which typically consist of quiescent BRAF<sup>V600E</sup> or NRAS<sup>Q61K</sup> mutant melanocytes that have undergone a process of oncogene induced senescence<sup>105,106</sup> (reviewed in Jones and Cichowski<sup>107</sup>). Canonical Wnt signaling has been found to delay the onset of oncogene induced senescence in both BRAF<sup>V600E</sup> or NRAS<sup>Q61K</sup> expressing primary melanocytes and thereby increase the chance of tumor development.<sup>108–110</sup>

Although canonical Wnt signaling appears to contribute to melanoma development, its role in disease progression is controversial.<sup>111,112</sup> Several clinical and translational studies have shown an increased overall survival rate of patients carrying melanoma with elevated nuclear β-catenin levels.<sup>113–115</sup> However, in a mouse model with a mutant PTEN and BRAF genotype,<sup>116</sup> activated β-catenin lead to accelerated melanoma development and promotion of metastasis. The impact of Wnt signaling on response towards BRAF inhibitors in melanoma is also unclear. Active Wnt signaling was shown to cooperate with BRAF<sup>V600E</sup> inhibition to induce apoptosis in melanoma cell lines.<sup>117</sup> However, clinical studies demonstrated that patients with lower nuclear β-catenin levels had a better prognosis under BRAF inhibitor treatment.<sup>118</sup>

The role of non-canonical Wnt signaling in melanoma progression has been investigated extensively. Activity of Wnt5a/ROR2 leads to increased cell motility as well as a pseudo-senescent phenotype, which is induced by external stresses.<sup>119–122</sup> In this reversible senescence-like state, melanoma cells are increasingly chemo- and radioresistant and show a senescence associated secretory phenotype<sup>120</sup> marked by the secretion of pro-angiogenic and pro-inflammatory cytokines, for example, IL-6.<sup>123</sup> Interestingly, stimulation with IL-6 has been shown to induce the expression of Wnt5a in melanoma cells itself,<sup>124</sup> thereby forming a positive feedback loop. Thus, Wnt5a mediated non-canonical Wnt signaling leads to self-promoting invasive and resistant phenotypes in melanomas. It is important to note that Wnt5a ligand binding to alternative co-receptors, such as LRP6, can result in a canonical Wnt signaling response in a subset of melanoma cells.<sup>125,126</sup> Consequently, the distinction between canonical and non-canonical signaling effects is not dichotomous and might explain controversial findings.

The progression of melanoma has been described by a phenotype switching model with melanoma cells changing between proliferative and invasive states.<sup>127,128</sup> These prevailing phenotypes are determined in part by the balance between canonical and non-canonical Wnt signaling. Recently, ROR1 and ROR2 co-receptor abundance was linked to the two different melanoma phenotypes. Wnt5a treatment of proliferative ROR1 positive melanoma cells led to ROR1 degradation, a high ROR2 expression and increased invasiveness of melanoma cells *in vivo*.<sup>122</sup> Hypoxic culture conditions were identified as a trigger for changing the cellular Wnt signaling response eventually leading to phenotypic switching.<sup>122</sup>

### Breast cancer

Wnt signaling is activated in over 50% of breast cancer patients and linked to reduced overall survival.<sup>129</sup> The role of canonical Wnt signaling in triple negative breast cancer development and progression has been studied intensively.<sup>130–132</sup> However, high levels of nuclear β-catenin were also found in other breast cancer subtypes.<sup>133</sup> Only a small fraction of tumors harbor somatic mutations of key pathway regulators such as β-catenin<sup>130</sup> (Figure 2), but canonical Wnt ligands and receptors are often overexpressed in breast cancers<sup>134–136</sup> whereas secreted antagonists are silenced.<sup>137</sup> In mice, MMTV-Wnt induced tumors are dependent on continuous Wnt signaling,<sup>138</sup> which leads to progenitor-like signatures in tumor cells.<sup>139</sup> Overexpression of

R-spondin2 alone was shown to initiate mammary tumors in mouse models.<sup>140</sup>

Recently the model of canonical Wnt signaling in mammary tumors has been refined by analysis of clonal heterogeneity within the tumor. Cleary *et al.*<sup>141</sup> identified two tumor cell-lineages of luminal and basal descent in a MMTV-Wnt model. The luminal subclone was characterized by secretion of canonical Wnt ligands, which was necessary for tumor growth of the basal-like recipient cells.<sup>141,142</sup> These findings indicate that mammary tumors can consist of polyclonal cell populations that cooperate to generate distinct, subpopulation specific Wnt activity levels.

### WNT SIGNALING AND CANCER STEM CELLS

The self-renewal potential of cancer cells is described by the cancer stemness model and has been used to explain many malignant phenotypes.<sup>143</sup> Although the concept of cancer stemness is still controversially discussed, the vital role of the Wnt pathway for the function of normal and cancer stem cells is commonly accepted (reviewed in Reya and Clevers<sup>144</sup>). One of the hallmarks of stem cells is their ability to maintain long telomeres by function of the TERT gene. TERT expression was found to be directly enhanced by binding of β-catenin to its promoter region and thereby links telomerase activity to Wnt signaling.<sup>145</sup> The R-spondin receptor Lgr5 is a marker of intestinal stem cells and can fuel tumor growth when APC is deleted in these cells.<sup>146</sup> Lineage tracing experiments demonstrate that single Lgr5-positive cells can give rise to additional Lgr5-positive cells and other cell types in colon adenoma, indicating that Lgr5 is a potential cancer stem cell marker.<sup>147</sup> Myant *et al.*<sup>148</sup> show that RAC1 is required for expansion of the Lgr5 population after APC loss. RAC1 activation drives ROS production and thereby activates NFκB signaling, which then enhances Wnt signaling. These findings are supported by another study showing that co-activation of the NFκB and Wnt pathway can induce dedifferentiation of normal intestinal cells into stem cells and thereby initiate tumor development in a mouse model.<sup>149</sup> The important role of the tumor environment for maintenance of cancer stemness is highlighted by several studies. Hepatocyte growth factor secreted by myofibroblasts in the tumor microenvironment can increase Wnt activity and induce stemness features in colorectal cancer cells.<sup>150</sup> Malanchi *et al.*<sup>151</sup> demonstrated that breast tumor cells induce the stromal expression of the extracellular matrix protein periostin in order to form a metastatic niche. Periostin interacts with Wnt1 and Wnt3a, thereby inducing Wnt signaling and sustaining a CSC phenotype.<sup>151</sup> In another study, MMP3 secreted by mammary epithelial cells was found to stimulate canonical Wnt signaling in mammary stem cells by sequestration of Wnt5b, thereby counteracting the inhibitory effect of the non-canonical Wnt pathway.<sup>152</sup> CD44v6 was described as another CSC marker in colorectal cancer and its expression is promoted by canonical Wnt signaling and cytokines secreted from tumor-associated cells, resulting in increased metastatic capacity.<sup>153</sup>

Recently, several studies uncovered potential links between non-coding RNAs and Wnt signaling in cancer stem cells. microRNA-146a was shown to stabilize β-catenin by repression of Numb, leading to maintenance of Wnt signaling and symmetric division of colorectal cancer stem cells.<sup>154</sup> In mammary stem cells, miR-142 recruits the APC mRNA for degradation and thereby increases canonical Wnt signaling.<sup>155</sup> The long non-coding RNA lncTCF7, which is highly expressed in hepatocellular carcinoma and liver stem cells, was found to activate expression of TCF7 by recruitment of the SWI/SNF complex to the promoter of TCF7. This activation of canonical Wnt signaling is associated with an increased self-renewal capacity of liver CSC.<sup>156</sup> In non-small cell lung cancer, overexpressed miR-582-3p maintains stemness features by targeting negative regulators of Wnt

signaling Axin2, DKK3 and SRP1 for degradation, thereby increasing  $\beta$ -catenin mediated Wnt activity.<sup>157</sup>

Expression signatures of intestinal stemness in tumor samples were correlated with disease prognosis in colorectal cancer.<sup>158,159</sup> Although both the intestinal stem cell and cancer stem cell signature could readily identify patients with poor prognosis, Melo *et al.* show that the expression of accepted Wnt target/stemness genes such as Axin2 and Lgr5 were lower in patients with poor prognosis, due to promoter methylation of those genes. No correlation was found between expression level of Wnt target/stemness genes and the number of CD133-positive stem cells or nuclear  $\beta$ -catenin levels. Thus, stem cell signatures likely reflect the general differentiation state of the tumor tissue rather than the number of Wnt driven cancer stem cells.

### WNT SIGNALING IN METASTASIS

Metastasis is a hallmark of late stage cancer and a major challenge to therapy. A main adaptive change of tumors during therapy is an epithelial to mesenchymal transition (EMT, reviewed in Scheel and Weinberg<sup>160</sup>). EMT describes the process by which polarized epithelial cells transform into migratory mesenchymal cells with invasive properties.<sup>161,162</sup> Transcriptional factors that are responsible for EMT include, among others, SNAI2. Cytoplasmic SNAI2 concentration is kept in check by GSK3 $\beta$  phosphorylation and subsequent ubiquitylation by  $\beta$ -TrCP. Activation of canonical Wnt signaling stabilizes SNAI2 by inhibiting GSK3 $\beta$  kinase activity and initiates EMT transcriptional programs in breast cancer cells.<sup>163</sup> Another candidate gene that regulates EMT is ASPP2, a protein that binds to a  $\beta$ -catenin/E-cadherin complex and inhibits N-terminal phosphorylation of  $\beta$ -catenin, leading to its stabilization. Reduced expression of ASPP2 leads to EMT and is associated with poor survival in hepatocellular and breast cancer.<sup>164</sup> In colon cancer cells with hyperactivated canonical Wnt signaling, pharmacological inhibition of the PI3K-Akt signaling leads to a nuclear accumulation of  $\beta$ -catenin and FOXO3a which results in increased cell scattering and metastasis.<sup>165</sup> These results show that both active and non-active canonical Wnt signaling can enhance EMT, depending on the tissue type. An involvement of the non-canonical Wnt pathway in EMT was implied by high co-expression of Fzd2, its ligands Wnt5a/b and EMT markers. It was shown that Fzd2 expression enhances EMT and cell migration via Fyn and Stat3. Targeting of Fzd2 by a specific antibody reduces tumor growth and metastasis in a xenograft mouse model of colon cancer.<sup>166</sup>

Recently, exosomes were found to be potential mechanism by which tumors prime their metastatic niche.<sup>167</sup> Exosomes are small vesicles secreted by cells and function in intercellular communication. It was shown that they can be vehicles for the transport of active Wnt ligands<sup>28</sup> or incorporate  $\beta$ -catenin.<sup>168</sup> Exosomes secreted from fibroblast in the tumor microenvironment can enhance motility and protrusive activity of breast cancer cells via the Wnt/PCP pathway.<sup>169</sup> Co-injection of breast cancer cells with fibroblast in orthotopic mouse models was shown to promote metastasis. Mechanistically, this results from a tethering of Wnt11 to fibroblast-derived exosomes.<sup>169</sup> Another route by which distant metastasis is proposed to spread is via circulating tumor cells (CTCs).<sup>170</sup> Single-cell RNA sequencing of CTCs was performed for prostate and pancreatic cancer and both studies identified a role for Wnt signaling. In CTCs of pancreatic cancer, Wnt2 expression increased anchorage-independent sphere formation and their metastatic propensity.<sup>171</sup> In another study, the non-canonical Wnt signaling pathway was found to be upregulated in CTCs of prostate cancer cells that are resistant to androgen receptor inhibition.<sup>172</sup> Taken together, there is increasing evidence that both canonical and non-canonical Wnt signaling can support tumor metastasis in a highly tissue-specific manner.

### WNT SIGNALING AND ANTI-TUMOR IMMUNITY

Overcoming immune evasion by cancer cells is a promising therapeutic approach and immune checkpoint blockade was shown to be highly effective in the treatment of melanoma<sup>173</sup> and other tumor types.<sup>174,175</sup> Wnt signaling controls proliferation, maturation and differentiation of T-cells and dendritic cells,<sup>176</sup> but a role of tumor intrinsic Wnt signaling in immune evasion has only recently emerged. Spranger *et al.* show that a Wnt signature in cutaneous melanoma samples correlates with T-cell exclusion. Using a mouse model of melanoma with Braf/PTEN mutant background and constitutively high  $\beta$ -catenin activity, the authors show that T-cell priming against tumor antigens is failing due to defective recruitment of CD103 $^{+}$  dendritic cells.<sup>177</sup>  $\beta$ -catenin signaling downregulates the chemokine CCL4, which negatively affects the recruitment of dendritic cells to the tumor. Restoration of intra-tumoral dendritic cells by injection could furthermore increase the efficiency of anti-CTLA4 and anti-PD-L1 therapy. Moreover, upregulation of IL-12 production in melanoma by increased  $\beta$ -catenin signaling can also lead to impaired dendritic cell maturation and induction of regulatory dendritic cells.<sup>178</sup> A different mechanism of immune evasion was recently demonstrated in lung and breast cancer. It was shown that latency competent cancers self-impose a slow-cycling state by autocrine inhibition of Wnt signaling by DKK1, thereby evading innate immune response.<sup>179</sup> As therapy against immune checkpoint inhibitors are showing promising results also in other tumor entities such as colorectal cancer,<sup>180</sup> further studies investigating the interplay between tumor intrinsic Wnt signaling and immune response are expected.

### PHARMACOLOGICAL INHIBITORS AND CLINICAL TRIALS

The concept that inhibition of Wnt signaling is an universal strategy for the treatment of cancer has been controversially discussed in the past.<sup>60</sup> As clinical data suggests, elevated Wnt signaling is only linked to a worse outcome for a subset of human cancers.<sup>181</sup> Therefore, current strategies aim at targeting Wnt signaling in distinct tumor subclasses or with specific mutational backgrounds. An overview of small molecule inhibitors and antibodies that are currently in clinical testing is presented in Figure 3 and Table 1.

In recent years, the knowledge on the role of Wnt secretion for carcinogenesis has advanced considerably and unveiled novel therapeutic targets. Small molecule inhibitors, including IWP<sup>182</sup> and LGK974, were shown to selectively inhibit the acyl-transferase Porcupine and thus Wnt secretion, leading to a size reduction of MMTV-Wnt1-driven tumors and head and neck cancer xenotransplants. Furthermore, Jiang *et al.* showed that mutations of RNF43 results in dependency of pancreatic adenocarcinomas on Wnt ligands.<sup>42</sup> Mutations of RNF43 and R-spondin fusion proteins, which occur mutually exclusive with APC mutations in colorectal cancer,<sup>41</sup> were subsequently presented as a predictors for an effective therapy targeting Wnt secretion.<sup>75,183</sup> Based on these results, a phase I/II trial of LGK974 was initiated for patients with metastatic colorectal cancer harboring mutations of RNF43 or R-spondin fusions. In addition, a novel orally available Porcupine inhibitor ETC-159<sup>184</sup> that was found to prevent growth of R-spondin-fusion positive CRC, is undergoing clinical testing since July 2015.<sup>185</sup> Although anti-Wnt secretion therapeutics appear promising, the number and impact of potential side effects are currently unclear.

Besides the intracellular perturbation of Wnt secretion, an array of drugs targeting extracellular Wnt ligands and their receptors are under development. OMP-54F28 is a fusion protein consisting of a Fzd8 and a human IgG1 Fc domain. This decoy receptor for Wnt ligands reduces the size of tumor xenografts and overall tumor initiating cell number in mouse models of hepatocellular

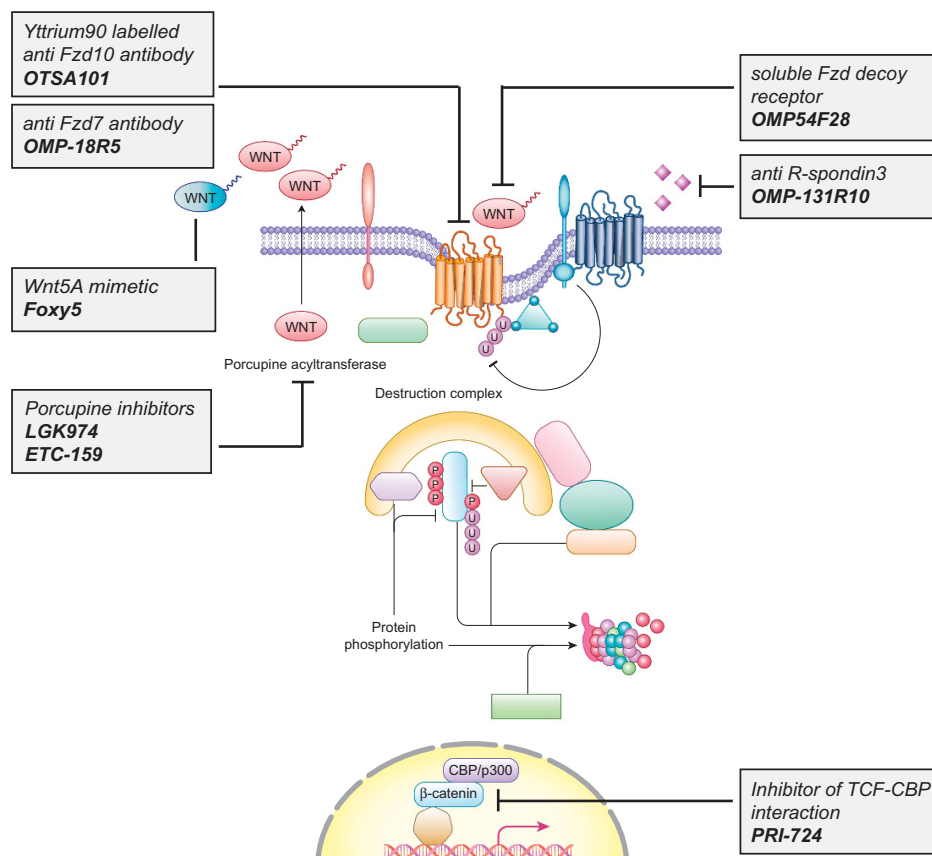


**Figure 3.** Currently tested pharmaceuticals targeting the Wnt pathway in cancer. Schematic representation of the canonical Wnt signaling pathway with pharmaceutical modulators. All depicted drugs are currently undergoing testing in Phase 1/2 against various types of cancer (see also Table 1).

carcinoma and ovarian cancer.<sup>186</sup> Currently, the substance is undergoing three phase 1b trials in liver, ovarian and pancreatic cancer in combination with established therapeutics. Furthermore, a phase I clinical trial testing the safety of OMP131R10, a RSPO3-binding antibody, has been initiated in June 2015 for patients with solid tumors and metastasized colorectal cancer.

OMP18R5 is a monoclonal antibody targeting five of ten human Fzd receptors. It was shown to inhibit the growth of human tumor xenografts and to synergize with standard-of-care therapeutic agents,<sup>187</sup> but first data from clinical studies suggested adverse effects on skeletal constitution.<sup>188</sup> This finding was considered as an on-target effect of Wnt inhibition since Wnt signaling has a key role in bone development and disease.<sup>189</sup> Currently, OMP18R5 is studied in phase I clinical trials alone or in combination with taxanes in breast and pancreatic cancer, as well as non-small cell lung cancer. Besides targeting key functional members of the Wnt signaling cascade, other pharmaceuticals exploit the specific expression patterns of Fzd receptors by cancer cells. For example, Fzd10 is almost exclusively overexpressed in a variety of defined cancer types.<sup>190</sup> OTSA101 is a radioactive anti-Fzd10 antibody which is currently in a phase I trial for the treatment of advanced synovial sarcoma.<sup>191</sup>

In addition to approaches targeting Wnt secretion and ligands, an inhibitor of the downstream Wnt pathway is currently undergoing clinical trials. PRI-724 and the closely related compound ICG-001 specifically target the complex formation of β-catenin and CBP while enhancing the formation of β-catenin/p300 complexes in ALL cells.<sup>192</sup> Treatment with PRI-724 therefore

inhibits the self-renewing downstream effects of β-catenin-CBP activity and leads to reduction of tumor burden.<sup>193</sup> Following promising results from phase I trials,<sup>194</sup> a new phase II trial of PRI-724 in combination with bevacizumab therapy in metastatic colorectal carcinoma patients is planned.<sup>195</sup> Tankyrase inhibitors such as XAV939, which stabilize Axin by blocking its PARsylation, have shown promising results as Wnt inhibitors.<sup>196</sup> Subsequently, additional compounds targeting this enzyme have been developed.<sup>197</sup> However, no tankyrase inhibitor is currently undergoing clinical testing, which may be linked to their toxicity in preclinical models.<sup>198</sup>

A better understanding of non-canonical Wnt signaling in tumor metastasis and growth has led to novel therapeutic approaches. Two Wnt5a analog small peptides, Foxy-5 and Box-5 have been developed to either activate or inhibit Wnt5a-dependent signaling, thereby reducing metastasis in selected tumors. First results from a phase I clinical trial of Foxy-5 suggest a good tolerability.<sup>199</sup>

The introduction of both Wnt5a agonists and antagonists, as well as the identification of anti-secretion therapy responsive tumor subsets further guide the clinical practice into the direction of personalized treatments. However, as data from selected clinical trials suggests, the possibility of serious on-target side effects across stem cell niches in the organism needs to be considered in future drug safety evaluations.

## OUTLOOK

In recent years, a multitude of studies have contributed to a deeper understanding of canonical and non-canonical Wnt

**Table 1.** Overview of clinical trials with drugs targeting the Wnt pathway

Compound	Mode of action	Trial Phase	Tumor entities	Originator	Preliminary clinical results	Starting date	Trial identifier
LGK974 (WNT94)	Inhibitor of Porcupine	1/2	Metastatic colorectal cancer with Wnt pathway mutations; head and neck squamous cell carcinoma with Notch receptor mutations Solid tumors	Novartis	None	October 2014 January 2016	NCT02278133 NCT02649530
ETC-159	Inhibitor of Porcupine	1	Hepatocellular carcinoma; ovarian cancer; pancreatic ductal adenocarcinoma	D3-Institute, experimental Therapeutics Centre (ETC), Duke-NUS Bayer HealthCare Pharmaceutical; OncoMed Pharmaceuticals	None	July 2015	NCT02521844
OMP-54F28 (Ipafriccept)	Fzd8-Fc Decoy receptor	1	Non-small cell lung cancer; pancreatic ductal adenocarcinoma; metastatic breast cancer	Bayer HealthCare Pharmaceuticals; OncoMed Pharmaceuticals	Well tolerated; Increased bone turnover; <sup>188</sup> LEF1 is a potential biomarker for treatment response <sup>209</sup>	February 2014	NCT02092363 NCT02092363 NCT02050178
OMP18R5 (Vantictumab)	Anti-Fzd7 antibody	1	Synovial sarcoma	OncoTherapy Science	Heterogeneous uptake; one case of thrombopenia complicated by hemoptysis with fatal outcome <sup>191</sup>	September 2013 December 2013 October 2013	NCT01957007 NCT02005315 NCT01973309
OTSA101	Yttrium90 radiolabeled Anti-Fzd10 antibody	1	RSPO3 biomarker-positive metastatic colorectal cancer	OncoMed Pharmaceutical; Celgene WntResearch	None	November 2011	NCT01469975
OMP131R10	Anti-R-spondin3 antibody	1	Breast cancer; colorectal cancer; prostate cancer	No dose-limiting toxicity identified; Phase 1b trial planned <sup>199</sup>	June 2015	NCT02482441	
Foxy-5	Wnt5a mimetic	1	Acute and chronic myelogenous leukemia; colorectal adenocarcinoma, pancreatic adenocarcinoma	PRISM Biolab and University of Southern California	January 2016	NCT02655952	
PRI-724	Inhibitor of TCF-CBP interaction	1/2	No dose-limiting toxicity in pancreatic cancer trial; some evidence of clinical activity <sup>194</sup>	April 2015	NCT01606579		
							NCT02413853 NCT01764477

Abbreviation: TCF, T-cell factor.

signaling on a mechanistic level. The effect of aberrant canonical Wnt signaling is not only restricted to cancer cells, but dynamically interacts with the microenvironment and immune system. It also became clear that the function of non-canonical Wnt signaling is similar in development and cancer. While non-canonical Wnt signaling regulates convergent extension and tissue mobility during development, it can also mediate motility of cancer cells during metastasis. Moreover, there is a better understanding of how canonical and non-canonical Wnt signaling interact. The balance between both pathways is maintained by mechanisms that are distinct for different tissue types and their corresponding tumors. This knowledge is currently translated into a refined approach of targeting the Wnt pathway in cancer, taking into account both the functional and mutational status of canonical and non-canonical Wnt pathways in different cancer types.

## CONFLICT OF INTEREST

The authors declare no conflict of interest.

## ACKNOWLEDGEMENTS

We thank Iris Augustin, Filip Port, Katharina Kober and Lucie Wolf for carefully reading the manuscript and contributing valuable ideas. T.Z. was supported by a DKFZ Postdoctoral Fellowship. We apologize to all colleagues whose work was not cited due to space constraints.

## REFERENCES

- Sharma R. Wingless, a new mutant in *D. melanogaster*. *Drosoph Inf Serv* 1973; **50**: 134.
- Nüsslein-Volhard C, Wieschaus E. Mutations affecting segment number and polarity in *Drosophila*. *Nature* 1980; **287**: 795–801.
- Tsukamoto AS, Grosschedl R, Guzman RC, Parslow T, Varmus HE. Expression of the int-1 gene in transgenic mice is associated with mammary gland hyperplasia and adenocarcinomas in male and female mice. *Cell* 1988; **55**: 619–625.
- Nusse R, van Ooyen A, Cox D, Fung YK, Varmus H. Mode of proviral activation of a putative mammary oncogene (int-1) on mouse chromosome 15. *Nature* 1988; **307**: 131–136.
- Nusse R, Varmus HE. Many tumors induced by the mouse mammary tumor virus contain a provirus integrated in the same region of the host genome. *Cell* 1982; **31**: 99–109.
- Rijsewijk F, Schuermann M, Wagenaar E, Parren P, Weigel D, Nusse R. The *Drosophila* homolog of the mouse mammary oncogene int-1 is identical to the segment polarity gene wingless. *Cell* 1987; **50**: 649–657.
- McMahon AP, Moon RT. Ectopic expression of the proto-oncogene int-1 in *Xenopus* embryos leads to duplication of the embryonic axis. *Cell* 1989; **58**: 1075–1084.
- Kinzler K, Nilbert M, Su L, Vogelstein B, Bryan T, Levy D et al. Identification of FAP locus genes from chromosome 5q21. *Science* 1991; **253**: 661–665.
- Nishisho I, Nakamura Y, Miyoshi Y, Miki Y, Ando H, Horii A et al. Mutations of chromosome 5q21 genes in FAP and colorectal cancer patients. *Science* 1991; **253**: 665–669.
- Rubinfeld B, Souza B, Albert I, Muller O, Chamberlain S, Masiarz F et al. Association of the APC gene product with beta-catenin. *Science* 1993; **262**: 1731–1734.
- Su L, Vogelstein B, Kinzler K. Association of the APC tumor suppressor protein with catenins. *Science* 1993; **262**: 1734–1737.
- Korinek V, Barker N, Morin PJ, van Wichen D, de Weger R, Kinzler KW et al. Constitutive transcriptional activation by a beta-catenin-Tcf complex in APC/colon carcinoma. *Science* 1997; **275**: 1784–1787.
- Vogelstein B, Papadopoulos N, Velculescu VE, Zhou S, Diaz LA, Kinzler KW. Cancer genome landscapes. *Science* 2013; **339**: 1546–1558.
- Pleasance ED, Cheetham RK, Stephens PJ, McBride DJ, Humphray SJ, Greenman CD et al. A comprehensive catalogue of somatic mutations from a human cancer genome. *Nature* 2010; **463**: 191–196.
- Clements WM, Wang J, Sarnaik A, Kim OJ, MacDonald J, Fenoglio-Preiser C et al. {beta}-Catenin mutation is a frequent cause of Wnt pathway activation in gastric cancer. *Cancer Res* 2002; **62**: 3503–3506.
- Satoh S, Daigo Y, Furukawa Y, Kato T, Miwa N, Nishiwaki T et al. AXIN1 mutations in hepatocellular carcinomas, and growth suppression in cancer cells by virus-mediated transfer of AXIN1. *Nat Genet* 2000; **24**: 245–250.
- Dahmen RP, Koch A, Denkhaus D, Tonn JC, Sorensen N, Berthold F et al. Deletions of AXIN1, a component of the WNT/wingless pathway, in poradic Medulloblastomas. *Cancer Res* 2001; **61**: 7039–7043.
- Segditsa S, Tomlinson I. Colorectal cancer and genetic alterations in the Wnt pathway. *Oncogene* 2006; **25**: 7531–7537.
- Kadowaki T, Wilder E, Klingensmith J, Zachary K, Perrimon N. The segment polarity gene porcupine encodes a putative multitransmembrane protein involved in Wingless processing. *Genes Dev* 1996; **10**: 3116–3128.
- Bartscherer K, Pelta N, Ingelfinger D, Boutros M. Secretion of Wnt ligands requires Evi, a conserved transmembrane protein. *Cell* 2006; **125**: 523–533.
- Bänziger C, Soldini D, Schütt C, Zipperlen P, Hausmann G, Basler K. Wntless, a conserved membrane protein dedicated to the secretion of Wnt proteins from signaling cells. *Cell* 2006; **125**: 509–522.
- Yu J, Chia J, Canning CA, Jones CM, Bard FA, Virshup DM. WLS Retrograde transport to the endoplasmic reticulum during Wnt secretion. *Dev Cell* 2014; **29**: 277–291.
- Buechling T, Chaudhary V, Spirohn K, Weiss M, Boutros M. p24 proteins are required for secretion of Wnt ligands. *EMBO Rep* 2011; **12**: 1265–1272.
- Port F, Hausmann G, Basler K. A genome-wide RNA interference screen uncovers two p24 proteins as regulators of Wingless secretion. *EMBO Rep* 2011; **12**: 1144–1152.
- Coudreuse DY, Roël G, Betist MC, Destree O, Korswagen HC. Wnt gradient formation requires retromer function in Wnt-producing cells. *Science* 2006; **312**: 921–924.
- Gasnereau I, Herr P, Chia PZC, Basler K, Gleeson PA. Identification of an endocytosis motif in an intracellular loop of Wntless protein, essential for its recycling and the control of Wnt protein signaling. *J Biol Chem* 2011; **286**: 43324–43333.
- Mulligan KA, Fuerer C, Ching W, Fish M, Willert K, Nusse R. Inaugural Article: Secreted Wingless-interacting molecule (Swim) promotes long-range signaling by maintaining Wingless solubility. *Proc Natl Acad Sci USA* 2012; **109**: 370–377.
- Gross JC, Chaudhary V, Bartscherer K, Boutros M. Active Wnt proteins are secreted on exosomes. *Nat Cell Biol* 2012; **14**: 1036–1045.
- Neumann S, Coudreuse DY, van der Westhuyzen DR, Eckhardt ERM, Korswagen HC, Schmitz G et al. Mammalian Wnt3a is released on lipoprotein particles. *Traffic* 2009; **10**: 334–343.
- Boutros M, Niehrs C. Sticking around: short-range activity of Wnt ligands. *Dev Cell* 2016; **36**: 485–486.
- Farin HF, Jordens I, Mosa MH, Basak O, Korving J, Tauriello DVF et al. Visualization of a short-range Wnt gradient in the intestinal stem-cell niche. *Nature* 2016; **530**: 340–343.
- Koch S, Acebron SP, Herbst J, Hatiboglu G, Niehrs C. Post-transcriptional Wnt signaling governs epididymal sperm maturation. *Cell* 2015; **163**: 1225–1236.
- Luga V, Zhang L, Viloria-Petit AM, Ogunjimi AA, Inanlou MR, Chiu E et al. Exosomes mediate stromal mobilization of autocrine Wnt-PCP signaling in breast cancer cell migration. *Cell* 2012; **151**: 1542–1556.
- Kazanskaia O, Glinka A, del Barco Barrantes I, Stannek P, Niehrs C, Wu W. R-Spondin2 is a secreted activator of Wnt/b-catenin signaling and is required for Xenopus myogenesis. *Dev Cell* 2004; **7**: 525–534.
- Glinka A, Dolde C, Kirsch N, Huang Y-L, Kazanskaia O, Ingelfinger D et al. LGR4 and LGR5 are R-spondin receptors mediating Wnt/b-catenin and Wnt/PCP signalling. *EMBO Rep* 2011; **12**: 1055–1061.
- Hao H-X, Xie Y, Zhang Y, Charlat O, Oster E, Avello M et al. ZNRF3 promotes Wnt receptor turnover in an R-spondin-sensitive manner. *Nature* 2012; **485**: 195–200.
- De Lau W, Barker N, Low TY, Koo B-K, Li VSW, Teunissen H et al. Lgr5 homologues associate with Wnt receptors and mediate R-spondin signalling. *Nature* 2011; **476**: 293–297.
- De Lau W, Peng WC, Gros P, Clevers H. The R-spondin / Lgr5 / Rnf43 module: regulator of Wnt signal strength the R-spondin / Lgr5 / Rnf43 module : regulator of Wnt signal strength. *Genes Dev* 2014; **28**: 305–316.
- Koo B-K, Spit M, Jordens I, Low TY, Stange DE, van de Wetering M et al. Tumour suppressor RNF43 is a stem-cell E3 ligase that induces endocytosis of Wnt receptors. *Nature* 2012; **488**: 665–669.
- Jiang X, Charlat O, Zamponi R, Yang Y, Cong F, Dishevelled promotes Wnt receptor degradation through recruitment of ZNRF3/RNF43 E3 ubiquitin ligases. *Mol Cell* 2015; **58**: 522–533.
- Giannakis M, Hodis E, Jasmine Mu X, Yamauchi M, Rosenbluh J, Cibulskis K et al. RNF43 is frequently mutated in colorectal and endometrial cancers. *Nat Genet* 2014; **46**: 1264–1266.
- Jiang X, Hao H-X, Grownay JD, Woolfenden S, Bottiglio C, Ng N et al. Inactivating mutations of RNF43 confer Wnt dependency in pancreatic ductal adenocarcinoma. *Proc Natl Acad Sci USA* 2013; **110**: 12649–12654.
- Azzolin L, Panciera T, Soligo S, Enzo E, Bicciato S, Dupont S et al. YAP/TAZ incorporation in the β-catenin destruction complex orchestrates the Wnt response. *Cell* 2014; **158**: 157–170.

- 44 Barry ER, Morikawa T, Butler BL, Shrestha K, de la Rosa R, Yan KS et al. Restriction of intestinal stem cell expansion and the regenerative response by YAP. *Nature* 2012; **493**: 106–110.
- 45 Varelas X, Miller BW, Sopko R, Song S, Gregorieff A, Fellouse FA et al. The Hippo pathway regulates Wnt/β-catenin signaling. *Dev Cell* 2010; **18**: 579–591.
- 46 Heallen T, Zhang M, Wang J, Bonilla-claudio M, Klysik E, Randy L et al. NIH public access. *Science* 2012; **332**: 458–461.
- 47 Rosenbluh J, Nijhawan D, Cox AG, Li X, James T, Schafer EJ et al. NIH public access. *Cell* 2013; **151**: 1457–1473.
- 48 Lien WH, Fuchs E. Wnt some lose some: transcriptional governance of stem cells by Wnt/β-catenin signaling. *Genes Dev* 2014; **28**: 1517–1532.
- 49 MacDonald BT, Tamai K, He X. Wnt/β-catenin signaling: components, mechanisms, and diseases. *Dev Cell* 2009; **17**: 9–26.
- 50 Li J, Chen X, Ding X, Cheng Y, Zhao B, Lai ZC et al. LATS2 suppresses oncogenic Wnt signaling by disrupting β-Catenin/BCL9 interaction. *Cell Rep* 2013; **5**: 1650–1663.
- 51 Takada K, Zhu D, Bird GH, Sukhdeo K, Zhao J-J, Mani M et al. Targeted disruption of the BCL9/β-catenin complex inhibits oncogenic Wnt signaling. *Sci Transl Med* 2012; **4**: 148ra117.
- 52 Jung H-Y, Jun S, Lee M, Kim H-C, Wang X, Ji H et al. PAF and EZH2 induce Wnt/β-catenin signaling hyperactivation. *Mol Cell* 2013; **52**: 193–205.
- 53 Davidson G, Shen J, Huang Y-L, Su Y, Karaulanov E, Bartscherer K et al. Cell cycle control of wnt receptor activation. *Dev Cell* 2009; **17**: 788–799.
- 54 Acebron SP, Karaulanov E, Berger BS, Huang Y-L, Niehrs C. Mitotic Wnt signaling promotes protein stabilization and regulates cell size. *Mol Cell* 2014; **54**: 663–674.
- 55 Taelman VF, Dobrowolski R, Plouhinec J-L, Fuentealba LC, Vorwald PP, Gumper I et al. Wnt Signaling requires sequestration of glycogen synthase kinase 3 inside multivesicular endosomes. *Cell* 2010; **143**: 1136–1148.
- 56 Xu C, Kim NG, Gumbiner BM. Regulation of protein stability by GSK3 mediated phosphorylation. *Cell Cycle* 2009; **8**: 4032–4039.
- 57 Stolz A, Neufeld K, Ertich N, Bastians H. Wnt-mediated protein stabilization ensures proper mitotic microtubule assembly and chromosome segregation. *EMBO Rep* 2015; **16**: 490–499.
- 58 Huang Y-L, Anvarian Z, Döderlein G, Acebron SP, Niehrs C. Maternal Wnt/STOP signaling promotes cell division during early Xenopus embryogenesis. *Proc Natl Acad Sci USA* 2015; **112**: 5732–5737.
- 59 Ploper D, Taelman VF, Robert L, Perez BS, Titz B, Chen H-W et al. MITF drives endolysosomal biogenesis and potentiates Wnt signaling in melanoma cells. *Proc Natl Acad Sci USA* 2015; **112**: E420–E429.
- 60 Anastas JN, Moon RT. WNT signalling pathways as therapeutic targets in cancer. *Nat Rev Cancer* 2013; **13**: 11–26.
- 61 Wang Y. Wnt/Planar cell polarity signaling: a new paradigm for cancer therapy. *Mol Cancer Ther* 2009; **8**: 2103–2109.
- 62 Katoh M. WNT/PCP signaling pathway and human cancer (Review). *Oncol Rep* 2005; **14**: 1583–1588.
- 63 De A. Wnt/Ca<sup>2+</sup> signaling pathway: a brief overview. *Acta Biochim Biophys Sin (Shanghai)* 2011; **43**: 745–756.
- 64 Yang Y, Mlodzik M. Wnt-frizzled/planar cell polarity signaling: cellular orientation by facing the wind (Wnt). *Annu Rev Cell Dev Biol* 2015; **31**: 623–646.
- 65 Nomachi A, Nishita M, Inaba D, Enomoto M, Hamasaki M, Minami Y. Receptor tyrosine kinase Ror2 mediates Wnt5a-induced polarized cell migration by activating c-Jun N-terminal kinase via actin-binding protein filamin A. *J Biol Chem* 2008; **283**: 27973–27981.
- 66 Endo M, Nishita M, Fujii M, Minami Y. Insight into the role of Wnt5a-induced signaling in normal and cancer cells. *Int Rev Cell Mol Biol* 2015; **314**: 117–148.
- 67 Polakis P. Wnt signaling in cancer. *Cold Spring Harb Perspect Biol* 2012; **4**: 9.
- 68 Matano M, Date S, Shimokawa M, Takano A, Fujii M, Ohta Y et al. Modeling colorectal cancer using CRISPR-Cas9-mediated engineering of human intestinal organoids. *Nat Med* 2015; **21**: 256–262.
- 69 Drost J, van Jaarsveld RH, Ponsioen B, Zimberlin C, van Boxtel R, Buijs A et al. Sequential cancer mutations in cultured human intestinal stem cells. *Nature* 2015; **521**: 43–47.
- 70 Christie M, Jorissen RN, Mouradov D, Sakthianandeswaren A, Li S, Day F et al. Different APC genotypes in proximal and distal sporadic colorectal cancers suggest distinct WNT/β-catenin signalling thresholds for tumourigenesis. *Oncogene* 2013; **32**: 4675–4682.
- 71 Buchert M, Athineos D, Abud HE, Burke ZD, Faux MC, Samuel MS et al. Genetic dissection of differential signaling threshold requirements for the Wnt/beta-catenin pathway *in vivo*. *PLoS Genet* 2010; **6**: e1000816.
- 72 Dow LE, O'Rourke KP, Simon J, Tschaхагане DF, van Es JH, Clevers H et al. Apc restoration promotes cellular differentiation and reestablishes crypt homeostasis in colorectal cancer. *Cell* 2015; **161**: 1539–1552.
- 73 Voloshanenko O, Erdmann G, Dubash TD, Augustin I, Metzig M, Moffa G et al. Wnt secretion is required to maintain high levels of Wnt activity in colon cancer cells. *Nat Commun* 2013; **4**: 2610.
- 74 Guinney J, Dienstmann R, Wang X, de Reyniès A, Schlicker A, Soneson C et al. The consensus molecular subtypes of colorectal cancer. *Nat Med* 2015; **21**: 1350–1356.
- 75 Seshagiri S, Stawiski EW, Durinck S, Modrusan Z, Storm EE, Conboy CB et al. Recurrent R-spondin fusions in colon cancer. *Nature* 2012; **488**: 660–664.
- 76 van de Wetering M, Francies HE, Francis JM, Bounova G, Iorio F, Pronk A et al. Prospective derivation of a living organoid Biobank of colorectal cancer patients. *Cell* 2015; **161**: 933–945.
- 77 Rusan NM, Peifer M. Original CIN: reviewing roles for APC in chromosome instability. *J Cell Biol* 2008; **181**: 719–726.
- 78 Caldwell CM, Green RA, Kaplan KB. APC mutations lead to cytokinetic failures in vitro and tetraploid genotypes in Min mice. *J Cell Biol* 2007; **178**: 1109–1120.
- 79 Aoki K, Aoki M, Sugai M, Harada N, Miyoshi H, Tsukamoto T et al. Chromosomal instability by beta-catenin/TCF transcription in APC or beta-catenin mutant cells. *Oncogene* 2007; **26**: 3511–3520.
- 80 Ertich N, Stolz A, Stenzinger A, Weichert W, Kaulfuß S, Burfeind P et al. Increased microtubule assembly rates influence chromosomal instability in colorectal cancer cells. *Nat Cell Biol* 2014; **16**: 779–791.
- 81 Zeng G, Germinaro M, Micsenyi A, Monga NK, Bell A, Sood A et al. Aberrant Wnt/beta-catenin signaling in pancreatic adenocarcinoma. *Neoplasia* 2006; **8**: 279–289.
- 82 White BD, Chien AJ, Dawson DW. Dysregulation of Wnt/β-catenin signaling in gastrointestinal cancers. *Gastroenterology* 2012; **142**: 219–232.
- 83 Morris JP, Cano DA, Sekine S, Wang SC, Hebrok M. Beta-catenin blocks Kras-dependent reprogramming of acini into pancreatic cancer precursor lesions in mice. *J Clin Invest* 2010; **120**: 508–520.
- 84 Zhang Y, Morris JP, Yan W, Schofield HK, Gurney A, Simeone DM et al. Canonical Wnt signaling is required for pancreatic carcinogenesis. *Cancer Res* 2013; **73**: 4909–4922.
- 85 Dougherty DM, Marsh-richard DM, Hatzis ES, Nouvion SO, Mathias CW. WNT7B mediates autocrine Wnt/β-catenin signaling and anchorage-independent growth in pancreatic adenocarcinoma. *Oncogene* 2014; **96**: 111–120.
- 86 Boultar L, Guest R V, Kendall TJ, Wilson DH, Wojtachka D, Robson AJ et al. WNT signaling drives cholangiocarcinoma growth and can be pharmacologically inhibited. *J Clin Invest* 2015; **125**: 1269–1285.
- 87 Loilome W, Bungkanjana P, Techasen A, Namwat N, Yongvanit P, Puapairoj A et al. Activated macrophages promote Wnt/beta-catenin signaling in cholangiocarcinoma cells. *Tumour Biol* 2014; **35**: 5357–5367.
- 88 Chan-On W, Nairismägi M-L, Ong CK, Lim WK, Dima S, Pairojkul C et al. Exome sequencing identifies distinct mutational patterns in liver fluke-related and non-infection-related bile duct cancers. *Nat Genet* 2013; **45**: 1474–1478.
- 89 Goepert B, Konermann C, Schmidt CR, Bogatyrova O, Geiselhart L, Ernst C et al. Global alterations of DNA methylation in cholangiocarcinoma target the Wnt signaling pathway. *Hepatology* 2014; **59**: 544–554.
- 90 Luis TC, Ichii M, Brugman MH, Kincade P, Staal FJT. Wnt signaling strength regulates normal hematopoiesis and its deregulation is involved in leukemia development. *Leukemia* 2012; **26**: 414–421.
- 91 Lento W, Congdon K, Voermans C, Kritzik M, Reya T. Wnt signaling in normal and malignant hematopoiesis. *Cold Spring Harb Perspect Biol*; e-pub ahead of print 1 February 2013; doi:10.1101/cshperspect.a008011.
- 92 Yeung J, Esposito MT, Gandillet A, Zeisig BB, Griessinger E, Bonnet D et al. β-Catenin mediates the establishment and drug resistance of MLL leukemic stem cells. *Cancer Cell* 2010; **18**: 606–618.
- 93 Lane SW, Wang YJ, Lo Celso C, Ragu C, Bullinger L, Stephen M et al. Differential niche and Wnt requirements during acute myeloid leukemia progression. *Blood* 2011; **118**: 2849–2856.
- 94 Wang Y, Krivtsov A, Sinha A, North T. The Wnt/β-catenin pathway is required for the development of leukemia stem cells in AML. *Science* 2010; **327**: 1650–1653.
- 95 Yeung J, Esposito MT, Gandillet A, Zeisig BB, Griessinger E, Bonnet D et al. Beta-catenin mediates the establishment and drug resistance of MLL leukemic stem cells. *Cancer Cell* 2010; **18**: 606–618.
- 96 Cheng CK, Li L, Cheng SH, Lau KM, Chan NPH, Wong RSM et al. Transcriptional repression of the RUNX3/AML2 gene by the t(8;21) and inv(16) fusion proteins in acute myeloid leukemia. *Blood* 2008; **112**: 3391–3402.
- 97 Müller-Tidow C, Steffen B, Cauvet T, Tickenbrock L, Ji P, Diederichs S et al. Translocation products in acute myeloid leukemia activate the Wnt signaling pathway in hematopoietic cells. *Mol Cell Biol* 2004; **24**: 2890–2904.
- 98 Ferrando AA. The role of NOTCH1 signaling in T-ALL. *Hematology Am Soc Hematol Educ Program* 2009; **2009**: 353–361.
- 99 Guo W, Lasky JL, Chang C-J, Mosessian S, Lewis X, Xiao Y et al. Multi-genetic events collaboratively contribute to Pten-null leukaemia stem-cell formation. *Nature* 2008; **453**: 529–533.
- 100 Kaveri D, Kastner P, Dembélé D, Nerlov C, Chan S, Kirstetter P. β-Catenin activation synergizes with Pten loss and Myc overexpression in Notch-independent T-ALL. *Blood* 2013; **122**: 694–704.

- 101 Giambra V, Jenkins CE, Lam SH, Hoofd C, Belmonte M, Wang X et al. Leukemia stem cells in T-ALL require active Hif1α and Wnt signaling. *Blood* 2015; **125**: 3917–3927.
- 102 Lu D, Zhao Y, Tawatao R, Cottam HB, Sen M, Leoni LM et al. Activation of the Wnt signaling pathway in chronic lymphocytic leukemia. *Proc Natl Acad Sci USA* 2004; **101**: 3118–3123.
- 103 Moskalev EA, Luckert K, Vorobjev IA, Mastitsky SE, Gladkikh AA, Stephan A et al. Concurrent epigenetic silencing of wnt / β -catenin pathway inhibitor genes in B cell chronic lymphocytic leukaemia. *BMC Cancer* 2012; **12**: 1.
- 104 Wang L, Shalek AK, Lawrence M, Ding R, Gaujolle JT, Pochet N et al. Somatic mutation as a mechanism of Wnt/beta-catenin pathway activation in CLL. *Blood* 2014; **124**: 1089–1098.
- 105 Stolz W, Schmoekel C, Landthaler M, Braun-Falco O. Association of early malignant melanoma with nevocytic nevi. *Cancer* 1989; **63**: 550–555.
- 106 Dhomen N, Reis-Filho JS, da Rocha Dias S, Hayward R, Savage K, Delmas V et al. Oncogenic Braf induces melanocyte senescence and melanoma in mice. *Cancer Cell* 2009; **15**: 294–303.
- 107 Jones SL, Cichowski K. Many roads lead to oncogene-induced senescence. *Oncogene* 2008; **27**: 2801–2809.
- 108 Delmas V, Beermann F, Martinuzzi S, Carreira S, Ackermann J, Kumada M et al. Beta-catenin induces immortalization of melanocytes by suppressing p16INK4a expression and cooperates with N-Ras in melanoma development. *Genes Dev* 2007; **21**: 2923–2935.
- 109 Juan J, Muraguchi T, Iezza G, Sears RC, McMahon M. Diminished WNT -> beta -catenin->c-MYC signaling is a barrier for malignant progression of BRAFV600E-induced lung tumors. *Genes Dev* 2014; **28**: 561–575.
- 110 Pawlikowski JS, McBryan T, van Tuyn J, Drotar ME, Hewitt RN, Maier AB et al. Wnt signaling potentiates neogenesis. *Proc Natl Acad Sci USA* 2013; **110**: 16009–16014.
- 111 Lim X, Nusse R. Wnt signaling in skin development, homeostasis, and disease. *Cold Spring Harb Perspect Biol*; e-pub ahead of print 1 February 2013; doi:10.1101/cshperspect.a008029.
- 112 Webster MR, Weeraratna AT. A Wnt-er migration: the confusing role of β-catenin in melanoma metastasis. *Sci Signal* 2013; **6**: pe11.
- 113 Kageshita T, Hamby CV, Ishihara T, Matsumoto K, Saida T, Ono T. Loss of beta-catenin expression associated with disease progression in malignant melanoma. *Br J Dermatol* 2001; **145**: 210–216.
- 114 Bachmann IM. Importance of P-Cadherin, -Catenin, and Wnt5a/Frizzled for progression of melanocytic tumors and prognosis in cutaneous melanoma. *Clin Cancer Res* 2005; **11**: 8606–8614.
- 115 Chien AJ, Moore EC, Lonsdorf AS, Kulikauskas RM, Rothberg BG, Berger AJ et al. Activated Wnt/beta-catenin signaling in melanoma is associated with decreased proliferation in patient tumors and a murine melanoma model. *Proc Natl Acad Sci USA* 2009; **106**: 1193–1198.
- 116 Damsky WE, Curley DP, Santhanakrishnan M, Rosenbaum LE, Platt JT, Gould Rothberg BE et al. β-catenin signaling controls metastasis in Braf-activated Ptene-deficient melanomas. *Cancer Cell* 2011; **20**: 741–754.
- 117 Biechele TL, Kulikauskas RM, Toroni R a, Lucero OM, Swift RD, James RG et al. Wnt/β-catenin signaling and AXIN1 regulate apoptosis triggered by inhibition of the mutant kinase BRAFV600E in human melanoma. *Sci Signal* 2012; **5**: ra3.
- 118 Chien AJ, Haydu LE, Biechele TL, Kulikauskas RM, Rizos H, Kefford RF et al. Targeted BRAF inhibition impacts survival in melanoma patients with high levels of Wnt/β-catenin signaling. *PLoS One* 2014; **9**: e94748.
- 119 O'Connell MP, Fiori JL, Baugher KM, Indig FE, French AD, Camilli TC et al. Wnt5A activates the calpain-mediated cleavage of filamin A. *J Invest Dermatol* 2009; **129**: 1782–1789.
- 120 Webster MR, Xu M, Kinzler KA, Kaur A, Appleton J, Connell MPO et al. Wnt5A promotes an adaptive, senescent-like stress response, while continuing to drive invasion in melanoma cells. *Pigment Cell Melanoma Res* 2015; **28**: 184–195.
- 121 Anastas JN, Kulikauskas RM, Tamir T, Rizos H, Long G V, von Euw EM et al. WNT5A enhances resistance of melanoma cells to targeted BRAF inhibitors. *J Clin Invest* 2014; **124**: 2877–2890.
- 122 O'Connell MP, Marchbank K, Webster MR, Valiga AA, Kaur A, Vultur A et al. Hypoxia induces phenotypic plasticity and therapy resistance in melanoma via the tyrosine kinase receptors ROR1 and ROR2. *Cancer Discov* 2013; **3**: 1378–1393.
- 123 Ekström EJ, Bergenfelz C, von Bülow V, Serfler F, Carlénalm E, Jönsson G et al. WNT5A induces release of exosomes containing pro-angiogenic and immunosuppressive factors from malignant melanoma cells. *Mol Cancer* 2014; **13**: 1–15.
- 124 Linnskog R, Jönsson G, Axelsson L, Prasad CP, Andersson T. Interleukin-6 drives melanoma cell motility through p38α-MAPK-dependent up-regulation of WNT5A expression. *Mol Oncol* 2014; **8**: 1365–1378.
- 125 Grossmann AH, Yoo JH, Clancy J, Sorensen LK, Sedgwick A, Tong Z et al. The small GTPase ARF6 stimulates β-catenin transcriptional activity during WNT5A-mediated melanoma invasion and metastasis. *Sci Signal* 2013; **6**: ra14.
- 126 Mikels AJ, Nusse R. Purified Wnt5a protein activates or inhibits beta-catenin-TCF signaling depending on receptor context. *PLoS Biol* 2006; **4**: e115.
- 127 Hoek KS, Schlegel NC, Brafford P, Sucker A, Ugurel S, Kumar R et al. Metastatic potential of melanomas defined by specific gene expression profiles with no BRAF signature. *Pigment Cell Res* 2006; **19**: 290–302.
- 128 Hoek KS, Eichhoff OM, Schlegel NC, Döbbeling U, Kobert N, Schaefer L et al. In vivo switching of human melanoma cells between proliferative and invasive states. *Cancer Res* 2008; **68**: 650–656.
- 129 Lin SY, Xia W, Wang JC, Kwong KY, Spohn B, Wen Y et al. Beta-catenin, a novel prognostic marker for breast cancer: its roles in cyclin D1 expression and cancer progression. *Proc Natl Acad Sci USA* 2000; **97**: 4262–4266.
- 130 Geyer FC, Lacroix-Triki M, Savage K, Arnedos M, Lambros MB, MacKay A et al. β-Catenin pathway activation in breast cancer is associated with triple-negative phenotype but not with CTNNB1 mutation. *Mod Pathol* 2011; **24**: 209–231.
- 131 Khratsov Al, Khratsova GF, Tretiakova M, Huo D, Olopade Ol, Goss KH. Wnt/{beta}-catenin pathway activation is enriched in basal-like breast cancers and predicts poor outcome. *Am J Pathol* 2010; **176**: 2911–2920.
- 132 Xu J, Prosperi JR, Choudhury N, Olopade Ol, Goss KH. B-catenin is required for the tumorigenic behavior of triple-negative breast cancer cells. *PLoS One* 2015; **10**: 1–11.
- 133 Li S, Li S, Sun Y, Li L. The expression of β-catenin in different subtypes of breast cancer and its clinical significance. *Tumour Biol* 2014; **35**: 7693–7698.
- 134 Howe LR, Brown AMC. Wnt signaling and breast cancer. *Cancer Biol Ther* 2004; **3**: 36–41.
- 135 Liu C-C, Prior J, Piwnica-Worms D, Bu G. LRP6 overexpression defines a class of breast cancer subtype and is a target for therapy. *Proc Natl Acad Sci USA* 2010; **107**: 5136–5141.
- 136 Yang L, Wu X, Wang Y, Zhang K, Wu J, Yuan Y-C et al. FZD7 has a critical role in cell proliferation in triple negative breast cancer. *Oncogene* 2011; **30**: 4437–4446.
- 137 Klarmann GJ, Decker A, Farrar WL. Epigenetic gene silencing in the Wnt pathway in breast cancer. *Epigenetics* 2008; **3**: 59–63.
- 138 Gunther EJ, Moody SE, Belka GK, Hahn KT, Innocent N, Dugan KD et al. Impact of p53 loss on reversal and recurrence of conditional Wnt-induced tumorigenesis. *Genes Dev* 2003; **17**: 488–501.
- 139 Li Y, Welch P, Podsypanina K, Huang S, Chamorro M, Zhang X et al. Evidence that transgenes encoding components of the Wnt signaling pathway preferentially induce mammary cancers from progenitor cells. *Proc Natl Acad Sci USA* 2003; **100**: 15853–15858.
- 140 Klauzinska M, Baljinnyam B, Raafat A, Rodriguez-Canales J, Strizzi L, Endo Greer Y et al. Rspo2/Int7 regulates invasiveness and tumorigenic properties of mammary epithelial cells. *J Cell Physiol* 2012; **227**: 1960–1971.
- 141 Cleary AS, Leonard TL, Gestl SA, Gunther EJ. Tumour cell heterogeneity maintained by cooperating subclones in Wnt-driven mammary cancers. *Nature* 2014; **508**: 113–117.
- 142 Kim S, Goel S, Alexander CM. Differentiation generates paracrine cell pairs that maintain basaloid mouse mammary tumors: proof of concept. *PLoS One* 2011; **6**: e19310.
- 143 Beck B, Blanpain C. Unravelling cancer stem cell potential. *Nat Rev Cancer* 2013; **13**: 727–738.
- 144 Reya T, Clevers H. Wnt signalling in stem cells and cancer. *Nature* 2005; **434**: 843–850.
- 145 Park J-I, Venteicher AS, Hong JY, Choi J, Jun S, Shkreli M et al. Telomerase modulates Wnt signalling by association with target gene chromatin. *Nature* 2009; **460**: 66–72.
- 146 Barker N, Ridgway RA, van de Wetering M, Begthel H, van den Born M et al. Crypt stem cells as the cells-of-origin of intestinal cancer. *Nature* 2008; **457**: 608–611.
- 147 Schepers AG, Snippert HJ, Stange DE, van den Born M, van Es JH, van de Wetering M et al. Lineage tracing reveals Lgr5+ stem cell activity in mouse intestinal adenomas. *Science* 2012; **337**: 730–735.
- 148 Myant KB, Cammareri P, McGhee EJ, Ridgway RA, Huels DJ, Cordero JB et al. ROS production and NF-κB activation triggered by RAC1 facilitate WNT-driven intestinal stem cell proliferation and colorectal cancer initiation. *Cell Stem Cell* 2013; **12**: 761–773.
- 149 Schwitalla S, Fingerle AA, Cammareri P, Nebelsiek T, Göktuna SI, Ziegler PK et al. Intestinal tumorigenesis initiated by dedifferentiation and acquisition of stem-cell-like properties. *Cell* 2013; **152**: 25–38.
- 150 Vermeulen L, De Souza E, Melo F, van der Heijden M, Cameron K, de Jong JH, Borovski T et al. Wnt activity defines colon cancer stem cells and is regulated by the microenvironment. *Nat Cell Biol* 2010; **12**: 468–476.
- 151 Malanchi I, Santamaría-Martínez A, Susanto E, Peng H, Lehr H-A, Delaloye J-F et al. Interactions between cancer stem cells and their niche govern metastatic colonization. *Nature* 2012; **481**: 85–89.

- 152 Kessenbrock K, Dijkgraaf GJP, Lawson DA, Littlepage LE, Shahi P, Pieper U et al. A role for matrix metalloproteinases in regulating mammary stem cell function via the Wnt signaling pathway. *Cell Stem Cell* 2013; **13**: 300–313.
- 153 Todaro M, Gaggianesi M, Catalano V, Benfante A, Iovino F, Biffoni M et al. CD44v6 is a marker of constitutive and reprogrammed cancer stem cells driving colon cancer metastasis. *Cell Stem Cell* 2014; **14**: 342–356.
- 154 Hwang W-L, Jiang J-K, Yang S-H, Huang T-S, Lan H-Y, Teng H-W et al. MicroRNA-146a directs the symmetric division of Snail-dominant colorectal cancer stem cells. *Nat Cell Biol* 2014; **16**: 268–280.
- 155 Isobe T, Hisamori S, Hogan DJ, Zabala M, Hendrickson DG, Dalerba P et al. miR-142 regulates the tumorigenicity of human breast cancer stem cells through the canonical WNT signaling pathway. *Elife* 2014; **3**: 1–23.
- 156 Wang Y, He L, Du Y, Zhu P, Huang G, Luo J et al. The long noncoding RNA lncTCF7 promotes self-renewal of human liver cancer stem cells through activation of Wnt signaling. *Cell Stem Cell* 2015; **16**: 413–425.
- 157 Fang L, Cai J, Chen B, Wu S, Li R, Xu X et al. Aberrantly expressed miR-582-3p maintains lung cancer stem cell-like traits by activating Wnt/β-catenin signalling. *Nat Commun* 2015; **6**: 8640.
- 158 Merlos-Suárez A, Barriga FM, Jung P, Iglesias M, Céspedes MV, Rossell D et al. The intestinal stem cell signature identifies colorectal cancer stem cells and predicts disease relapse. *Cell Stem Cell* 2011; **8**: 511–524.
- 159 de Sousa E, Melo F, Colak S, Buikhuisen J, Koster J, Cameron K, de Jong JH et al. Methylation of cancer-stem-cell-associated Wnt target genes predicts poor prognosis in colorectal cancer patients. *Cell Stem Cell* 2011; **9**: 476–485.
- 160 Scheel C, Weinberg RA. Cancer stem cells and epithelial-mesenchymal transition: concepts and molecular links. *Semin Cancer Biol* 2012; **22**: 396–403.
- 161 Kalluri R. EMT: when epithelial cells decide to become mesenchymal-like cells. *J Clin Invest* 2009; **119**: 1417–1419.
- 162 De Craene B, Berx G. Regulatory networks defining EMT during cancer initiation and progression. *Nat Rev Cancer* 2013; **13**: 97–110.
- 163 Wu Z-Q, Li X-Y, Hu CY, Ford M, Kleer CG, Weiss SJ. Canonical Wnt signaling regulates Slug activity and links epithelial-mesenchymal transition with epigenetic Breast Cancer 1, Early Onset (BRCA1) repression. *Proc Natl Acad Sci USA* 2012; **109**: 16654–16659.
- 164 Wang Y, Bu F, Royer C, Serres S, Larkin JR, Soto MS et al. ASPP2 controls epithelial plasticity and inhibits metastasis through β-catenin-dependent regulation of ZEB1. *Nat Cell Biol* 2014; **16**: 1092–1104.
- 165 Tenbaum SP, Ordóñez-Morán P, Puig I, Chicote I, Arqués O, Landolfi S et al. β-catenin confers resistance to PI3K and AKT inhibitors and subverts FOXO3a to promote metastasis in colon cancer. *Nat Med* 2012; **18**: 892–901.
- 166 Gujral TS, Chan M, Peshkin L, Sorger PK, Kirschner MW, MacBeath G. A Non-canonical frizzled2 pathway regulates epithelial-mesenchymal transition and metastasis. *Cell* 2014; **159**: 844–856.
- 167 Kahler C, Kalluri R. Exosomes in tumor microenvironment influence cancer progression and metastasis. *J Mol Med (Berl)* 2013; **91**: 431–437.
- 168 Chairoungdua A, Smith DL, Pochard P, Hull M, Caplan MJ. Exosome release of β-catenin: a novel mechanism that antagonizes Wnt signaling. *J Cell Biol* 2010; **190**: 1079–1091.
- 169 Luga V, Zhang L, Viloria-Petit AM, Ogunjimi A a, Inanlou MR, Chiu E et al. Exosomes mediate stromal mobilization of autocrine Wnt-PCP signaling in breast cancer cell migration. *Cell* 2012; **151**: 1542–1556.
- 170 Maheswaran S, Haber DA. Circulating tumor cells: a window into cancer biology and metastasis. *Curr Opin Genet Dev* 2010; **20**: 96–99.
- 171 Yu M, Ting DT, Stott SL, Wittner BS, Ozsolak F, Paul S et al. RNA sequencing of pancreatic circulating tumour cells implicates WNT signalling in metastasis. *Nature* 2012; **487**: 510–513.
- 172 Miyamoto DT, Zheng Y, Wittner BS, Lee RJ, Zhu H, Broderick KT et al. RNA-Seq of single prostate CTCs implicates noncanonical Wnt signaling in antiandrogen resistance. *Science* 2015; **349**: 1351–1356.
- 173 Larkin J, Chiarioti-Silén V, Gonzalez R, Grob JJ, Cowey CL, Lao CD et al. Combined nivolumab and ipilimumab or monotherapy in untreated melanoma. *N Engl J Med* 2015; **373**: 23–34.
- 174 Borghaei H, Paz-Ares L, Horn L, Spigel DR, Steins M, Ready NE et al. Nivolumab versus docetaxel in advanced nonsquamous non-small-cell lung cancer. *N Engl J Med* 2015; **373**: 1627–1639.
- 175 Motzer RJ, Escudier B, McDermott DF, George S, Hammers HJ, Srinivas S et al. Nivolumab versus everolimus in advanced renal-cell carcinoma. *N Engl J Med* 2015; **373**: 1803–1813.
- 176 Staal FJT, Luis TC, Tiemessen MM. WNT signalling in the immune system: WNT is spreading its wings. *Nat Rev Immunol* 2008; **8**: 581–593.
- 177 Spranger S, Bao R, Gajewski TF. Melanoma-intrinsic β-catenin signalling prevents anti-tumour immunity. *Nature* 2015; **523**: 231–235.
- 178 Yaguchi T, Goto Y, Kido K, Mochimaru H, Sakurai T, Tsukamoto N et al. Immune suppression and resistance mediated by constitutive activation of Wnt/β-catenin signalling in human melanoma cells. *J Immunol* 2012; **189**: 2110–2117.
- 179 Malladi S, Macalinao DG, Jin X, He L, Basnet H, Zou Y et al. Metastatic latency and immune evasion through autocrine inhibition of WNT. *Cell* 2016; **165**: 45–60.
- 180 Le DT, Uram JN, Wang H, Bartlett BR, Kemberling H, Eyring AD et al. PD-1 blockade in tumors with mismatch-repair deficiency. *N Engl J Med* 2015; **372**: 2509–2520.
- 181 Kahn M. Can we safely target the WNT pathway? *Nat Rev Drug Discov* 2014; **13**: 513–532.
- 182 Dodge ME, Moon J, Tuladhar R, Lu J, Jacob LS, Zhang L et al. Diverse chemical scaffolds support direct inhibition of the membrane-bound O-acetyltransferase porcupine. *J Biol Chem* 2012; **287**: 23246–23254.
- 183 van de Wetering M, Francies HE, Francis JM, Bouanova G, Iorio F, Pronk A et al. Prospective derivation of a living organoid biobank of colorectal cancer patients. *Cell* 2015; **161**: 933–945.
- 184 Madan B, Ke Z, Harmston N, Ho SY, Frois AO, Alam J et al. Wnt addiction of genetically defined cancers reversed by PORCN inhibition. *Oncogene* 2016; **35**: 2197–2207.
- 185 D3 (Drug Product and Development) BSI. A Study to Evaluate the Safety and Tolerability of ETC-1922159 in Advanced Solid Tumours. ClinicalTrials.gov, 2015, p NCT02521844.
- 186 Yeung P, Beviglia L, Cancilla B, Dee-Hoskins C, Evans JW, Fischer MM et al. Abstract 1907: Wnt pathway antagonist OMP-54F28 (FZD8-Fc) inhibits tumor growth and reduces tumor-initiating cell frequency in patient-derived hepatocellular carcinoma and ovarian cancer xenograft models. *Cancer Res* 2014; **74**: 1907–1907.
- 187 Gurney A, Axelrod F, Bond CJ, Cain J, Chartier C, Donigan L et al. Wnt pathway inhibition via the targeting of Frizzled receptors results in decreased growth and tumorigenicity of human tumors. *Proc Natl Acad Sci USA* 2012; **109**: 11717–11722.
- 188 Smith DC, Rosen LS, Chugh R, Goldman JW, Xu L, Kapoun A et al. General Poster Session (Board # 1H), Mon, 8: 00 AM-11: 45 AM First-in-human evaluation of the human monoclonal antibody vantictumab (OMP-18RS; anti-Frizzled) targeting the WNT pathway in a phase I study for patients with advanced solid tumors. ASCO Annu Meet Abstr 2013; *J Clin Onc*: 1345201.
- 189 Baron R, Kneissel M. WNT signaling in bone homeostasis and disease: from human mutations to treatments. *Nat Med* 2013; **19**: 179–192.
- 190 Nagayama S, Yamada E, Kohno Y, Aoyama T, Fukukawa C, Kubo H et al. Inverse correlation of the up-regulation of FZD10 expression and the activation of β-catenin in synchronous colorectal tumors. *Cancer Sci* 2009; **100**: 405–412.
- 191 Giraudet A-L, Badel J-N, Cassier P, Desuzinges C, Kriza D, Perol D et al. SYNFRIZZ-A phase Ia/Ib of a radiolabelled monoclonal AB for the treatment of relapsing synovial sarcoma. *J Nucl Med* 2014; **55**: 223.
- 192 Gang EJ, Hsieh Y-T, Pham J, Zhao Y, Nguyen C, Huantes S et al. Small-molecule inhibition of CBP/catenin interactions eliminates drug-resistant clones in acute lymphoblastic leukemia. *Oncogene* 2014; **33**: 2169–2178.
- 193 Rebel VI, Kung AL, Tanner EA, Yang H, Bronson RT, Livingston DM. Distinct roles for CREB-binding protein and p300 in hematopoietic stem cell self-renewal. *Proc Natl Acad Sci USA* 2002; **99**: 14789–14794.
- 194 Robert R, McWilliams Andrew H, Ko E, Gabriela Chiorean, Eunice Lee Kwak et al. A phase Ib dose-escalation study of PRI-724, a CBP/beta-catenin modulator, plus gemcitabine (GEM) in patients with advanced pancreatic adenocarcinoma (APC) as second-line therapy after FOLFIRINOX or FOLFOX. *J Clin Oncol* 2015; **33**: abstr e15270.
- 195 University of Southern California. Combination Chemotherapy and Bevacizumab With or Without PRI-724 in Treating Patients With Newly Diagnosed Metastatic Colorectal Cancer (PRIMIER). In: Clinicaltrials.Gov. 2015, p NCT02413853.
- 196 Huang S-MA, Mishina YM, Liu S, Cheung A, Stegmeier F, Michaud GA et al. Tankyrase inhibition stabilizes axin and antagonizes Wnt signalling. *Nature* 2009; **461**: 614–620.
- 197 Riffell JL, Lord CJ, Ashworth A. Tankyrase-targeted therapeutics: expanding opportunities in the PARP family. *Nat Rev Drug Discov* 2012; **11**: 923–936.
- 198 Lau T, Chan E, Callow M, Waaler J, Boggs J, Blake RA et al. A novel Tankyrase small-molecule inhibitor suppresses APC mutation-driven colorectal tumor growth. *Cancer Res* 2013; **73**: 3132–3144.
- 199 Andersson T, Axelsson L, Mohapatra P, Prasad C, Soerensen PG, Mau-Soerensen M et al. Abstract A116: targeting the Wnt-5a signaling pathway as a novel anti-metastatic therapy. *Mol Cancer Ther* 2015; **14**: A116–A116.
- 200 Latres E, Chiaur DS, Pagano M. The human F box protein beta-Trcp associates with the Cul1/Skp1 complex and regulates the stability of beta-catenin. *Oncogene* 1999; **18**: 849–854.

- 201 Metcalfe C, Mendoza-Topaz C, Miesczanek J, Bienz M. Stability elements in the LRP6 cytoplasmic tail confer efficient signalling upon DIX-dependent polymerization. *J Cell Sci* 2010; **123**: 1588–1599.
- 202 Clevers H. Wnt/Beta-catenin signaling in development and disease. *Cell* 2006; **127**: 469–480.
- 203 Tree DRP, Shulman JM, Scott MP, Gubb D, Axelrod JD. Prickle mediates feedback amplification to generate asymmetric planar cell polarity signaling. *Cell* 2002; **109**: 371–381.
- 204 Habas R, Kato Y, He X. Wnt / frizzled activation of Rho regulates vertebrate gastrulation and requires a novel formin homology protein Daam1. *Cell* 2001; **107**: 843–854.
- 205 Kikuchi A, Yamamoto H, Sato A, Matsumoto S. New insights into the mechanism of Wnt signaling pathway activation. *Int Rev Cell Mol Biol* 2011; **291**: 21–71.
- 206 Gao B, Song H, Bishop K, Elliot G, Garrett L, English MA et al. Wnt signaling gradients establish planar cell polarity by inducing Vangl2 phosphorylation through Ror2. *Dev Cell* 2011; **20**: 163–176.
- 207 Gao C, Chen Y. Dishevelled: the hub of Wnt signaling. *Cell Signal* 2010; **22**: 717–727.
- 208 Sheldahl LC, Slusarski DC, Pandur P, Miller JR, Kuhl M, Moon RT. Dishevelled activates Ca<sup>2+</sup> flux, PKC, and CamKII in vertebrate embryos. *J Cell Biol* 2003; **161**: 769–777.
- 209 Zhang C, Cattaruzza F, Yeung P, Yen W-C, Fischer M, Brunner A et al. Abstract A30: Predictive and pharmacodynamic biomarkers of vantictumab (OMP-18R5; anti-Frizzled) in non-small cell lung cancer. *Mol Cancer Ther* 2015; **14**: A30–A30.



This work is licensed under a Creative Commons Attribution-NonCommercial-NoDerivs 4.0 International License. The images or other third party material in this article are included in the article's Creative Commons license, unless indicated otherwise in the credit line; if the material is not included under the Creative Commons license, users will need to obtain permission from the license holder to reproduce the material. To view a copy of this license, visit <http://creativecommons.org/licenses/by-nc-nd/4.0/>

© The Author(s) 2017



Review

## CRISPR/Cas9 for cancer research and therapy

Tianzuo Zhan<sup>a,b,1</sup>, Niklas Rindtorff<sup>a,c,1</sup>, Johannes Betge<sup>a,b</sup>, Matthias P. Ebert<sup>b</sup>, Michael Boutros<sup>a,d,\*</sup>



<sup>a</sup> German Cancer Research Center (DKFZ), Division Signaling and Functional Genomics, and Heidelberg University, Department Cell and Molecular Biology, Faculty of Medicine Mannheim, Heidelberg, Germany

<sup>b</sup> Heidelberg University, Department of Internal Medicine II, Medical Faculty Mannheim, Mannheim, Germany

<sup>c</sup> Heidelberg University, Medical Faculty Heidelberg, Heidelberg, Germany

<sup>d</sup> German Cancer Consortium (DKTK), Heidelberg, Germany

### ARTICLE INFO

**Keywords:**

CRISPR  
Cas9  
Genome-engineering  
Cancer  
High-throughput screening  
Organoids  
Immune therapy  
Synthetic lethality

### ABSTRACT

CRISPR/Cas9 has become a powerful method for making changes to the genome of many organisms. First discovered in bacteria as part of an adaptive immune system, CRISPR/Cas9 and modified versions have found a widespread use to engineer genomes and to activate or to repress the expression of genes. As such, CRISPR/Cas9 promises to accelerate cancer research by providing an efficient technology to dissect mechanisms of tumorigenesis, identify targets for drug development, and possibly arm cells for cell-based therapies. Here, we review current applications of the CRISPR/Cas9 technology for cancer research and therapy. We describe novel Cas9 variants and how they are used in functional genomics to discover novel cancer-specific vulnerabilities. Furthermore, we highlight the impact of CRISPR/Cas9 in generating organoid and mouse models of cancer. Finally, we provide an overview of the first clinical trials that apply CRISPR/Cas9 as a therapeutic approach against cancer.

### 1. Introduction

Cancer is one of the main causes of disease-associated mortality, with a rising incidence worldwide [1]. At the same time, progress has been made in the prevention and treatment of many cancers, leading to prolonged survival or even cures. A main pillar of innovation in cancer therapy has been an improved understanding of the underlying tumor biology. This knowledge has led to the development of small molecules and antibodies targeting key proteins of oncogenic signaling pathways. Some of the prominent examples include targeting BCR-ABL by imatinib in chronic myeloid leukemia [2] or EGFR by specific antibodies in colorectal cancer [3]. While these agents have improved survival for selected cancer entities, for many others, treatment options are still limited and resistance mechanisms are poorly understood. Thus, concerted efforts by the scientific community were undertaken to characterize the genetic landscape of cancer and thereby deepen the understanding of its role in carcinogenesis and treatment response [4,5]. Large-scale sequencing projects have revealed genetic alterations that are either specific to a certain type of cancer or common to many cancer entities. However, while most genetic variations of cancer genomes have been structurally characterized, much less is known about the

function of many mutated genes [6]. This particularly applies to the „long tail“ of molecular alterations which are recurrently found only at low frequency.

The systematic functional analysis of genes and mutations have been slow and laborious. Discovery of mutations that cause phenotypes relied either on random mutagenesis or indirectly on perturbation of transcripts by RNAi. The development of engineered nucleases such as zinc finger nucleases or TALENs opened up the possibility to directly target and modify the genomic sequence [7,8]. Recently, genome engineering was greatly accelerated by the development of CRISPR/Cas9 technologies. Since its first use as a genome editing tool in 2013 in mammalian cells [9,10], the toolbox of CRISPR/Cas9 has been continuously expanded, enabling not only the modification of the genomic sequence of cells and organisms, but also the introduction of epigenetic and transcriptional modifications.

In this review, we describe how CRISPR/Cas9 opens new avenues for cancer research. In addition to its application as an effective screening method in functional cancer genomics, we outline how CRISPR/Cas9 can be used to explore the non-coding genome of cancer. Furthermore, we describe novel *in vitro* and *in vivo* cancer models that can be engineered by CRISPR/Cas9. Finally, we review the first clinical

\* Corresponding author.

E-mail address: [m.boutros@dkfz.de](mailto:m.boutros@dkfz.de) (M. Boutros).

<sup>1</sup> Equal contribution.

trials that apply CRISPR as a therapy against cancer.

## 2. CRISPR/Cas9 – a versatile tool for genome engineering

Clustered regularly interspersed short palindromic repeats (CRISPR) were first found in *E. coli* in 1987 [11] and later in many other bacteria species [12]. For several years, the role of the short repeat sequences remained obscure, until in 2005 several groups described similarities of these sequences to phage DNA, raising the hypothesis that these sequences are part of an adaptive immune system in bacteria [13–15]. These studies were later extended to experimentally demonstrate that CRISPR and its CRISPR-associated proteins (Cas) are linked to the adaptive immunity targeting foreign viral DNA [16]. Mechanistically, two distinct RNAs – the CRISPR targeting (crRNA) and the trans-activating RNA (tracrRNA) – activate and guide Cas proteins to bind viral DNA sequences which are subsequently cleaved [17–19]. A subgroup of these CRISPR systems, the type II system, relies on a single Cas protein to target a defined DNA sequence and is therefore particularly attractive to be used as a tool for genome editing [19]. Combining crRNAs with tracrRNAs into a single guide RNA (sgRNA) further simplified the system [19]. In 2013 the type II Cas protein from *Streptococcus pyogenes* (SpCas9) was used for RNA guided DNA cleavage in mammalian cells for the first time, laying the basis for using CRISPR/Cas9 as a widely applicable genome-editing tool [9,10]. Before cleaving the target DNA, the Cas9 nuclease undergoes conformational changes upon sgRNA binding and is directed to its target site [19–21]. The binding specificity is determined by a 20 nucleotides sequence preceding the three nucleotide protospacer adjacent motif (PAM, consisting of a NGG or NAG sequence) [19,21,22]. After unwinding the DNA, binding to the PAM and DNA-sgRNA hybrid formation, two nuclease domains introduce a double strand break (DSB) in the target sequence [18,21] (Fig. 1A). The host cell responds to a DSB with two different mechanisms of repair. Non-homologous end joining (NHEJ) is an error-prone repair mechanism that often leads to insertions or deletions (indel). These indels can cause frameshift mutations, premature stop codons or/and nonsense mediated decay to the target gene, which result in loss-of-function. In contrast, homology directed repair (HDR) uses assisted recombination of DNA donor templates to reconstruct cleaved DNA. This mechanism can be exploited to introduce well defined mutations by transferring altered donor templates into targeted cells (Fig. 1A). The strength of the nuclease activity is determined largely by the binding efficiency of Cas9. Systematic modifications of the sgRNA scaffold identified an optimized scaffold structure that is associated with a higher binding efficiency of Cas9 to the target DNA [23] (see Fig. 1B). Besides Cas9, other CRISPR Type II nucleases that use alternative PAM sites (Cpf1 [24]) or target RNAs (Cas13a/b [25,26]) have been developed into genome engineering tools.

In addition to the use of wildtype SpCas9 for DNA cleavage, a nuclease-deficient SpCas9 modification (dCas9) was developed [27], which can be fused to a variety of effector domains to mediate specific local DNA manipulation (Fig. 1C). CRISPR interference (CRISPRi) and activation (CRISPRa) exploit fused transcriptional regulators to repress or induce gene transcription when dCas9 is directed to the transcription start site of a target gene [12]. In most cases, CRISPR interference systems rely on dCas9 fusions with a KRAB repressor domain to downregulate gene transcription [28]. Interestingly, dCas9-KRAB can also modify enhancer regions by changing the methylation status at the target site, thereby repressing gene transcription [29].

In contrast, CRISPR activation systems have been using diverse strategies to enhance gene expression. The first CRISPRa system relied on a single VP64 activator domain fused to dCas9, thereby activating transcription [28,30]. This system was further improved by changing VP64 for a tripartite activator VP64-p65-Rta (VPR) [31] or by recruiting multiple transcriptional activators to dCas9. The latter is achieved by either adding a long epitope tail to dCas9 (termed SunTag) [32] or by modifying the sgRNA scaffold to include aptamers to

generate additional binding sites for activator domains (termed SAM) [33]. Currently VPR, SAM and SunTag are considered to be to the most effective CRISPRa systems [34].

To investigate the epigenome, dCas9-fusion proteins have been developed that allow region-specific epigenetic modifications (Fig. 1C). dCas9-DNMT3A or -DNMT3A-DNMT3L fusion proteins can selectively increase DNA methylation of CpG motifs in targeted genomic regions [35–37], thereby repressing gene transcription. In contrast, dCas9 coupled to TET1 can be used to decrease DNA methylation [38] and dCas9-p300-domain fusions act as programmable histone acetyltransferases to increase accessibility of genomic regions [39]. Both systems can be used for transcriptional activation of target genes. In fact, the dCas9-p300 system was shown to outperform dCas9-VP64 in activation of gene expression, especially when targeting more distal regulator regions of a gene [39].

Recently, Cas9 variants have been engineered that induce specific single nucleotide base-changes. These base-editors do not introduce DSBs but rely on Cas9-nickases coupled to cytidine deaminase domains to induce targeted transitions from C to T or G to A. For example, Komor et al. designed an efficient base-editor by fusing Cas9-nickase to rat APOBEC1 and an inhibitor of base-excision-repair [40]. They used this BE3 named construct to correct the Y163C hotspot mutation of TP53 in breast cancer cell lines with high efficiency and very low rates of indel formations. Kuscu et al. recently demonstrated how the BE3 system can be adapted for pooled CRISPR screens [41]. While wildtype Cas9 based screens rely on indel formation for functional depletion of genes, CRISPR-STOP targets BE3 to selected nucleotide motifs where it introduces premature stop codons. Although this approach is limited by a smaller number of potential sgRNA binding sites, it offers an alternative solution to avoid viability artefacts caused by repetitive DSBs when targeting amplified genes. An alternative base-editor system relies on the AID protein for cytidine deamination [42–44]. While some constructs show comparable base-editing performance to BE3 [43], their main application is to introduce a diverse set of point mutations at targeted loci, including all three alternative nucleotides. Hence, these systems can be used to generate local nucleotide diversity which was exploited to uncover new mechanisms of resistance to the small molecule inhibitors imatinib and bortezomib [43,44].

## 3. Design of sgRNAs and bioinformatics resources

Unlike previous technologies, the use of CRISPR/Cas9 as a genome editing tool rapidly spread across the scientific community. This distribution of knowledge was supported by the development of open bioinformatics resources for the design and analysis of CRISPR-associated experiments. Currently, several online tools exist that select sgRNAs based on their calculated efficiency and specificity. The algorithms that determine sgRNA on-target efficiency are derived from large screening data and integrate both the nucleotide composition of the binding site as well as its relative position within the gene model [45,46]. In contrast, predicting the specificity of sgRNAs is more difficult as most off-targets do not result in a detectable phenotype, and thus need to be identified experimentally. Different approaches have been developed to detect off-targets, such as integration of a synthetic oligos into DSBs in living cells [47] or detection of Cas9 cut sites by deep sequencing of *in vitro* cleaved genomic DNA [48,49]. The most important lesson learned from these experiments is that off-targets share sequence similarities with the target site, but the precise bioinformatic prediction of all off-targets is not possible based on the currently available data [49]. Furthermore, for the design of custom sgRNA libraries and the analysis of pooled CRISPR/Cas9 screens, specific web-based and local bioinformatics solutions have been developed [50,51]. A selection of frequently used tools can be found in Table 1.

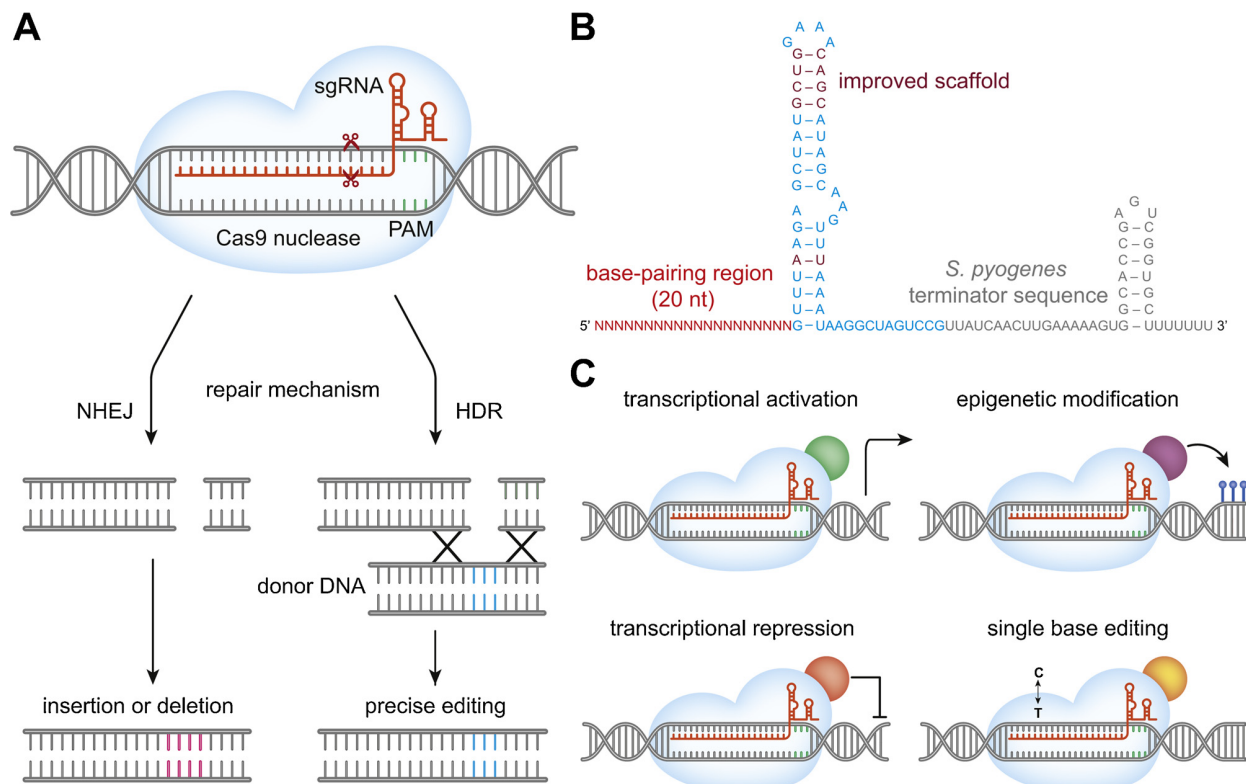


**Fig. 1.** CRISPR/Cas9 function and different SpCas9 variants. Overview of Cas9 activity, sgRNA structure and modifications. (A) The Cas9 nuclease is directed to the target DNA by complementary base-pairing with its bound sgRNA. The target site must be followed by a 3' PAM sequence (NGG, NAG). The following cleavage of double stranded DNA (dsDNA) triggers either the error prone non-homologous end joining (NHEJ) or homology directed repair (HDR) mechanisms. (B) Structure of a sgRNA. The sgRNA consists of 20 nt stretch defining the homologous target sequence and a tracr-RNA inspired handle region for Cas9 binding. Furthermore, the sgRNA scaffold was optimized by addition of specific bases into the hairpin. (C) Selected SpCas9 fusion proteins with distinct biological effects: dCas9 fusion to VP64 transcriptional activator (green) to activate transcription of the target gene by binding upstream of the transcription start site. dCas9 fusion to KRAB repressor (red) to downregulate transcription by binding to the transcription start site. dCas9 fusion to epigenetic modifiers (e.g. DNMT3A, purple) for modification of local methylation patterns. dCas9 fusion to base-editors (e.g. AID, yellow) for precise single nucleotide exchanges.

#### 4. Target discovery by CRISPR/Cas9 screens

CRISPR/Cas9 screens are a powerful functional genomics tool to discover novel targets for cancer therapy. For pooled screening with CRISPR/Cas9, a cell population with a diversity of gene knockouts needs to be generated. This process involves several bioinformatics and

experimental steps (see Fig. 2 for a schematic workflow). First, sgRNAs which are predicted to be efficient are selected for every target gene. In most sgRNA design tools, algorithms that predict sgRNA efficiency are already integrated [50,51]. The sgRNA library is synthesized as a pool of oligonucleotides and cloned into a lentiviral plasmid backbone, followed by generation of viral particles. The lentiviral particles are then

**Table 1**  
Software for the design and analysis of CRISPR experiments.

Software for the design of single sgRNAs				
Software	Platform	Reference	Organism	URL
E-CRISP	Web-based	[126]	Multiple	<a href="http://www.e-crisp.org/">http://www.e-crisp.org/</a>
CRISPR Design Tool	Web-based	[127]	Multiple	<a href="http://crispr.mit.edu/">http://crispr.mit.edu/</a>
CHOPCHOP v2	Web-based	[128]	Multiple	<a href="http://chopchop.cbu.uib.no/">http://chopchop.cbu.uib.no/</a>
Protospacer Workbench	Offline/graphical interface	[129]	Multiple	<a href="http://www.protospacer.com">www.protospacer.com</a>
CRISPRScan	Web-based	[130]	Multiple	<a href="http://www.crisprscan.org/">http://www.crisprscan.org/</a>
sgRNA Scorer 1.0	Web-based	[131]	Human	<a href="http://crispr.med.harvard.edu/sgRNAScorer">http://crispr.med.harvard.edu/sgRNAScorer</a>
Software for design of sgRNA libraries				
Software	Platform	Reference	Organisms	URL
GUIDES	Web-based	[50]	Human and mouse	<a href="http://guides.sanjanalab.org/#/">http://guides.sanjanalab.org/#/</a>
CRISPR Library Designer (CLD)	Offline/graphical interface	[51]	Multiple	<a href="https://github.com/boutroslab/cld">https://github.com/boutroslab/cld</a>
Software for analysis of pooled CRISPR screens				
Software	Platform	Reference	Organism	URL
caPools	R/Bioconductor	[132]	/	<a href="http://github.com/boutroslab/caPools">http://github.com/boutroslab/caPools</a>
MAGECK-VISPR	Offline/graphical interface	[133]	/	<a href="https://bitbucket.org/lulab/mageck-vispr">https://bitbucket.org/lulab/mageck-vispr/</a>
ScreenBEAM	Offline/graphical interface	[134]	/	<a href="https://github.com/jyyu/ScreenBEAM">https://github.com/jyyu/ScreenBEAM</a>
CRISPRAnalyzeR (CAR)	Web-based and Offline/graphical interface	[135]	/	<a href="http://www.crispr-analyzer.org">http://www.crispr-analyzer.org</a> <a href="http://www.github.com/boutroslab/CRISPRAnalyzeR">http://www.github.com/boutroslab/CRISPRAnalyzeR</a>

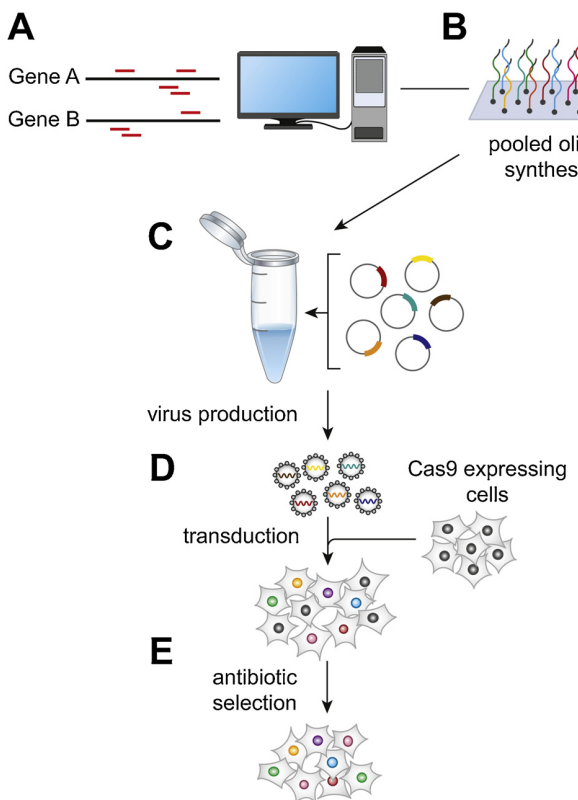


**Fig. 2.** Pipeline for generation knockout cell pools. Overview of individual steps in the design and cloning of sgRNA libraries and generation of knockout cell pools. Appropriate sgRNA binding sites for selected genes are identified *in silico* by library design software tools (A). A pool of oligos containing the sgRNA sequences are then produced by chip-based synthesis (B) and cloned into a lentiviral backbone vector (C). Lentiviral particles each containing a distinct sgRNA expression cassette are produced and used to infect Cas9 expressing cells at a low multiplicity of infection (MOI) (D). After antibiotic selection, the pool contains cells with distinct gene knockout that can be used for a variety of different screening approaches.

used to infect Cas9-expressing cells at a low multiplicity of infection, so that every cell potentially carries a distinct sgRNA cassette and specific gene knockout. Subsequently, this pool of knockout cells is kept in culture for a fixed period of time or exposed to selected perturbations, after which the cells are harvested and their genomic DNA is extracted. By amplification and sequencing of the integrated sgRNA cassettes, the abundance of cells carrying a specific knockout can be determined. By this means, it is possible to monitor the phenotypic effect of specific gene knockouts within the cell population. This set-up of a CRISPR screen can be modified by using different Cas9 variants to perform *e.g.* gain-of-function screens, or to investigate drug-gene interactions by adding small molecules as perturbations (Fig. 3).

One main goal of pooled CRISPR/Cas9 screens in cancer research is to identify genotype-specific vulnerabilities (Fig. 3A). These ‘essential’ genes can be potential drug targets, as their functional depletion leads to a reduced viability. Compared to shRNAs, CRISPR was shown to be more sensitive in detecting essential genes [52]. Hence, large-scale CRISPR/Cas9 screens have been conducted to systematically discover essential genes across many cancer cell lines [53–55]. In genome-scale CRISPR/Cas9 screens in ten cancer cell lines, approximately 1500 essential genes were identified, which was five times higher than previously detected by shRNA screens [54]. However, cutting of Cas9 at highly amplified genes can generate a lethal DNA damage response, thereby creating false positive hits in pooled screens [53,55]. To correct for this effect, different computational approaches have been recently

proposed [56]. A main observation from negative selection screens was that some genes were essential in the majority of cell lines (termed “core essentiality”), while other genes were essential only for cell lines with a specific genetic or tissue background (termed “context-dependent essentiality”) (see Fig. 4). For example, to identify essential genes for acute myeloid leukemia, Tzelepis et al. focused on eight AML cell lines and identified 429 candidates, among which KAT2A was characterized as a druggable and leukemia specific target [57]. Since the so far published CRISPR screens have revealed many unknown essential genes, there are ongoing research efforts that apply this method to determine gene essentiality in a larger panel of cancer cell lines [56]. Along these lines, Rauscher et al. recently demonstrated how gene essentiality data from diverse CRISPR screens can be integrated to generate a map of genetic interactions in cancer cells, thereby revealing novel context-dependent essential genes [58].

The concept of gene essentiality can also be narrowed down to gene regions encoding essential protein domains. As opposed to RNAi that depletes transcripts of target genes, it is possible to disrupt specific protein domains using CRISPR/Cas9, by targeting the corresponding genomic sequence. This screening approach – termed domain screen – was used to pinpoint protein domains that determine the essentiality of a specific gene, which can further facilitate drug development. For example, a CRISPR screen targeting exons of chromatin regulatory domains revealed several novel domains that were essential for AML [59]. A similar approach identified that AML cell lines harboring a mutation in the NPM1 gene specifically depend on the menin binding site of the MLL1 protein [60]. Supporting this observation, pharmacological inhibition of this binding site has a pronounced anti-leukemic effect. While screens for essential genes and domains have revealed many genes that show a lethal phenotype upon disruption, a major drawback is that only few of these candidates are directly targetable by drugs.

A complementary screening approach to identify druggable targets relies on the concept of synthetic lethality, which is a specific form of context-dependent gene essentiality (see Fig. 4B–C). In brief, synthetic lethality occurs if a cell can compensate the functional alteration of gene A or B, but is unable to survive if gene A and B are simultaneously altered (Fig. 4B, right). Translated into cancer biology, this means that previously non-essential genes can become essential due to the loss of a specific tumor suppressor or the activation of an oncogene [61]. With the increasing knowledge on the structural alterations of cancer, this approach could vastly enlarge the spectrum of potential drug target. The translational relevance of this concept was recently demonstrated by a clinical trial that showed higher sensitivity of breast cancer bearing a germline mutation of BRCA to PARP inhibition [62]. Several CRISPR/Cas9 screens were performed to identify synthetic lethal interactions. In a genome-wide CRISPR screen, Steinhart et al. discovered that pancreatic cell lines harboring a mutation in the ubiquitin-ligase RNF43 are particularly vulnerable to knockout of the Wnt ligand receptor FZD5 [63]. Interestingly, this effect is exclusive for FZD5 and targeting the receptor with an antibody reduced viability in tumor organoids derived from RNF43 mutant pancreatic and colorectal cancer [63]. In another genome-wide screen performed in a panel of 14 RAS mutant and non-mutant AML cell lines, a set of genes was found to be synthetic lethal with oncogenic RAS mutations [64]. Selecting the gene PREX1 as an example, it was shown that most of the identified candidates directly interact with the RAS pathway. A similar approach was used to identify targets in leukemia cells that harbor a MLL-AF4 fusion oncogene. By means of a genome-scale CRISPR screen, the previously uncharacterized gene ENL was found to be required for growth and proliferation in MLL-AF4 positive AML lines [60]. ENL is a component of the super elongation complex and degradation of ENL decreased transcription of oncogenes such as MYC [60]. However, the molecular mechanism by which ENL interacts in a synthetic lethal manner with MLL-AF4 was not resolved. Together, these studies highlight that CRISPR screens can reveal a wealth of synthetic lethal interactions. The

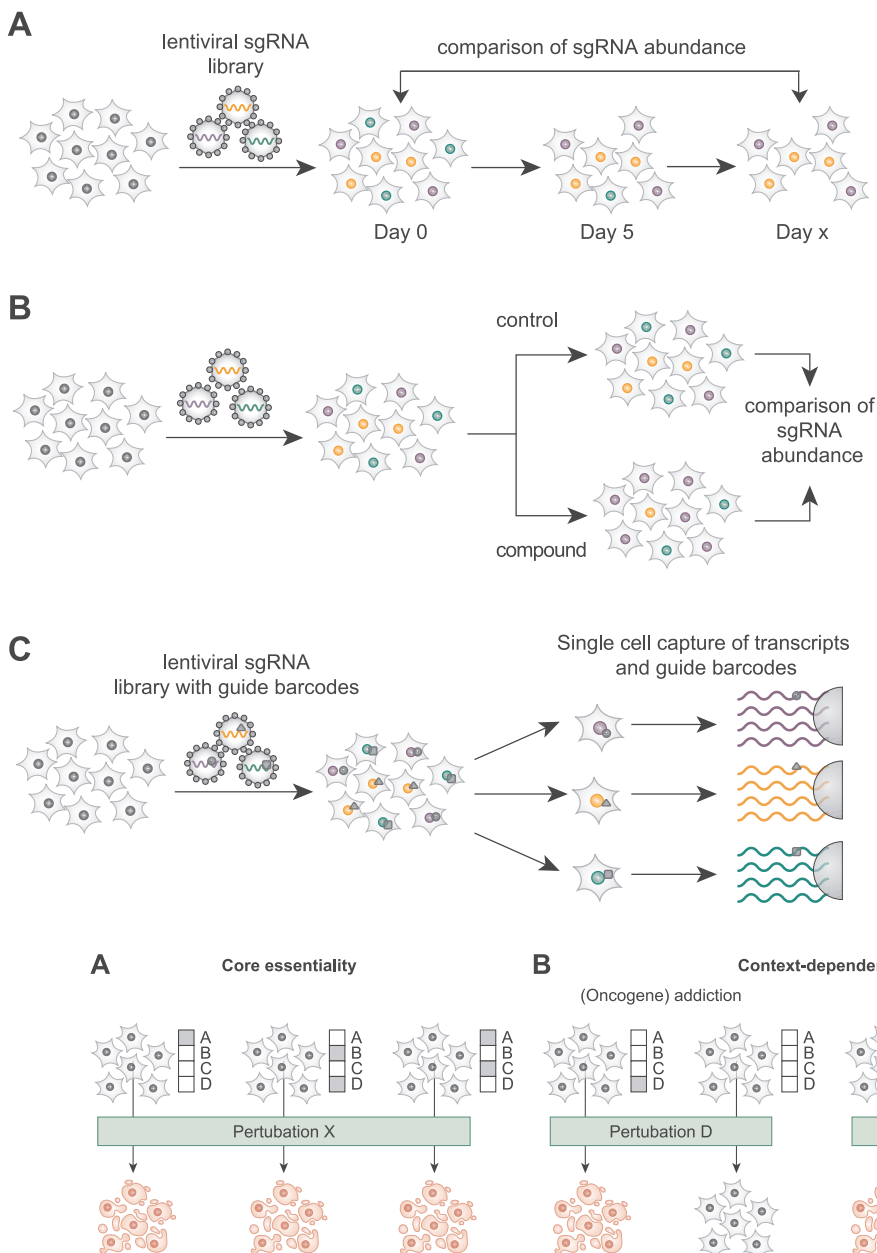


**Fig. 3. Pooled CRISPR/Cas9 screening approaches.** Three different screening approaches are schematically presented. In a negative selection screen (e.g. to identify essential genes) (A), the pool of knockout cells is incubated for a defined time span. The abundance of different sgRNAs within the pool is determined at an early time-point (Day 0) and at the end of the screen (Day X) by deep sequencing. Cells carrying sgRNAs targeting essential genes will be depleted in the cell pool during incubation. To investigate gene-drug interactions (B), the pool of knockout cell is separated and treated either with a compound or the carrier solution (control) for a defined time period. The abundance of cells with different sgRNA cassettes is determined in the drug-treated and control pool. Cells with sgRNAs targeting genes that confer drug resistance upon knockout will be enriched while those resulting in increased sensitivity to the drug will be depleted in the final pool. To screen for single cell transcriptome changes induced by gene knockouts (C), an additional highly expressed barcode is encoded on the lentiviral vector (depicted as small icons). After sorting out single cells from the pool of knockout cells, mRNA of individual cells including the barcode is captured by beads and then sequenced. The cellular transcriptomes are then assigned to the corresponding sgRNAs using the barcodes.

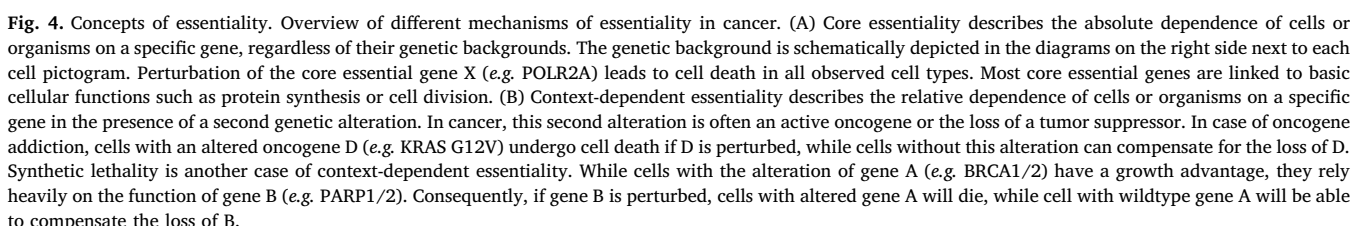


**Fig. 4. Concepts of essentiality.** Overview of different mechanisms of essentiality in cancer. (A) Core essentiality describes the absolute dependence of cells or organisms on a specific gene, regardless of their genetic backgrounds. The genetic background is schematically depicted in the diagrams on the right side next to each cell pictogram. Perturbation of the core essential gene X (e.g. POLR2A) leads to cell death in all observed cell types. Most core essential genes are linked to basic cellular functions such as protein synthesis or cell division. (B) Context-dependent essentiality describes the relative dependence of cells or organisms on a specific gene in the presence of a second genetic alteration. In cancer, this second alteration is often an active oncogene or the loss of a tumor suppressor. In case of oncogene addiction, cells with an altered oncogene D (e.g. KRAS G12V) undergo cell death if D is perturbed, while cells without this alteration can compensate for the loss of D. Synthetic lethality is another case of context-dependent essentiality. While cells with the alteration of gene A (e.g. BRCA1/2) have a growth advantage, they rely heavily on the function of gene B (e.g. PARP1/2). Consequently, if gene B is perturbed, cells with altered gene A will die, while cells with wildtype gene A will be able to compensate the loss of B.

future challenge will be to disentangle the underlying molecular mechanisms and identify (druggable) synthetic lethal interactions that can be translated into therapies.

Another major application of CRISPR/Cas9 screening is the dissection of chemico-genetic interactions, which enables insights into how cancer responds to drug treatment. Combining pooled CRISPR screening with a drug as a perturbation can identify gene knockouts that act synergistically with or confer resistance to the agent (Fig. 3B). In one of the first pooled CRISPR screens, treatment of a genome scale

knockout library of melanoma cells with the BRAF inhibitor vemurafenib recovered genes that were known to confer resistance to the drug [65]. Likewise, a pooled CRISPR screen could reliably identify both positive and negative regulators of the TRAIL pathway, when cancer cells were treated with the TRAIL ligand [51]. Later, a series of CRISPR screens have been performed to identify genes that modulate cellular response to specific drugs, such as ATR [66] or Ras pathway inhibitors [67]. This strategy was also used to explore the mode of action of poorly characterized anti-neoplastic drugs. For example, apilimod is a known

phosphatidylinositol-3-phosphate 5-kinase inhibitor, but the mechanism of its cytotoxic effect has not been understood. A CRISPR screen revealed that genes involved in the endosomal/lysosomal pathway conferred resistance upon knockout, indicating that the cytotoxicity of apilimod critically relies on endosomal/lysosomal homeostasis [68]. Recently, combinatorial CRISPR screening approaches were developed that use lentiviral plasmids that encode two pre-defined sgRNAs. This approach allows not only the dissection of genetic interaction of pairwise gene knockouts, but also enables identification of synergistic drug targets. Han et al. generated a large double-sgRNA library targeting 21,321 pairs of potential drug targets to test for synergistic combinations in an AML cell line [69]. They identified a strong synergism between knockout of MCL1 and BCL2L1 which could be reproduced using chemical inhibitors of the two genes. Similarly, Shen et al. used the double-knockout screening approach to pairwise target 73 cancer genes and discovered a number of known (e.g. BRCA-PARP) and unknown synthetic lethal interactions, some of which could be phenocopied using drug combinations [70]. Since drug resistance can also result from overexpression of genes, Konermann et al. used CRISPRa to perform a pilot, genome-scale activator screen to identify genes that confer resistance to BRAF inhibition [33]. Among the top hits were many regulators of the Ras pathway, including EGFR as a known resistance gene. It is expected that CRISPR screens will be used to dissect chemico-genetic interactions of many more drugs, allowing to understand the contribution of tissue and genetic background to drug response.

While most pooled CRISPR screening techniques are designed to identify genes that show a specific phenotype upon depletion, novel screening approaches aim to obtain a more global insight into biological changes associated with a specific gene perturbation. As recently described, combining single cell RNA-sequencing platforms with pooled CRISPR screening increases the explanatory power of CRISPR based assays [71–73] (Fig. 3C). In brief, a pool of cells carrying different knockouts is generated, followed by single cell capturing and RNA sequencing of the individual transcriptomes of each cell. In order to link the transcriptome of a cell to the identity of the transduced sgRNA with high confidence, an additional highly expressed guide barcode or marker [74] is incorporated into the lentiviral vector. These assays, referred to as Perturb- or CROP-Seq, allow the comparison of transcriptomes of cells with different gene knockouts, and thereby group and assign genes to specific biological processes. Using these methods, new regulators [71] of immune cell differentiation and unknown bifurcations [73] of the unfolded protein response in phenotypically homogenous cell populations were identified.

## 5. Interrogation of the non-coding genome of cancer

The vast majority of the human genome consists of non-protein coding regions that contain many regulatory elements such as enhancers or non-coding RNAs. To date, most of the non-coding genome has not been functionally characterized, mainly due to a lack of appropriate experimental tools. In cancer, the expression of non-coding RNAs is known to be dysregulated [75] and the transcription of oncogenes can be controlled by near and distant enhancer elements [74]. Therefore, the comprehensive understanding of non-coding elements will provide deeper insights into cancer biology. Recently, CRISPR/Cas9 has been shown to be a potent tool for the interrogation of non-coding elements. To identify enhancer regions of the three cancer associated genes CUL3, NF1 and NF2, a CRISPR screen was performed targeting genomic regions of 700 kb surrounding the open reading frame of the candidates [76]. Since direct knockout of either candidate leads to resistance against the BRAF inhibitor vemurafenib, disruption of any enhancer elements that results in downregulation of the gene will phenocopy the drug resistance. In fact, alterations of specific genomic sites down- and upstream of the CUL3 gene changed the occupancy of specific transcription factors and reduced CUL3 expression.

Another study used CRISPR to identify functional enhancers of TP53 target genes [77]. For this purpose, sgRNA libraries against genomic regions that show both TP53 binding property and enhancer markers were designed. Knockout of a relevant enhancer element would result in resistance of cells against HRAS<sup>G12V</sup> induced senescence, which depends on TP53. The authors identified several enhancers in the proximity of CDKN1A which upon editing resulted in downregulation of CDKN1A and escape from oncogene induced senescence. Another class of poorly understood genetic elements are non-coding RNAs. To systematically dissect the role of lncRNA in cancer cells, three screening approaches using different Cas9 variants were applied. Zhu et al. used paired-sgRNAs to delete genomic sequences of 651 lncRNAs and thereby identified 51 lncRNAs that show an altered proliferation phenotype upon knockout [78]. In contrast, CRISPRi was used by Liu et al. to screen 16401 lncRNA loci in six cell lines for effects on cell viability [79]. A total of 499 lncRNAs were found to be essential for cellular growth. Interestingly, the overwhelming majority of these lncRNAs were required in a cell line specific manner, supporting previous observations that expression of lncRNAs varies greatly between cancers from different tissue backgrounds [80]. In a similar approach, CRISPRa was used to identify lncRNAs that mediate resistance to BRAF inhibition upon transcriptional activation [81]. Several candidate loci were found, but the phenotypes were mostly caused by the activation of neighbouring protein coding genes. This result reflects one of the major caveats of using CRISPRi/a to target lncRNAs. Since many lncRNA have bidirectional promoters or are located within protein-coding genes, it is rarely possible to target lncRNAs without affecting neighbouring protein coding genes [82]. Therefore, it remains yet to be determined which CRISPR/Cas9 technology is best suited to investigate lncRNA function.

## 6. Genome editing to generate organoid cancer models

Adult stem cell derived organoids are an increasingly popular *in vitro* model of intact and diseased human epithelia [83]. Stem cells from multiple adult tissue types can be isolated and cultivated in 3D. By stimulation with tissue specific growth factors, stem cells proliferate, differentiate and form organoids in a cell culture dish. The possibility to culture both healthy and cancerous tissue enables the study of tumor development and progression *in vitro*.

Schwank et al. were the first to use the CRISPR/Cas9 system in mouse derived intestinal organoids [84]. Two years later two groups simultaneously reported to have transformed healthy human colon organoids into their cancerous counterparts by recapitulating the adenoma-carcinoma sequence of colon cancer using CRISPR/Cas9 [85,86]. Disruption of tumor suppressors such as APC, TP53 and SMAD4 as well as genetic editing of oncogenes such as KRAS and PI3K lead to organoid models of colon cancer *in vitro* (Fig. 5). Of note, these cells were growing independently of any growth factors normally needed for the culture of untransformed organoids, thereby enabling phenotype dependent selection of genetically modified organoids. Recently, Drost et al. [87] also modelled mismatch-repair deficient colorectal cancer by deleting DNA repair genes in colon organoids. This allowed the detection of mutational signatures which were also observed in patient cohorts with similar defects. By uniting scalable culture and nearly intact physiology, organoids can be used to validate findings from other model systems in an *ex vivo* setting [88]. Moreover, new insights can be gained by using patient derived material for functional assays such as compound or CRISPR screens, further reviewed in Driehuis et al. [89].

## 7. Methods for *in vivo* delivery of CRISPR/Cas9

To apply CRISPR/Cas9 *in vivo*, an efficient delivery of both Cas9 and the sgRNA to the target cell is required. Ideally, the method should provide high editing efficiency, cause low immunogenicity and enable the Cas9/sgRNA to be directed to the organ or cell type of choice. The

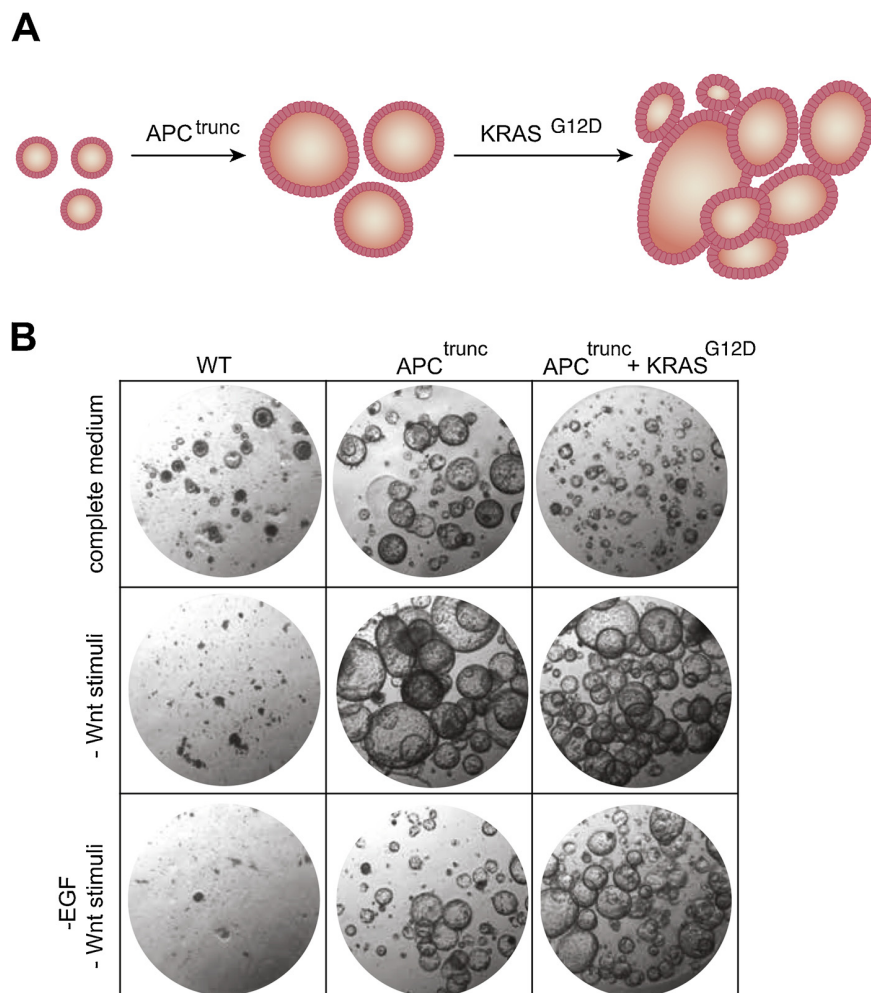


**Fig. 5.** Modelling of the adenoma-carcinoma sequence in mouse colon organoids. Genetic perturbation of colon organoids *in vitro* affects both phenotype (A) and niche requirements (B) of organoids. (A) Sequential loss of tumor suppressors and activation of oncogenes lead to enlarged highly proliferative organoids with an enhanced capacity to form colonies. (B) Hyperactivated Wnt signaling by loss of APC leads to independence from Wnt activating growth factors (Wnt3A and R-Spondin1) in the medium. The same principle applies to a sequential KRAS mutation, which renders organoids less dependent on EGF (Rindtorff et al., unpublished).

first genome editing approaches in mammalian cells relied on the plasmid based expression of Cas9 and sgRNA [9,10]. In model organisms such as mice, this method is also suitable for *in vivo* applications since the plasmid can be delivered to the tissue by hydrodynamic injection [90] or electroporation [91,92]. However, the editing efficiency is low and the Cas9 activity can be poorly controlled. In order to improve *in vivo* delivery of Cas9/sgRNA, different viral and non-viral methods have been developed.

Adeno-associated virus (AAV) are regarded as a potent tool, as they are non-integrating, possess a high transduction efficiency and are serologically compatible with a large fraction of the human population [93]. Furthermore, the family of AAVs is characterized by a rich diversity of serotypes with distinct tissue tropisms, enabling the selective targeting of different organs [94]. However, due to the limited cargo size of AAVs, the spCas9 and sgRNA need to be encoded on separate vectors [95]. For genome editing, AAVs can be directly applied to the target organ or administrated systemically. Wu et al. showed that subretinal injections of AAVs could efficiently edit the NRL gene in postmitotic retinal photoreceptors [96]. Similarly, direct injections of AAVs into the striatum of mice could locally modify the huntingtin gene [97]. For systemic applications of AAVs, the tissue selectivity of genome editing is achieved by using appropriate AAV serotypes and tissue specific promoters for Cas9. This approach has been successfully used

for editing the ornithine transcarbamylase gene in murine liver [98] and the dystrophin gene in muscle tissue [99,100]. After systemic application, the editing frequency ranged from 10% [98] up to 70% [99], which was sufficient to measure phenotypical improvements in mouse model of hereditary diseases [98,99]. Although both Cas9 expression and AAVs caused a humoral immune response, no extensive cellular damage was observed [101]. An alternative approach to viral delivery is the application of lipid nanoparticles. A major advantage of nanoparticles is that they can be manufactured on an industrial scale and allow a dosing that is more similar to commonly used drugs [102]. Lipid nanoparticles has been used to successfully deliver siRNA [102] or mRNA [103] in clinical trials. Recently, a series of studies have shown that the Cas9 mRNA and the sgRNA can be loaded onto lipid nanoparticles and delivered to murine liver with high efficiency [104–106]. Furthermore, modified nanoparticles can be additionally loaded with a donor template and thereby also allow homology directed repair [107]. A correction of the dystrophin gene was observed after intramuscular injection of nanoparticles carrying a donor template, but the editing efficiency was low (5.3%) [107]. Since major efforts are currently undertaken to establish and improve CRISPR/Cas9 as a gene repair tool, it is expected that this knowledge will also be used to develop CRISPR/Cas9 into a therapeutic agent against cancer. The success of such an approach will strongly depend on advances in the tissue

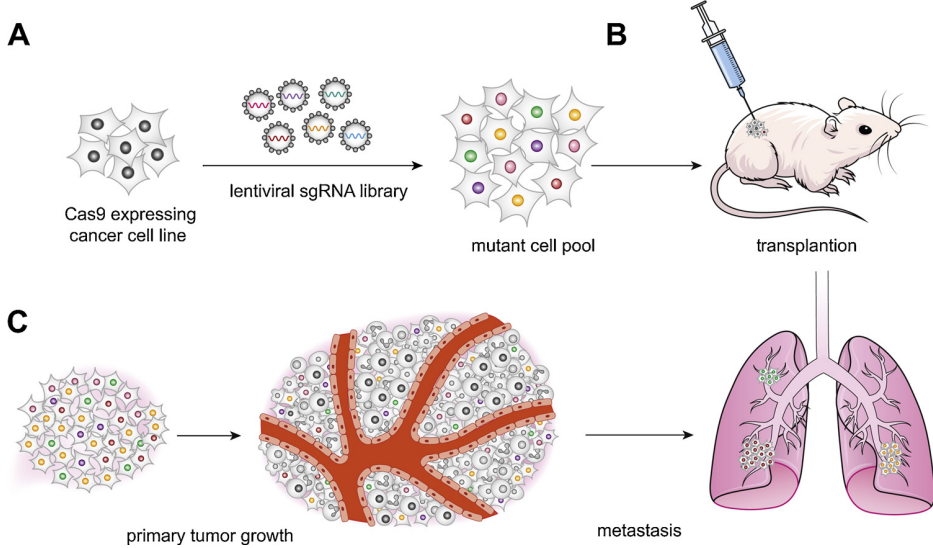


**Fig. 6.** Pooled CRISPR/Cas9 screens in mouse. The concept is illustrated by a study performed by Chen et al. [109]. Non-metastasizing Cas9 expressing cancer cells were infected with a (genome-wide) sgRNA library *ex vivo* (A), before the mutant cell pool was subcutaneously transplanted into immunodeficient mice (B). By molecular analysis of enriched sgRNA sequences in advanced tumors and metastases, genes involved in tumor progression and the metastatic process were identified (C). This principle has been adopted to several other cancer types to identify genes involved in tumor progression and metastasis.

specific delivery of Cas9/sgRNA and on experiences gained from current and future trials with RNA therapeutics [108].

#### 8. In vivo genome editing and genetic screens in mice

*In vivo* CRISPR screening differs from *in vitro* based screening assays with respect to stronger growth competition between transplanted cells and additional influencing factors of the microenvironment such as the host immune system. Two basic concepts of *in vivo* screening exist: implanting of *ex vivo* edited cancer cells and *in vivo* delivery of CRISPR/Cas9 components to mouse tissues, thereby generating tumors.

Transplanting *ex vivo* CRISPR edited cells enables screening of sgRNAs with high-throughput. For example, Chen et al. performed a genome-wide CRISPR loss-of-function screen in murine lung cancer cells to identify genes driving progression and metastasis [109]. They transduced a non-metastatic lung cancer line with an sgRNA library and subcutaneously transplanted these cells into mice. The implanted cells formed local tumors and lung metastasis which were extracted and analyzed for the enrichment of specific sgRNAs, thereby identifying drivers of tumor growth and metastasis (Fig. 6). Another loss-of-function screen was performed with murine liver progenitor cells deficient for TP53 and overexpressing MYC [110]. These cells were also subcutaneously transplanted after transduction with a genome-scale sgRNA library. Analysis of engrafted tumors suggested new key tumor suppressor genes in hepatocellular carcinoma. Besides adherent cell lines, a recent study by Roper et al. demonstrated feasibility of orthotopic implantation of CRISPR edited colon organoids [111]. APC mutant organoids engrafted efficiently in the colon within a few weeks. Moreover, patient derived tumor organoids recapitulated tissue infiltration and metastasis upon orthotopic transplantation. Combining CRISPR based screening in organoids with orthotopic transplantation might therefore be a suitable approach to validate putative tumor drivers in different phases of disease progression.

Direct *in vivo* genome editing is a potent approach to study the effect of genetic alterations on carcinogenesis in a native tissue microenvironment. The first evidence that *in vivo* gene editing can result in tumor formation was provided by Xue et al. [90]. In this study, a plasmid encoding Cas9 and sgRNAs against PTEN and TP53 was transfected into murine liver cells by hydrodynamic tail vein injection, resulting in the formation of liver cancer. Subsequently, the same method was used to deliver Cas9/sgRNA encoding plasmids targeting a set of ten genes, which led to the development of hepatocellular and cholangiocellular carcinoma in a murine model with oncogenic KRAS background [112]. Similarly, multiplexed electroporation of sgRNA-

encoding plasmids into the pancreas of mice with oncogenic KRAS caused the formation of pancreatic tumors [91]. Another approach applied *in utero* electroporation of the developing prosencephalon with multiple sgRNAs targeting key tumor suppressors, which resulted in mice developing glioblastomas within less than six months [92]. However, it should be noted that unwanted chromosomal translocations can be a consequence of multiplexed sgRNA targeting [91]. Introduction of sgRNAs by adeno-associated virus (AAV) offers an alternative to transfection based approaches. In a proof of principle study, Platt et al. delivered AAV encoding three sgRNAs targeting *LKB1*, *TP53* and *KRAS* combined with a donor template for oncogenic KRAS to the lungs of Cas9 expressing mice [113]. As a result, macroscopic lung cancer formation could be observed. In another study, Chow et al. injected a focused AAV-mediated CRISPR library into brains of conditionally Cas9 expressing mice and sequenced targeted genetic loci after visible tumor development [114]. sgRNA targeting genes that are frequently mutated in human glioblastoma were also found to be enriched in extracted lesions. Moreover, co-occurring sgRNAs were identified which suggest a set of synergistic mutations in glioblastoma. In summary, both *in vivo* and *ex vivo* delivery of sgRNAs and Cas9 for loss-of-function screens can be performed and continue to yield new insights into the function of cancer-associated genes.

#### 9. First clinical applications of CRISPR

The ability to edit genes, not only in cell culture models and model organisms, but also in humans, has been discussed long before genome-editing technologies had been developed. Somatic gene therapy traditionally means the introduction of novel genetic material into somatic cells (any other cells than gametes or germ cells) to express therapeutic gene products for the treatment of diseases. Gene therapy trials have been performed already since the eighties and have been largely unsuccessful for many years due to problems with somatic silencing of gene products, host immune response, viral vectors and mutagenesis [115]. Even though most of these problems have not been fundamentally resolved, promising results of somatic gene therapy have been published recently [116–119]. The new technologies of gene editing may overcome some of the current issues and allow permanent modification of somatic cells. As in animal studies, both *in vivo* and *ex vivo* approaches are studied.

The first clinical trial showing feasibility of gene editing in the clinical setting was published 2014 and did not use CRISPR/Cas9, but zinc finger nucleases (ZFN) [120]. In this trial, the major HIV co-receptor CCR5 was targeted by ZFN in autologous T-cells *ex vivo* to induce

resistance to infection with the virus. The study revealed well tolerability of CCR5 modified T-cell infusions and indeed, CCR5 knockout cells declined significantly less upon viremia than unmodified counterparts. Even though the treatment did not have a lasting therapeutic effect [121], this trial paved the way for other *ex vivo* gene-editing trials.

The first clinical trial using CRISPR for cancer therapy has enrolled the first patient at Sichuan University's West China Hospital in Chengdu in 2016 [122]. In this non-randomized, open-label phase I study (NCT02793856), the safety of programmed cell death protein-1 (PD-1) knockout engineered T cells *ex vivo* is evaluated in treating metastatic non-small cell lung cancer that has progressed after all standard treatments. Immune checkpoint regulator PD-1 is a T-cell receptor responsible for inhibition of T-cell activation, thereby regulating immune tolerance and decreasing autoimmune reactions, but also allowing immune escape of cancers [123]. Antibodies that neutralize PD-1 or its ligand PD-L1 are successfully used for the treatment of lung cancers, among others [124]. Patients enrolled in the gene-editing trial are providing peripheral blood lymphocytes and PD-1 knockout of T-cells by CRISPR/Cas9 is performed *ex vivo*. The edited lymphocytes are selected, expanded and subsequently infused back into the patients (Fig. 7). Four other trials applying the same concept of PD-1 knockout for the treatment of other cancer types, including prostate, bladder, esophageal and renal cell cancer have been registered (see Table 2).

Even though the concept is promising, there are doubts that PD-1 knockout engineered T-cells are preferable over PD-1 or PD-L1 antibodies in the clinical setting, since the process of genetically modifying, propagating and infusing T-cells is laborious [122]. Hence, these trials can be regarded as first proof-of-concept studies for applying *ex vivo* CRISPR/Cas9 knockout in cancer treatment, while other targets for knockout or combinations with PD-1 knockout may be more promising for future clinical applications. An example is another registered phase I/II trial (NCT03044743) that adds PD-1 knockout to Epstein-Barr virus (EBV)-specific autologous T-cells for the treatment of EBV positive cancers. Another *ex vivo* approach is the generation of chimeric antigen

receptor (CAR) T-cells with the help of CRISPR/Cas9. CARs are synthetic receptors that are transduced into the T-cells of a patient to reprogram T-cells to attack malignant cells. In a recent preclinical study targeted gene delivery of a CAR to the T-cell receptor  $\alpha$  chain (TRAC) locus using CRISPR Cas9 produced T-cells with immensely enhanced tumor rejection activity compared to conventionally produced CAR T-cells using randomly integrating vectors [125]. These interesting data from mouse models will very likely prompt clinical trials in the near future. Of note, by knocking out the TRAC locus, it is even possible to produce non-alloreactive CAR T cells that could be generated from T cells of healthy donors to be stored and then transfused to a wide range of patients when needed. This approach has previously been done using TALENs (reviewed by [121]).

Compared to *ex vivo* genome editing, *in vivo* genome editing is yet less implemented in clinical trials. A single registered clinical trial that is not yet recruiting (NCT03057912) plans to use TALEN or CRISPR/Cas9 plasmids targeting HPV16 and HPV18 E6/E7 DNA. The constructs are delivered with a gel that is locally applied to the HPV infected cervix. Next to safety and dosing regime, the change of HPV 16 or 18, as well as cervical cytology and histology shall be evaluated in this phase 1 trial that is expected to start early 2018. Of note, a study with a very similar concept using ZFN has already finished the data collection phase (NCT02800369). Improvements in specificity of Cas9 for targeting defined genomic regions without off-target effects and advancements in delivery methods to target specific organs or tumors with CRISPR/Cas9 constructs will certainly fuel the development of further *in vivo* gene editing clinical trials in the future.

## 10. Future perspectives of CRISPR for cancer research

Since its development into a genome editing tool, the CRISPR/Cas9 technology has revolutionized biology by providing a simple and versatile method to manipulate the genome, transcriptome and epigenome across a broad range of organisms. The potential of CRISPR/Cas9 for both basic and translational cancer research is yet beginning to unfold. In the future, pooled CRISPR screens will provide a comprehensive set of essential genes across most cancer cell lines. This resource, combined with the already available information on the genetic and epigenetic characteristics of cancer cell line, will enable the extensive identification of synthetic lethal interactions and facilitate the discovery of novel drug targets. However, it will require considerable experimental research to fully understand the biological mechanisms underlying the many genetic interactions revealed by CRISPR/Cas9 screens. Furthermore, CRISPR/Cas9 provides a tool to manipulate non-coding regions of the genome and will accelerate the functional exploration of a so far poorly characterized aspect of the cancer genome. The precise engineering of common and rare mutations by CRISPR/Cas9 – combined with advanced organoid culture – will enable cancer researchers to copy the genetic sequence of carcinogenesis of many cancer entities. This will provide deeper insights into the biological changes that are elicited by individual mutations and to separate driver from passenger mutations. Finally, we expect to see the yet unpredictable results from pilot clinical trials that apply CRISPR/Cas9 as a therapeutic tool to target the immune system against cancer. The future use of CRISPR/Cas9 in translational medicine will largely depend on the ability to develop Cas9 variants with minimal or no off-target effect and novel methods to improve the yet inefficient engineering of precise genetic changes by homology directed repair. Furthermore, future improvements of viral and non-viral delivery methods will be necessary to improve the *in vivo* application of CRISPR/Cas9, laying the ground for the therapeutic use of CRISPR in the future. In summary, the development of the CRISPR/Cas9 technology has and will greatly accelerate cancer research in many areas.

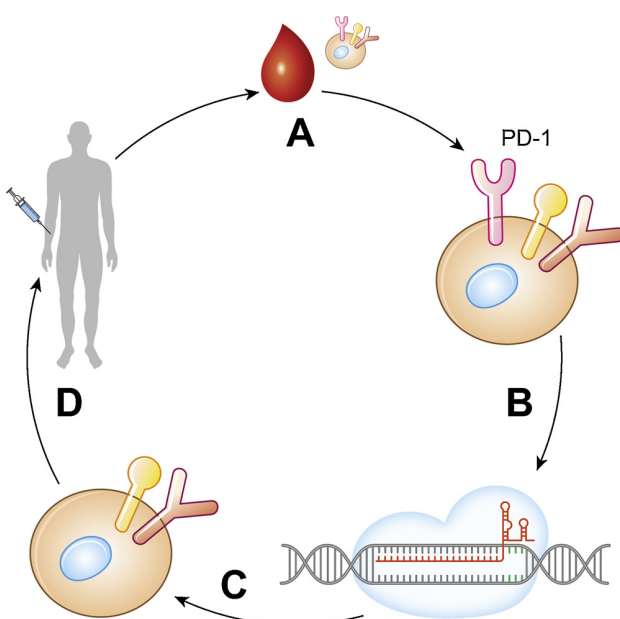


**Fig. 7.** CRISPR/Cas9 as a therapeutic tool. The principle of the first phase I clinical trials using a CRISPR/cas9 *ex vivo* knockout is shown: Peripheral blood lymphocytes are collected from the patient with a solid tumor (A) and CRISPR/Cas9 mediated knockout of the immune checkpoint gene PD1 is performed in T-cells (B-C). The PD1-knockout T-cells are expanded *ex vivo* and then transfused back to the patient (D), where they are supposed to induce immunological response against tumor cells.

**Table 2**

Registered clinical trials using CRISPR/Cas9 for treatment of neoplasms.  
from clinicaltrials.gov, accessed 03-18-2018.

Identifier	Condition	Phase	Treatment
NCT03081715	Esophageal cancer	II	PD-1 knockout T cells
NCT02863913	Bladder cancer	I	PD-1 knockout T cells
NCT02867345	Hormone refractory prostate cancer	I	PD-1 knockout T cells
NCT02867332	Renal cell carcinoma	I	PD-1 knockout T cells
NCT02793856	Non small cell lung cancer	I	PD-1 knockout T cells
NCT03044743	EBV positive advanced stage malignancies	I/II	PD-1 knockout EBV-CTL
NCT03166878	B cell lymphoma / leukemia	I/II	CRISPR-Cas9 edited CAR-T cells targeting CD19
NCT03057912	HPV related cervical intraepithelial neoplasia	I	CRISPR/Cas9-sg HPV E6/E7 gel to disrupt HPV DNA
NCT03399448	Multiple myeloma, synovial sarcoma, myxoid/round cell liposarcoma, melanoma	I	autologous T cells targeting tumor antigen NY-ESO-1, edited with CRISPR-Cas9 to disrupt endogenous TCR $\alpha$ , TCR $\beta$ and PD-1 (NYCE T Cells)
NCT03398967	B cell lymphoma / leukemia	I/II	CRISPR-Cas9 edited CAR-T Cells Targeting CD19 and CD20 or CD22

### Conflict of interest

None.

### Acknowledgements

We thank Florian Heigwer and Luisa Henkel for carefully reading the manuscript and contributing valuable ideas. T.Z. was supported by the research program “Nicht codierende RNA” of the Baden-Württemberg Stiftung. J.B. was supported by the “Translational Physician Scientist (TRAPS)” program of the Medical Faculty Mannheim, Heidelberg University and the State of Baden-Württemberg. M.P.E was supported by grants from the State of Baden-Württemberg for the “Center of Geriatric Oncology (ZOBEL) – Perspektivförderung” and “Biology of Frailty – Sonderlinie Medizin”. The groups of M.B. and M.P.E. were supported by the Hector Foundation II. We apologize to all colleagues whose work could not be cited due to space constraints.

### References

- [1] L.A. Torre, F. Bray, R.L. Siegel, J. Ferlay, J. Lortet-Tieulent, A. Jemal, Global cancer statistics, 2012, CA. Cancer J. Clin. 65 (2015) 87–108, <http://dx.doi.org/10.3322/caac.21262>.
- [2] H. Kantarjian, C. Sawyers, A. Hochhaus, F. Guilhot, C. Schiffer, C. Gambacorti-Passerini, D. Niederwieser, D. Resta, R. Capdeville, U. Zoellner, M. Talpaz, B. Druker, J. Goldman, S.G. O'Brien, N. Russell, T. Fischer, O. Ottmann, P. Cony-Makhoul, T. Facon, R. Stone, C. Miller, M. Tallman, R. Brown, M. Schuster, T. Loughran, A. Gratwohl, F. Mandelli, G. Saglio, M. Lazzarino, D. Russo, M. Baccarani, E. Morra, Hematologic and cytogenetic responses to imatinib mesylate in chronic myelogenous leukemia, N. Engl. J. Med. 346 (2002) 645–652, <http://dx.doi.org/10.1056/NEJMoa011573>.
- [3] D. Cunningham, Y. Humblet, S. Siena, D. Khayat, H. Bleiberg, A. Santoro, D. Bets, M. Mueser, A. Harstrick, C. Verslype, I. Chau, E. Van Cutsem, Cetuximab monotherapy and cetuximab plus irinotecan in irinotecan-refractory metastatic colorectal cancer, N. Engl. J. Med. 351 (2004) 337–345, <http://dx.doi.org/10.1056/NEJMoa033025>.
- [4] K. Chang, C.J. Creighton, C. Davis, L. Donehower, J. Drummond, D. Wheeler, A. Ally, M. Balasundaram, I. Birol, Y.S.N. Butterfield, A. Chu, E. Chuah, H.-J.E. Chun, N. Dhalla, R. Guin, M. Hirst, C. Hirst, R.A. Holt, S.J.M. Jones, D. Lee, H.I. Li, M.A. Marra, M. Mayo, R.A. Moore, A.J. Mungall, A.G. Robertson, J.E. Schein, P. Sipahimalani, A. Tam, N. Thiessen, R.J. Varhol, R. Beroukhim, A.S. Bhatt, A.N. Brooks, A.D. Cherniack, S.S. Freeman, S.B. Gabriel, E. Helman, J. Jung, M. Meyerson, A.I. Ojesina, C.S. Pedamallu, G. Saksena, S.E. Schumacher, B. Tabak, T. Zack, E.S. Lander, C.A. Bristow, A. Hadjipanayis, P. Haseley, R. Kucherlapati, S. Lee, E. Lee, L.J. Luquette, H.S. Mahadehwari, A. Pantazi, M. Parfenov, P.J. Park, A. Protopopov, X. Ren, N. Santoso, J. Seidman, S. Seth, X. Song, J. Tang, R. Xi, A.W. Xu, L. Yang, D. Zeng, J.T. Auman, S. Balu, E. Buda, C. Fan, K.A. Hoadley, C.D. Jones, S. Meng, P.A. Mieczkowski, J.S. Parker, C.M. Perou, J. Roach, Y. Shi, G.O. Silva, D. Tan, U. Veluvolu, S. Waring, M.D. Wilkerson, J. Wu, W. Zhao, T. Bodenheimer, D.N. Hayes, A.P. Hoyle, S.R. Jeffreys, L.E. Mose, J.V. Simons, M.G. Soloway, S.B. Baylin, B.P. Berman, M.S. Bootwalla, L. Danilova, J.G. Herman, T. Hinoue, P.W. Laird, S.K. Rhee, H. Shen, T. Triche, D.J. Weisenberger, S.L. Carter, K. Cibulskis, L. Chin, J. Zhang, G. Getz, C. Sougnez, M. Wang, G. Saksena, S.L. Carter, K. Cibulskis, L. Chin, J. Zhang, G. Getz, H. Dinh, H.V. Doddapaneni, R. Gibbs, P. Gunaratne, Y. Han, D. Kalra, C. Kovar, L. Lewis, M. Morgan, D. Morton, D. Muzny, J. Reid, L. Xi, J. Cho, D. DiCara, S. Frazer, N. Gehlenborg, D.I. Heiman, J. Kim, M.S. Lawrence, P. Lin, Y. Liu, M.S. Noble, P. Stojanov, D. Voet, H. Zhang, L. Zou, C. Stewart, B. Bernard, R. Bressler, A. Eakin, L. Iype, T. Knijnenburg, R. Kramer, R. Kreisberg, K. Leinonen, J. Lin, Y. Liu, M. Miller, S.M. Reynolds, H. Rovira, I. Shmulevich, V. Thorsson, D. Yang, W. Zhang, S. Amin, C.-J. Wu, C.-C. Wu, R. Akbani, K. Aldape, K.A. Baggerly, B. Broom, T.D. Casasent, J. Cleland, C. Creighton, D. Dodd, M. Edgerton, L. Han, S.M. Herbrich, Z. Ju, H. Kim, S. Lerner, J. Li, H. Liang, W. Liu, P.L. Lorenzi, Y. Lu, J. Melott, G.B. Mills, L. Nguyen, X. Su, R. Verhaak, W. Wang, J.N. Weinstein, A. Wong, Y. Yang, J. Yao, R. Yao, K. Yoshihara, Y. Yuan, A.K. Yung, N. Zhang, S. Zheng, M. Ryan, D.W. Kane, B.A. Aksoy, G. Ciriello, G. Dresdner, J. Gao, B. Gross, A. Jacobsen, A. Kahles, M. Ladanyi, W. Lee, K.-V. Lehmann, M.L. Miller, R. Ramirez, G. Rätsch, B. Reva, C. Sander, N. Schultz, Y. Senbabaooglu, R. Shen, R. Sinha, S.O. Sumer, Y. Sun, B.S. Taylor, N. Weinhold, S. Fei, P. Spellman, C. Benz, D. Carlin, M. Cline, B. Craft, K. Ellrott, M. Goldman, D. Haussler, S. Ma, S. Ng, E. Paull, A. Radenbaugh, S. Salama, A. Sokolov, J.M. Stuart, T. Swatloski, V. Uzunangelov, P. Waltman, C. Yau, J. Zhu, S.R. Hamilton, G. Getz, C. Sougnez, S. Abbott, R. Abbott, N.D. Dees, K. Delehaunty, L. Ding, D.J. Dooling, J.M. Eldred, C.C. Fronick, R. Fulton, L.L. Fulton, J. Kallicki-Veizer, K.-L. Kanchi, C. Kandoth, D.C. Koboldt, D.E. Larson, T.J. Ley, L. Lin, C. Lu, V.J. Magrini, E.R. Mardis, M.D. McLellan, J.F. McMichael, C.A. Miller, M. O'Laughlin, C. Pohl, H. Schmidt, S.M. Smith, J. Walker, J.W. Wallis, M.C. Wendt, R.K. Wilson, T. Wylie, Q. Zhang, R. Burton, M.A. Jensen, A. Kahn, T. Pihl, D. Pot, Y. Wan, D.A. Levine, A.D. Black, J. Bowen, J. Frick, J.M. Gastier-Foster, H.A. Harper, C. Helsel, K.M. Leraas, T.M. Lichtenberg, C. McAllister, N.C. Ramirez, S. Sharpe, L. Wise, E. Zmuda, S.J. Chanock, T. Davidsen, J.A. Demchok, G. Eley, I. Felau, B.A. Ozemberger, M. Sheth, H. Sofia, L. Staudt, R. Tarnuzzer, Z. Wang, L. Yang, J. Zhang, L. Omberg, A. Margolin, B.J. Raphael, F. Vandin, H.-T. Wu, M.D.M. Leiserson, S.C. Benz, C.J. Vaske, H. Noushmehr, T. Knijnenburg, D. Wolf, L.V. Veer, E.A. Collisson, D. Anastassiou, T.-H.O. Yang, N. Lopez-Bigas, A. Gonzalez-Perez, D. Tamborero, Z. Xia, W. Li, D.-Y. Cho, T. Przytycka, M. Hamilton, S. McGuire, S. Nelander, P. Johansson, R. Jörnsten, T. Kling, J. Sanchez, J.N. Weinstein, E.A. Collisson, G.B. Mills, K.R.M. Shaw, B.A. Ozemberger, K. Ellrott, I. Shmulevich, C. Sander, J.M. Stuart, The cancer genome atlas pan-cancer analysis project, Nat. Genet. 45 (2013) 1113–1120, <http://dx.doi.org/10.1038/ng.2764>.
- [5] T.I.C.G. International Cancer Genome Consortium, T.J. Hudson, W. Anderson, A. Artez, A.D. Barker, C. Bell, R.R. Bernabé, M.K. Bhan, F. Calvo, I. Eerola, D.S. Gerhard, A. Guttmacher, M. Guyer, F.M. Hemsley, J.L. Jennings, D. Kerr, P. Klatt, P. Kolar, J. Kusada, D.P. Lane, F. Laplace, L. Youyong, G. Nettekoven, B. Ozemberger, J. Peterson, T.S. Rao, J. Remacle, A.J. Schafer, T. Shibata, M.R. Stratton, J.G. Vockley, K. Watanabe, H. Yang, M.M.F. Yuen, B.M. Knoppers, M. Bobrow, A. Cambon-Thomsen, L.G. Dressler, S.O.M. Dyke, Y. Joly, K. Kato, K.L. Kennedy, P. Nicolás, M.J. Parker, E. Rial-Sebbag, C.M. Romeo-Casabona, K.M. Shaw, S. Wallace, G.L. Wiesner, N. Zeps, P. Lichter, A.V. Biankin, C. Chabannon, L. Chin, B. Clément, E. de Alava, F. Degos, M.L. Ferguson, P. Geary, D.N. Hayes, T.J. Hudson, A.L. Johns, A. Kasprzyk, H. Nakagawa, R. Penny, M.A. Piris, R. Sarin, A. Scarpa, T. Shibata, M. van de Vijver, P.A. Futreal, H. Aburatani, M. Bayés, D.D.L. Bowtell, P.J. Campbell, X. Estivill, D.S. Gerhard, S.M. Grimmond, I. Gut, M. Hirst, C. López-Otín, P. Majumder, M. Marra, J.D. McPherson, H. Nakagawa, Z. Ning, X.S. Puente, Y. Ruan, T. Shibata, M.R. Stratton, H.G. Stunnenberg, H. Swerdlow, V.E. Velculescu, R.K. Wilson, H.H. Xue, L. Yang, P.T. Spellman, G.D. Bader, P.C. Boutros, P.J. Campbell, P. Flicek, G. Getz, R. Guigó, G. Guo, D. Haussler, S. Heath, T.J. Hubbard, T. Jiang, S.M. Jones, Q. Li, N. López-Bigas, R. Luo, L. Muthuswamy, B.F.F. Ouellette, J.V. Pearson, X.S. Puente, V. Quesada, B.J. Raphael, C. Sander, T. Shibata, T.P. Speed, L.D. Stein, J.M. Stuart, J.W. Teague, Y. Totoki, T. Tsunoda, A. Valencia, D.A. Wheeler, H. Wu, S. Zhao, G. Zhou, L.D. Stein, R. Guigó, T.J. Hubbard, Y. Joly, S.M. Jones, A. Kasprzyk, M. Lathrop, N. López-Bigas, B.F.F. Ouellette, P.T. Spellman, J.W. Teague, G. Thomas, A. Valencia, T. Yoshida, K.L. Kennedy, M. Axton, S.O.M. Dyke, P.A. Futreal, D.S. Gerhard, C. Gunter, M. Guyer, T.J. Hudson, J.D. McPherson, L.J. Miller, B. Ozemberger, K.M. Shaw, A. Kasprzyk, L.D. Stein, J. Zhang, S.A. Haider, J. Wang, C.K. Yung, A. Cros, A. Cross, Y. Liang, S. Gnaneshan, J. Guberman, J. Hsu, M. Bobrow, D.R.C. Chalmers, K.W. Hasel, Y. Joly, T.S.H. Kaan, K.L. Kennedy, B.M. Knoppers, W.W. Lowrance, T. Masui, P. Nicolás, E. Rial-Sebbag, L.L. Rodriguez, C. Vergely, T. Yoshida, S.M. Grimmond, A.V. Biankin, D.L. Bowtell, N. Cloonan, A. Defazio, J.R. Eshleman, D. Etemadmoghadam, B.B. Gardiner, B.A. Gardiner, J.G. Kench, A. Scarpa, R.L. Sutherland, M.A. Tempere, N.J. Waddell, P.J. Wilson,

- J.D. McPherson, S. Gallinger, M.-S. Tsao, P.A. Shaw, G.M. Petersen, D. Mukhopadhyay, L. Chin, R.A. DePinho, S. Thayer, L. Muthuswamy, K. Shazand, T. Beck, M. Sam, L. Timms, V. Ballin, Y. Lu, J. Ji, X. Zhang, F. Chen, X. Hu, G. Zhou, Q. Yang, G. Tian, L. Zhang, X. Xing, X. Li, Z. Zhu, Y. Yu, J. Yu, H. Yang, M. Lathrop, J. Tost, P. Brennan, I. Holcatovala, D. Zaridze, A. Brazma, L. Egevad, E. Prokhortchouk, R.E. Banks, M. Uhlén, A. Cambon-Thomsen, J. Viksna, F. Ponten, K. Skryabin, M.R. Stratton, P.A. Futreal, E. Birney, A. Borg, A.-L. Børresen-Dale, C. Caldas, J.A. Foekens, S. Martin, J.S. Reis-Filho, A.L. Richardson, C. Sotiriou, H.G. Stuennenberg, G. Thoms, M. van de Vijver, L. van't Veer, F. Calvo, D. Birnbaum, H. Blanche, P. Boucher, S. Boyault, C. Chabannon, I. Gut, J.D. Masson-Jacquemier, M. Lathrop, I. Pauporté, X. Pivot, A. Vincent-Salomon, E. Tabone, C. Theillet, G. Thomas, J. Tost, I. Treilleux, F. Calvo, P. Bioulac-Sage, B. Clément, T. Decaens, F. Degos, D. Franco, I. Gut, M. Gut, S. Heath, M. Lathrop, D. Samuel, G. Thomas, J. Zucman-Rossi, P. Lichter, R. Eils, B. Brors, J.O. Korbel, A. Korshunov, P. Landgraf, H. Lehrach, S. Pfister, B. Radlwiller, G. Reifenberger, M.D. Taylor, C. von Kalle, P.P. Majumder, R. Sarin, T.S. Rao, M.K. Khan, A. Scarpa, P. Pederzoli, R.A. Lawlor, M. Delledonne, A. Bardelli, A.V. Biankin, S.M. Grimmind, T. Gress, D. Klimstra, G. Zamboni, T. Shibata, Y. Nakamura, H. Nakagawa, J. Kusada, T. Tsunoda, S. Miyano, H. Aburatani, K. Kato, A. Fujimoto, T. Yoshida, E. Campo, C. López-Otín, X. Estivill, R. Guigó, S. de Sanjose, M.A. Piris, E. Montserrat, M. González-Díaz, X.S. Puente, P. Jares, A. Valencia, H. Himmelbauer, H. Himmelbaue, V. Quesada, S. Bea, M.R. Stratton, P.A. Futreal, P.J. Campbell, A. Vincent-Salomon, A.L. Richardson, J.S. Reis-Filho, M. van de Vijver, G. Thomas, J.D. Masson-Jacquemier, S. Aparicio, A. Borg, A.-L. Børresen-Dale, C. Caldas, J.A. Foekens, H.G. Stuennenberg, L. van't Veer, D.F. Easton, P.T. Spellman, S. Martin, A.D. Barker, L. Chin, F.S. Collins, C.C. Compton, M.L. Ferguson, D.S. Gerhard, G. Getz, C. Gunter, A. Guttmacher, M. Guyer, D.N. Hayes, E.S. Lander, B. Ozemberger, R. Penny, J. Peterson, C. Sander, K.M. Shaw, T.P. Speed, P.T. Spellman, J.G. Vockley, D.A. Wheeler, R.K. Wilson, T.J. Hudson, L. Chin, B.M. Knoppers, E.S. Lander, P. Lichter, L.D. Stein, M.R. Stratton, W. Anderson, A.D. Barker, C. Bell, M. Bobrow, W. Burke, F.S. Collins, C.C. Compton, R.A. DePinho, D.F. Easton, P.A. Futreal, D.S. Gerhard, A.R. Green, M. Guyer, S.R. Hamilton, T.J. Hubbard, O.P. Kallioniemi, K.L. Kennedy, T.J. Ley, E.T. Liu, Y. Lu, P. Majumder, M. Marra, B. Ozemberger, J. Peterson, A.J. Schafer, P.T. Spellman, H.G. Stuennenberg, B.J. Wainwright, R.K. Wilson, H. Yang, International network of cancer genome projects, *Nature* 464 (2010) 993–998, <http://dx.doi.org/10.1038/nature08987>.
- [6] L.A. Garraway, E.S. Lander, Lessons from the cancer genome, *Cell* 153 (2013) 17–37, <http://dx.doi.org/10.1016/j.cell.2013.03.002>.
- [7] J.K. Joung, J.D. Sander, TALENs: a widely applicable technology for targeted genome editing, *Nat. Rev. Mol. Cell Biol.* 14 (2012) 49–55, <http://dx.doi.org/10.1038/nrm3486>.
- [8] F.D. Urnov, E.J. Rebar, M.C. Holmes, H.S. Zhang, P.D. Gregory, Genome editing with engineered zinc finger nucleases, *Nat. Rev. Genet.* 11 (2010) 636–646, <http://dx.doi.org/10.1038/nrg2842>.
- [9] L. Cong, F.A. Ran, D. Cox, S. Lin, R. Barretto, N. Habib, P.D. Hsu, X. Wu, W. Jiang, L.A. Marrapponi, F. Zhang, Multiplex genome engineering using CRISPR/Cas systems, *Science* 339 (2013) 819–823, <http://dx.doi.org/10.1126/science.1231143>.
- [10] P. Mali, L. Yang, K.M. Esvelt, J. Aach, M. Guell, J.E. DiCarlo, J.E. Norville, G.M. Church, RNA-guided human genome engineering via Cas9, *Science* 339 (2013) 823–826 <http://www.pubmedcentral.nih.gov/articlerender.fcgi?artid=3712628&tool=pmcentrez&rendertype=abstract>.
- [11] Y. Ishino, H. Shinagawa, K. Makino, M. Amemura, A. Nakata, Nucleotide sequence of the iap gene, responsible for alkaline phosphatase isozyme conversion in *Escherichia coli*, and identification of the gene product, *J. Bacteriol.* 169 (1987) 5429–5433, <http://dx.doi.org/10.1128/jb.169.12.5429-5433.1987>.
- [12] M. Kampmann, CRISPRi and CRISPRa screens in mammalian cells for precision biology and medicine, *ACS Chem. Biol.* (2017), <http://dx.doi.org/10.1021/acschembio.7b00657>.
- [13] A. Bolotin, B. Quinquis, A. Sorokin, S.D. Ehrlich, Clustered regularly interspaced short palindromic repeats (CRISPRs) have spacers of extrachromosomal origin, *Microbiology* 151 (2005) 2551–2561, <http://dx.doi.org/10.1099/mic.0.28048-0>.
- [14] C. Pourcel, G. Salvignol, G. Vergnaud, CRISPR elements in *Yersinia pestis* acquire new repeats by preferential uptake of bacteriophage DNA, and provide additional tools for evolutionary studies, *Microbiology* 151 (2005) 653–663, <http://dx.doi.org/10.1099/mic.0.27437-0>.
- [15] F.J.M. Mojica, C. Díez-Villaseñor, J. García-Martínez, E. Soria, Intervening sequences of regularly spaced prokaryotic repeats derive from foreign genetic elements, *J. Mol. Evol.* 60 (2005) 174–182, <http://dx.doi.org/10.1007/s00239-004-0046-3>.
- [16] R. Barrangou, C. Fremaux, H. Deveau, M. Richards, P. Boyaval, S. Moineau, D.A. Romero, P. Horvath, CRISPR provides acquired resistance against viruses in prokaryotes, *Science* 315 (2007) 1709–1712, <http://dx.doi.org/10.1126/science.1138140>.
- [17] E. Deltcheva, K. Chylinski, C.M. Sharma, K. Gonzales, Y. Chao, Z.A. Pirzada, M.R. Eckert, J. Vogel, E. Charpentier, CRISPR RNA maturation by trans-encoded small RNA and host factor RNase III, *Nature* 471 (2011) 602–607, <http://dx.doi.org/10.1038/nature09886>.
- [18] G. Gasijnas, R. Barrangou, P. Horvath, V. Siksny, Cas9-crRNA ribonucleoprotein complex mediates specific DNA cleavage for adaptive immunity in bacteria, *Proc. Natl. Acad. Sci. U. S. A.* 109 (2012), [http://dx.doi.org/10.1073/pnas.1208507109 E2579–86](http://dx.doi.org/10.1073/pnas.1208507109).
- [19] M. Jinek, K. Chylinski, I. Fonfara, M. Hauer, J.A. Doudna, E. Charpentier, A programmable dual-RNA-guided DNA endonuclease in adaptive bacterial immunity, *Science* 337 (2012) 816–821, <http://dx.doi.org/10.1126/science.1225829>.
- [20] H. Deveau, R. Barrangou, J.E. Garneau, J. Labonté, C. Fremaux, P. Boyaval, D.A. Romero, P. Horvath, S. Moineau, Phage response to CRISPR-encoded resistance in *Streptococcus thermophilus*, *J. Bacteriol.* 190 (2008) 1390–1400, <http://dx.doi.org/10.1128/JB.01412-07>.
- [21] S.H. Sternberg, S. Redding, M. Jinke, E.C. Greene, J.A. Doudna, DNA interrogation by the CRISPR RNA-guided endonuclease Cas9, *Nature* 507 (2014) 62–67, <http://dx.doi.org/10.1038/nature13011>.
- [22] H. Deveau, R. Barrangou, J.E. Garneau, J. Labonté, C. Fremaux, P. Boyaval, D.A. Romero, P. Horvath, S. Moineau, Phage response to CRISPR-encoded resistance in *Streptococcus thermophilus*, *J. Bacteriol.* 190 (2008) 1390–1400, <http://dx.doi.org/10.1128/JB.01412-07>.
- [23] B. Chen, L.A. Gilbert, B.A. Cimini, J. Schnitzbauer, W. Zhang, G.W. Li, J. Park, E.H. Blackburn, J.S. Weissman, L.S. Qi, B. Huang, Dynamic imaging of genomic loci in living human cells by an optimized CRISPR/Cas system, *Cell* 155 (2013) 1479–1491, <http://dx.doi.org/10.1016/j.cell.2013.12.001>.
- [24] B. Zetsche, J.S. Gootenber, O.O. Abudayeh, I.M. Slaymaker, K.S. Makarova, P. Essletzbichler, S.E. Volz, J. Joung, J. van der Oost, A. Regev, E.V. Koonin, F. Zhang, Cpf1 is a single RNA-guided endonuclease of a class 2 CRISPR/Cas system, *Cell* 163 (2015) 759–771, <http://dx.doi.org/10.1016/j.cell.2015.09.038>.
- [25] O.O. Abudayeh, J.S. Gootenber, S. Konermann, J. Joung, I.M. Slaymaker, D.B.T. Cox, S. Shmakov, K.S. Makarova, E. Semenova, L. Minakhin, K. Severinov, A. Regev, E.S. Lander, E.V. Koonin, F. Zhang, C2c2 is a single-component programmable RNA-guided RNA-targeting CRISPR effector, *Science* 353 (2016), <http://dx.doi.org/10.1126/science.aaf5573>.
- [26] A.A. Smargon, D.B.T. Cox, N.K. Pyzocha, K. Zheng, I.M. Slaymaker, J.S. Gootenber, O.A. Abudayeh, P. Essletzbichler, S. Shmakov, K.S. Makarova, E.V. Koonin, F. Zhang, Cas13b is a type VI-B CRISPR-associated RNA-guided RNases differentially regulated by accessory proteins Csx27 and Csx28, *Mol. Cell* 65 (2017) 618–630, [http://dx.doi.org/10.1016/j.molcel.2016.12.023 e7](http://dx.doi.org/10.1016/j.molcel.2016.12.023).
- [27] L.S. Qi, M.H. Larson, L.A. Gilbert, J.A. Doudna, J.S. Weissman, A.P. Arkin, W.A. Lim, Repurposing CRISPR as an RNA-guided platform for sequence-specific control of gene expression, *Cell* 152 (2013) 1173–1183, <http://dx.doi.org/10.1016/j.cell.2013.02.022>.
- [28] L.A. Gilbert, M.H. Larson, L. Morsut, Z. Liu, CRISPR-mediated modular RNA-guided regulation of transcription in eukaryotes, *Cell* (2013) 1–10, <http://dx.doi.org/10.1016/j.cell.2013.06.044>.
- [29] P.I. Thakore, A.M. D'ippolito, L. Song, A. Safi, N.K. Shivakumar, A.M. Kabadi, T.E. Reddy, G.E. Crawford, C.A. Gersbach, Highly specific epigenome editing by CRISPR-Cas9 reporters for silencing of distal regulatory elements, *Nat. Methods* 12 (2015) 1143–1149, <http://dx.doi.org/10.1038/nmeth.3630>.
- [30] M.L. Maeder, S.J. Linder, V.M. Cascio, Y. Fu, Q.H. Ho, J.K. Joung, CRISPR RNA-guided activation of endogenous human genes, *Nat. Methods* 10 (2013) 977–979, <http://dx.doi.org/10.1038/nmeth.2598>.
- [31] A. Chavez, J. Scheiman, S. Vora, B.W. Pruitt, M. Tuttle, E.P.R. Iyer, S. Lin, S. Kiani, C.D. Guzman, D.J. Wiegand, D. Ter-Ovanesyan, J.L. Braff, N. Davidsohn, B.E. Housden, N. Perrimon, R. Weiss, J. Aach, J.J. Collins, G.M. Church, Highly efficient Cas9-mediated transcriptional programming, *Nat. Methods* 12 (2015) 326–328, <http://dx.doi.org/10.1038/nmeth.3312>.
- [32] M.E. Tanenbaum, L.A. Gilbert, L.S. Qi, J.S. Weissman, R.D. Vale, A protein-tagging system for signal amplification in gene expression and fluorescence imaging, *Cell* 159 (2014) 635–646, <http://dx.doi.org/10.1016/j.cell.2014.09.039>.
- [33] S. Konermann, M.D. Brigham, A.E. Trevino, J. Joung, O.O. Abudayeh, C. Barcena, P.D. Hsu, N. Habib, J.S. Gootenber, H. Nishimatsu, O. Nureki, F. Zhang, Genome-scale transcriptional activation by an engineered CRISPR-Cas9 complex, *Nature* 517 (2014) 583–588, <http://dx.doi.org/10.1038/nature14136>.
- [34] A. Chavez, M. Tuttle, B.W. Pruitt, B. Ewen-Campen, R. Chari, D. Ter-Ovanesyan, S.J. Haque, R.J. Cecchi, E.J.K. Kowal, J. Buchthal, B.E. Housden, N. Perrimon, J.J. Collins, G. Church, Comparison of Cas9 activators in multiple species, *Nat. Methods* 13 (2016) 563–567, <http://dx.doi.org/10.1038/nmeth.3871>.
- [35] J.I. McDonald, H. Celik, L.E. Rois, G. Fishberger, T. Fowler, R. Rees, A. Kramer, A. Martens, J.R. Edwards, G.A. Challen, Reprogrammable CRISPR/Cas9-based system for inducing site-specific DNA methylation, *Biol. Open* 5 (2016) 866–874, <http://dx.doi.org/10.1242/bio.019067>.
- [36] A. Vojta, P. Dobrnić, V. Tadić, L. Bočkor, P. Korać, B. Julg, M. Klasić, V. Zoldoš, Repurposing the CRISPR-Cas9 system for targeted DNA methylation, *Nucleic Acids Res.* 44 (2016) 5615–5628, <http://dx.doi.org/10.1093/nar/gkw159>.
- [37] P. Stepper, G. Kungulovski, R.Z. Jurkowska, T. Chandra, F. Krueger, R. Reinhardt, W. Reik, A. Jeltsch, T.P. Jurkowski, Efficient targeted DNA methylation with chimeric dCas9-Dnmt3a-Dnmt3L methyltransferase, *Nucleic Acids Res.* 45 (2017) 1703–1713, <http://dx.doi.org/10.1093/nar/gkw1112>.
- [38] X. Xu, Y. Tao, X. Gao, L. Zhang, X. Li, W. Zou, K. Ruan, F. Wang, G. Xu, R. Hu, A CRISPR-based approach for targeted DNA demethylation, *Cell Discov.* 2 (2016) 16009, <http://dx.doi.org/10.1038/celldisc.2016.9>.
- [39] I.B. Hilton, A.M. D'Ippolito, C.M. Vockley, P.I. Thakore, G.E. Crawford, T.E. Reddy, C.A. Gersbach, Epigenome editing by a CRISPR-Cas9-based acetyltransferase activates genes from promoters and enhancers, *Nat. Biotechnol.* 33 (2015) 510–517, <http://dx.doi.org/10.1038/nbt.3199>.
- [40] A.C. Komor, Y.B. Kim, M.S. Packer, J.A. Zuris, D.R. Liu, Programmable editing of a target base in genomic DNA without double-stranded DNA cleavage, *Nature* 533 (2016) 420–424, <http://dx.doi.org/10.1038/nature17946>.
- [41] C. Kuscu, M. Parlak, T. Tufan, J. Yang, K. Szlachta, X. Wei, R. Mammadov, M. Adli, CRISPR-STOP: gene silencing through base-editing-induced nonsense mutations, *Nat. Methods* 14 (2017) 710–712, <http://dx.doi.org/10.1038/nmeth.4327>.
- [42] K. Nishida, T. Arazoe, N. Yachie, S. Banno, M. Kakimoto, M. Tabata, M. Mochizuki, A. Miyabe, M. Araki, K.Y. Hara, Z. Shimatani, A. Kondo, Targeted nucleotide editing using hybrid prokaryotic and vertebrate adaptive immune systems, *Science*

- 353 (2016), <http://dx.doi.org/10.1126/science.aaf8729>.
- [43] Y. Ma, J. Zhang, W. Yin, Z. Zhang, Y. Song, X. Chang, Targeted AID-mediated mutagenesis (TAM) enables efficient genomic diversification in mammalian cells, *Nat. Methods* 13 (2016) 1029–1035, <http://dx.doi.org/10.1038/nmeth.4027>.
- [44] G.T. Hess, L. Fréard, K. Han, C.H. Lee, A. Li, K.A. Cimprich, S.B. Montgomery, M.C. Bassik, Directed evolution using dCas9-targeted somatic hypermutation in mammalian cells, *Nat. Methods* 13 (2016) 1036–1042, <http://dx.doi.org/10.1038/nmeth.4038>.
- [45] T. Hart, A.H.Y. Tong, K. Chan, J. Van Leeuwen, A. Seetharaman, M. Aregger, M. Chandrashekhar, N. Hustedt, S. Seth, A. Noonan, A. Habsid, O. Sizova, L. Nedyalkova, R. Clime, L. Tworzanski, K. Lawson, M.A. Sartori, S. Alibeh, D. Tieu, S. Masud, P. Mero, A. Weiss, K.R. Brown, M. Usaj, M. Billmann, M. Rahman, M. Costanzo, C.L. Myers, B.J. Andrews, C. Boone, D. Durocher, J. Moffat, Evaluation and design of genome-wide CRISPR/SpCas9 knockout screens, *Genes Genom. Genet.* 7 (2017) 2719–2727, <http://dx.doi.org/10.1534/g3.117.041277>.
- [46] J.G. Doench, N. Fusi, M. Sullender, M. Hegde, E.W. Vainberg, K.F. Donovan, I. Smith, Z. Tothova, C. Wilen, R. Orchard, H.W. Virgin, J. Listgarten, D.E. Root, Optimized sgRNA design to maximize activity and minimize off-target effects of CRISPR-Cas9, *Nat. Biotechnol.* (2016), <http://dx.doi.org/10.1038/nbt.3437>.
- [47] S.Q. Tsai, Z. Zheng, N.T. Nguyen, M. Liebers, V.V. Topkar, V. Thapar, N. Wyckens, C. Khayter, A.J. Iafrate, L.P. Le, M.J. Aryee, J.K. Joung, GUIDE-seq enables genome-wide profiling of off-target cleavage by CRISPR-Cas nucleases, *Nat. Biotechnol.* 33 (2014) 187–197, <http://dx.doi.org/10.1038/nbt.3117>.
- [48] D. Kim, S. Bae, J. Park, E. Kim, S. Kim, H.R. Yu, J. Hwang, J.-I. Kim, J.-S. Kim, Digenome-seq: genome-wide profiling of CRISPR-Cas9 off-target effects in human cells, *Nat. Methods* 12 (2015) 237–243, <http://dx.doi.org/10.1038/nmeth.3284>.
- [49] S.Q. Tsai, N.T. Nguyen, J. Malagon-Lopez, V.V. Topkar, M.J. Aryee, J.K. Joung, CIRCLE-seq: a highly sensitive in vitro screen for genome-wide CRISPR-Cas9 nuclease off-targets, *Nat. Methods* 14 (2017) 607–614, <http://dx.doi.org/10.1038/nmeth.4278>.
- [50] J.A. Meier, F. Zhang, N.E. Sanjana, GUIDES: sgRNA design for loss-of-function screens, *Nat. Methods* 14 (2017) 831–832, <http://dx.doi.org/10.1038/nmeth.4423>.
- [51] F. Heigwer, T. Zhan, M. Breinig, J. Winter, D. Brügemann, S. Leible, M. Boutros, CRISPR library designer (CLD): software for multispecies design of single guide RNA libraries, *Genome Biol.* 17 (2016) 55, <http://dx.doi.org/10.1186/s13059-016-0915-2>.
- [52] B. Evers, K. Jastrzebski, J.P.M. Heijmans, W. Gremmum, R.L. Beijersbergen, R. Bernards, CRISPR knockout screening outperforms shRNA and CRISPRi in identifying essential genes, *Nat. Biotechnol.* 34 (2016) 631–633, <http://dx.doi.org/10.1038/nbt.3536>.
- [53] D.M. Munoz, P.J. Cassiani, L. Li, E. Billy, J.M. Korn, M.D. Jones, J. Golji, D.A. Ruddy, K. Yu, G. McAllister, A. Deweck, D. Abramowski, J. Wan, M.D. Shirley, S.Y. Neshat, D. Rakiec, R. De Beaumont, O. Weber, A. Kauffmann, E. Robert McDonald, N. Keen, F. Hofmann, W.R. Sellers, T. Schmelzle, F. Stegmeier, M.R. Schlabach, CRISPR screens provide a comprehensive assessment of cancer vulnerabilities but generate false-positive hits for highly amplified genomic regions, *Cancer Discov.* 6 (2016) 900–913, <http://dx.doi.org/10.1158/2159-8290.CD-16-0178>.
- [54] T. Hart, M. Chandrashekhar, M. Aregger, Z. Steinhart, K.R. Brown, G. MacLeod, M. Mis, M. Zimmermann, A. Fradet-Turcotte, S. Sun, P. Mero, P. Dirks, S. Sidhu, F.P. Roth, O.S. Rissland, D. Durocher, S. Angers, J. Moffat, High-resolution CRISPR screens reveal fitness genes and genotype-specific cancer liabilities, *Cell* 163 (2015) 1515–1526, <http://dx.doi.org/10.1016/j.cell.2015.11.015>.
- [55] A.J. Aguirre, R.M. Meyers, B.A. Weir, F. Vazquez, C.-Z. Zhang, U. Ben-David, A. Cook, G. Ha, W.F. Harrington, M.B. Doshi, M. Kost-Alimova, S. Gill, H. Xu, L.D. Ali, G. Jiang, S. Pantel, Y. Lee, A. Goodale, A.D. Cherniack, C. Oh, G. Kryukov, G.S. Cowley, L.A. Garraway, K. Stegmaier, C.W. Roberts, T.R. Golub, M. Meyerson, D.E. Root, A. Tsherniak, W.C. Hahn, Genomic copy number dictates a gene-independent cell response to CRISPR/Cas9 targeting, *Cancer Discov.* 6 (2016) 914–929, <http://dx.doi.org/10.1158/2159-8290.CD-16-0154>.
- [56] R.M. Meyers, J.G. Bryan, J.M. McFarland, B.A. Weir, A.E. Sizemore, H. Xu, N.V. Dharia, P.G. Montgomery, G.S. Cowley, S. Pantel, A. Goodale, Y. Lee, L.D. Ali, G. Jiang, R. Lubonja, W.F. Harrington, M. Strickland, T. Wu, D.C. Hawes, V.A. Zhivich, M.R. Wyatt, Z. Kalani, J.J. Chang, M. Okamoto, K. Stegmaier, T.R. Golub, J.S. Boehm, F. Vazquez, D.E. Root, W.C. Hahn, A. Tsherniak, Computational correction of copy number effect improves specificity of CRISPR-Cas9 essentiality screens in cancer cells, *Nat. Genet.* 49 (2017) 1779–1784, <http://dx.doi.org/10.1038/ng.3984>.
- [57] K. Tzelepis, H. Koike-Yusa, E. De Braekeleer, Y. Li, E. Metzakopian, O.M. Dovey, A. Mupo, V. Grinkevich, M. Li, M. Mazan, M. Gozdecka, S. Ohnishi, J. Cooper, M. Patel, T. McKerrell, B. Chen, A.F. Domingues, P. Gallipoli, S. Teichmann, H. Ponstingl, U. McDermott, J. Saez-Rodriguez, B.J.P. Huntly, F. Iorio, C. Pina, G.S. Vassiliou, K. Yusa, A CRISPR dropout screen identifies genetic vulnerabilities and therapeutic targets in acute myeloid leukemia, *Cell Rep.* 17 (2016) 1193–1205, <http://dx.doi.org/10.1016/j.celrep.2016.09.079>.
- [58] B. Rauscher, F. Heigwer, L. Henkel, T. Hielscher, O. Voloshanenko, M. Boutros, Toward an integrated map of genetic interactions in cancer cells, *Mol. Syst. Biol.* 14 (2018) e7656, <http://dx.doi.org/10.15252/msb.20177656>.
- [59] J. Shi, E. Wang, J.P. Milazzo, Z. Wang, J.B. Kinney, C.R. Vakoc, Discovery of cancer drug targets by CRISPR-Cas9 screening of protein domains, *Nat. Biotechnol.* 33 (2015) 661–667, <http://dx.doi.org/10.1038/nbt.3235>.
- [60] M.A. Erb, T.G. Scott, B.E. Li, H. Xie, J. Paulk, H.-S. Seo, A. Souza, J.M. Roberts, S. Dastjerdi, D.L. Buckley, N.E. Sanjana, O. Shalem, B. Nabat, R. Zeid, N.K. Offei-Addo, S. Dhe-Paganon, F. Zhang, S.H. Orkin, G.E. Winter, J.E. Bradner, Transcription control by the ENL YEATS domain in acute leukaemia, *Nature* 543 (2017) 270–274, <http://dx.doi.org/10.1038/nature21688>.
- [61] T. Zhan, M. Boutros, Towards a compendium of essential genes - from model organisms to synthetic lethality in cancer cells, *Crit. Rev. Biochem. Mol. Biol.* (2015) 1–12, <http://dx.doi.org/10.3109/10409238.2015.1117053>.
- [62] M. Robson, S.-A. Im, E. Senkus, B. Xu, S.M. Domchek, N. Masuda, S. Delaloge, W. Li, N. Tung, A. Armstrong, W. Wu, C. Goessl, S. Runswick, P. Conte, Olaparib for metastatic breast cancer in patients with a germline BRCA mutation, *N. Engl. J. Med.* 377 (2017) 523–533, <http://dx.doi.org/10.1056/NEJMoa1706450>.
- [63] Z. Steinhart, Z. Pavlovic, M. Chandrashekhar, T. Hart, X. Wang, X. Zhang, M. Robitaille, K.R. Brown, S. Jakani, R. Overmeer, S.F. Boj, J. Adams, J. Pan, H. Clevers, S. Sidhu, J. Moffat, S. Angers, Genome-wide CRISPR screens reveal a Wnt-FZD5 signaling circuit as a druggable vulnerability of RNF43-mutant pancreatic tumors, *Nat. Med.* 23 (2017) 60–68, <http://dx.doi.org/10.1038/nm.4219>.
- [64] T. Wang, H. Yu, N.W. Hughes, B. Liu, A. Kendirci, K. Klein, W.W. Chen, E.S. Lander, D.M. Sabatini, Gene essentiality profiling reveals gene networks and synthetic lethal interactions with oncogenic ras, *Cell* 168 (2017) 890–903, <http://dx.doi.org/10.1016/j.cell.2017.01.013> e15.
- [65] O. Shalem, N.E. Sanjana, F. Zhang, High-throughput functional genomics using CRISPR-Cas9, *Nat. Rev. Genet.* 16 (2015) 299–311, <http://dx.doi.org/10.1038/ng.3899>.
- [66] S. Ruiz, C. Mayor-Ruiz, V. Lafarga, M. Murga, M. Vega-Sendino, S. Ortega, O. Fernandez-Capetillo, A genome-wide CRISPR screen identifies CDC25A as a determinant of sensitivity to ATR inhibitors, *Mol. Cell.* 62 (2016) 307–313, <http://dx.doi.org/10.1016/j.molcel.2016.03.006>.
- [67] E.B. Krall, B. Wang, D.M. Munoz, N. Ilic, S. Raghavan, M.J. Niederst, K. Yu, D.A. Ruddy, A.J. Aguirre, J.W. Kim, A.J. Redig, J.F. Gainor, J.A. Williams, J.M. Asara, J.G. Doench, P.A. Janne, A.T. Shaw, R.E. McDonald, J.A. Engelman, F. Stegmeier, M.R. Schlabach, W.C. Hahn, KEAP1 loss modulates sensitivity to kinase targeted therapy in lung cancer, *Elife*. 6 (2017), <http://dx.doi.org/10.7554/elife.18970>.
- [68] S. Gayle, S. Landrette, N. Beecharry, C. Conrad, M. Hernandez, P. Beckett, S.M. Ferguson, T. Mandelkern, M. Zheng, T. Xu, J. Rothberg, H. Lichenstein, Identification of apilimod as a first-in-class PIKfyve kinase inhibitor for treatment of B-cell non-Hodgkin lymphoma, *Blood* 129 (2017) 1768–1778, <http://dx.doi.org/10.1182/blood-2016-09-736892>.
- [69] K. Han, E.E. Jeng, G.T. Hess, D.W. Morgens, A. Li, M.C. Bassik, Synergistic drug combinations for cancer identified in a CRISPR screen for pairwise genetic interactions, *Nat. Biotechnol.* 35 (2017) 463–474, <http://dx.doi.org/10.1038/nbt.3834>.
- [70] J.P. Shen, D. Zhao, R. Sasik, J. Luebeck, A. Birmingham, A. Bojorquez-Gomez, K. Licon, K. Klepper, D. Pekin, A.N. Beckett, K.S. Sanchez, A. Thomas, C.-C. Kuo, D. Du, A. Rogue, N.E. Lewis, A.N. Chang, J.F. Kreisberg, N. Krogan, L. Qi, T. Ideker, P. Malai, Combinatorial CRISPR-Cas9 screens for de novo mapping of genetic interactions, *Nat. Methods* 14 (2017) 573–576, <http://dx.doi.org/10.1038/nmeth.4225>.
- [71] D.A. Jaitin, A. Weinert, I. Yofe, D. Lara-Astiaso, H. Keren-Shaul, E. David, T.M. Salame, A. Tanay, A. van Oudenaarden, I. Amit, Dissecting immune circuits by linking CRISPR-Pooled screens with single-cell RNA-Seq, *Cell* 167 (2016) 1883–1896, <http://dx.doi.org/10.1016/j.cell.2016.11.039> e15.
- [72] A. Dixit, O. Parnas, B. Li, J. Chen, C.P. Fulco, L. Jerby-Aron, N.D. Marjanovic, D. Dionne, T. Burks, R. Raychowdhury, B. Adamson, T.M. Norman, E.S. Lander, J.S. Weissman, N. Friedman, A. Regev, Perturb-Seq: dissecting molecular circuits with scalable single-cell RNA profiling of pooled genetic screens, *Cell* 167 (2016) 1853–1866, <http://dx.doi.org/10.1016/j.cell.2016.11.038> e17.
- [73] B. Adamson, T.M. Norman, M. Jost, M.Y. Cho, J.K. Nuñez, Y. Chen, J.E. Villalta, L.A. Gilbert, M.A. Horlbeck, M.Y. Hein, R.A. Pak, A.N. Gray, C.A. Gross, A. Dixit, O. Parnas, A. Regev, J.S. Weissman, A multiplexed single-cell CRISPR screening platform enables systematic dissection of the unfolded protein response, *Cell* 167 (2016) 1867–1882, <http://dx.doi.org/10.1016/j.cell.2016.11.048> e21.
- [74] P. Datlinger, A.F. Rendeiro, C. Schmidl, T. Krausgruber, P. Traxler, J. Klughammer, L.C. Schuster, A. Kuchler, D. Alpar, C. Bock, Pooled CRISPR screening with single-cell transcriptome readout, *Nat. Methods* 14 (2017) 297–301, <http://dx.doi.org/10.1038/nmeth.4177>.
- [75] M. Huarte, The emerging role of lncRNAs in cancer, *Nat. Med.* 21 (2015) 1253–1261, <http://dx.doi.org/10.1038/nm.3981>.
- [76] N.E. Sanjana, J. Wright, K. Zheng, O. Shalem, P. Fontanillas, J. Joung, C. Cheng, A. Regev, F. Zhang, High-resolution interrogation of functional elements in the noncoding genome, *Science* 353 (2016) 1545–1549, <http://dx.doi.org/10.1126/science.aaf7613>.
- [77] G. Korkmaz, R. Lopes, A.P. Ugalde, E. Nevedomskaya, R. Han, K. Myacheva, W. Zwart, R. Elkorn, R. Agami, Functional genetic screens for enhancer elements in the human genome using CRISPR-Cas9, *Nat. Biotechnol.* 34 (2016) 192–198, <http://dx.doi.org/10.1038/nbt.3450>.
- [78] S. Zhu, W. Li, J. Liu, C.-H. Chen, Q. Liao, P. Xu, H. Xu, T. Xiao, Z. Cao, J. Peng, P. Yuan, M. Brown, X.S. Liu, W. Wei, Genome-scale deletion screening of human long non-coding RNAs using a paired-guide RNA CRISPR-Cas9 library, *Nat. Biotechnol.* 34 (2016) 1279–1286, <http://dx.doi.org/10.1038/nbt.3715>.
- [79] S.J. Liu, M.A. Horlbeck, S.W. Cho, H.S. Birk, M. Malatesta, D. He, F.J. Attenello, J.E. Villalta, M.Y. Cho, Y. Chen, M.A. Mandegar, M.P. Olvera, L.A. Gilbert, B.R. Conklin, H.Y. Chang, J.S. Weissman, D.A. Lim, CRISPR-based genome-scale identification of functional long noncoding RNA loci in human cells, *Science* 355 (2017), <http://dx.doi.org/10.1126/science.aah7111> eaah7111.
- [80] X. Yan, Z. Hu, Y. Feng, X. Hu, J. Yuan, S.D. Zhao, Y. Zhang, L. Yang, W. Shan, Q. He, L. Fan, L.E. Kandalaf, J.L. Tanyi, C. Li, C.-X. Yuan, D. Zhang, H. Yuan, K. Hua, Y. Lu, D. Katsaros, Q. Huang, K. Montone, Y. Fan, G. Coukos, J. Boyd,

- A.K. Sood, T. Rebbeck, G.B. Mills, C.V. Dang, L. Zhang, Comprehensive genomic characterization of long non-coding RNAs across human cancers, *Cancer Cell* 28 (2015) 529–540, <http://dx.doi.org/10.1016/j.ccr.2015.09.006>.
- [81] J. Joung, J.M. Engeleit, S. Konermann, O.O. Abudayyeh, V.K. Verdine, F. Aguet, J.S. Gootenberg, N.E. Sanjana, J.B. Wright, C.P. Fulco, Y.-Y. Tseng, C.H. Yoon, J.S. Boehm, E.S. Lander, F. Zhang, Genome-scale activation screen identifies a lncRNA locus regulating a gene neighbourhood, *Nature* 548 (2017) 343–346, <http://dx.doi.org/10.1038/nature23451>.
- [82] A. Goyal, K. Myacheva, M. Grof, M. Klingenberg, B. Duran Arqué, S. Diederichs, Challenges of CRISPR/Cas9 applications for long non-coding RNA genes, *Nucleic Acids Res.* 45 (2016), <http://dx.doi.org/10.1093/nar/gkw883> gkw883.
- [83] H. Clevers, Modeling development and disease with organoids, *Cell* 165 (2016) 1586–1597, <http://dx.doi.org/10.1016/j.cell.2016.05.082>.
- [84] G. Schwank, B.K. Koo, V. Sasselli, J.F. Dekkers, I. Heo, T. Demircan, N. Sasaki, S. Boymans, E. Cuppen, C.K. Van Der Ent, E.E.S. Nieuwenhuis, J.M. Beekman, H. Clevers, Functional repair of CFTR by CRISPR/Cas9 in intestinal stem cell organoids of cystic fibrosis patients, *Cell Stem Cell* 13 (2013) 653–658, <http://dx.doi.org/10.1016/j.stem.2013.11.002>.
- [85] J. Drost, R.H. van Jaarsveld, B. Ponsioen, C. Zimberlin, R. van Boxtel, A. Buijs, N. Sachs, R.M. Overmeer, G.J. Offerhaus, H. Begthel, J. Korving, M. van de Wetering, G. Schwank, M. Logtenberg, E. Cuppen, H.J. Snippert, J.P. Medema, G.J.P.L. Kops, H. Clevers, Sequential cancer mutations in cultured human intestinal stem cells, *Nature* 521 (2015) 43–47, <http://dx.doi.org/10.1038/nature14415>.
- [86] M. Matano, S. Date, M. Shimokawa, A. Takano, M. Fujii, Y. Ohta, T. Watanabe, T. Kanai, T. Sato, Modeling colorectal cancer using CRISPR-Cas9-mediated engineering of human intestinal organoids, *Nat. Med.* 21 (2015) 256–262, <http://dx.doi.org/10.1038/nm.3802>.
- [87] J. Drost, Use of CRISPR-modified human stem cell organoids to study the origin of mutational signatures in cancer, *Science* (2017) 3130.
- [88] L. Tao, J. Zhang, P. Meraner, A. Tovaglieri, X. Wu, R. Gerhard, X. Zhang, W.B. Stallcup, J. Miao, X. He, J.G. Hurdle, D.T. Breact, A.L. Brass, M. Dong, Frizzled proteins are colonic epithelial receptors for *C. difficile* toxin B, *Nature* (2016), <http://dx.doi.org/10.1038/nature19799>.
- [89] E. Driehuis, H. Clevers, CRISPR/Cas 9 genome editing and its applications in organoids, *Am. J. Physiol. Gastrointest. Liver Physiol.* (2017), <http://dx.doi.org/10.1152/ajpgi.00410.2016>.
- [90] W. Xue, S. Chen, H. Yin, T. Tammela, T. Papagiannakopoulos, N.S. Joshi, W. Cai, G. Yang, R. Bronson, D.G. Crowley, F. Zhang, D.G. Anderson, P.A. Sharp, T. Jacks, CRISPR-mediated direct mutation of cancer genes in the mouse liver, *Nature* 514 (2014) 380–384, <http://dx.doi.org/10.1038/nature13589>.
- [91] R. Maresch, S. Mueller, C. Veltkamp, R. Öllinger, M. Friedrich, I. Heid, K. Steiger, J. Weber, T. Engleitner, M. Barenboim, S. Klein, S. Louzada, R. Banerjee, A. Strong, T. Stauber, N. Gross, U. Geumann, S. Lange, M. Ringelhan, I. Varela, K. Unger, F. Yang, R.M. Schmid, G.S. Vassiliou, R. Braren, G. Schneider, M. Heikenwalder, A. Bradley, D. Saur, R. Rad, Multiplexed pancreatic genome engineering and cancer induction by transfection-based CRISPR/Cas9 delivery in mice, *Nat. Commun.* 7 (2016) 10770, <http://dx.doi.org/10.1038/ncomms10770>.
- [92] M. Zuckermann, V. Hovestadt, C.B. Knobbe-Thomsen, M. Zapata, P.A. Northcott, K. Schramm, J. Belic, D.T.W. Jones, B. Tschida, B. Moriarity, D. Largaespada, M.F. Roussel, A. Korshunov, G. Reifenberger, S.M. Pfister, P. Lichter, D. Kawauchi, J. Gronych, Somatic CRISPR/Cas9-mediated tumour suppressor disruption enables versatile brain tumour modelling, *Nat. Commun.* 6 (2015) 7391, <http://dx.doi.org/10.1038/ncomms8391>.
- [93] J. Luo, Y. Luo, J. Sun, Y. Zhou, Y. Zhang, X. Yang, Adeno-associated virus-mediated cancer gene therapy: current status, *Cancer Lett.* 356 (2015) 347–356, <http://dx.doi.org/10.1016/j.canlet.2014.10.045>.
- [94] C. Zinicarelli, S. Solty, G. Rengo, J.E. Rabkinowitz, Analysis of AAV serotypes 1–9 mediated gene expression and tropism in mice after systemic injection, *Mol. Ther.* 16 (2008) 1073–1080, <http://dx.doi.org/10.1038/mt.2008.76>.
- [95] E. Senis, C. Fatouros, S. Große, E. Wiedtke, D. Niopel, A.K. Mueller, K. Börner, D. Grimm, CRISPR/Cas9-mediated genome engineering: an adeno-associated viral (AAV) vector toolbox, *Biotechnol. J.* 9 (2014) 1402–1412, <http://dx.doi.org/10.1002/biot.201400046>.
- [96] W. Yu, S. Mookherjee, V. Chaitankar, S. Hiriyanna, J.W. Kim, M. Brooks, Y. Ataeijannati, X. Sun, L. Dong, T. Li, A. Swaroop, Z. Wu, Nrl knockdown by AAV-delivered CRISPR/Cas9 prevents retinal degeneration in mice, *Nat. Commun.* 8 (2017) 14716, <http://dx.doi.org/10.1038/ncomms14716>.
- [97] S. Yang, R. Chang, H. Yang, T. Zhao, Y. Hong, H.E. Kong, X. Sun, Z. Qin, P. Jin, S. Li, X.-J. Li, CRISPR/Cas9-mediated gene editing ameliorates neurotoxicity in mouse model of Huntington's disease, *J. Clin. Invest.* 127 (2017) 2719–2724, <http://dx.doi.org/10.1172/JCI92087>.
- [98] Y. Yang, L. Wang, P. Bell, D. McMenamin, Z. He, J. White, H. Yu, C. Xu, H. Morizono, K. Musunuru, M.L. Batshaw, J.M. Wilson, A dual AAV system enables the Cas9-mediated correction of a metabolic liver disease in newborn mice, *Nat. Biotechnol.* 34 (2016) 334–338, <http://dx.doi.org/10.1038/nbt.3469>.
- [99] N.E. Bengtsson, J.K. Hall, G.L. Odom, M.P. Phelps, C.R. Andrus, R.D. Hawkins, S.D. Hauschka, J.R. Chamberlain, J.S. Chamberlain, Muscle-specific CRISPR/Cas9 dystrophin gene editing ameliorates pathophysiology in a mouse model for Duchenne muscular dystrophy, *Nat. Commun.* 8 (2017) 14454, <http://dx.doi.org/10.1038/ncomms14454>.
- [100] M. Tabebordbar, K. Zhu, J.K.W. Cheng, W.L. Chew, J.J. Widrick, W.X. Yan, C. Maesner, E.Y. Wu, R. Xiao, F.A. Ran, L. Cong, F. Zhang, L.H. Vandenberghe, G.M. Church, A.J. Wagers, In vivo gene editing in dystrophic mouse muscle and muscle stem cells, *Science* 351 (2016) 407–411, <http://dx.doi.org/10.1126/science.aad5177>.
- [101] W.L. Chew, M. Tabebordbar, J.K.W. Cheng, P. Mali, E.Y. Wu, A.H.M. Ng, K. Zhu, A.J. Wagers, G.M. Church, A multifunctional AAV-CRISPR-Cas9 and its host response, *Nat. Methods* 13 (2016) 868–874, <http://dx.doi.org/10.1038/nmeth.3993>.
- [102] W. Mehnert, K. Mäder, Solid lipid nanoparticles: production, characterization and applications, *Adv. Drug Deliv. Rev.* 64 (2012) 83–101, <http://dx.doi.org/10.1016/j.addr.2012.09.021>.
- [103] N. Pardi, M.J. Hogan, R.S. Pelc, H. Muramatsu, H. Andersen, C.R. DeMaso, K.A. Dowd, L.L. Sutherland, R.M. Scarce, R. Parks, W. Wagner, A. Granados, J. Greenhouse, M. Walker, E. Willis, J.-S. Yu, C.E. McGee, G.D. Sempowski, B.L. Mui, Y.K. Tam, Y.-J. Huang, D. Vanlandingham, V.M. Holmes, H. Balachandran, S. Sahu, M. Lifton, S. Higgs, S.E. Hensley, T.D. Madden, M.J. Hope, K. Karikó, S. Santra, B.S. Graham, M.G. Lewis, T.C. Pierson, B.F. Haynes, D. Weissman, Zika virus protection by a single low-dose nucleoside-modified mRNA vaccination, *Nature* 543 (2017) 248–251, <http://dx.doi.org/10.1038/nature21428>.
- [104] J.D. Finn, A.R. Smith, M.C. Patel, L. Shaw, M.R. Youniss, J. van Heteren, T. Dirstine, C. Ciullo, R. Lescarbeau, J. Seitzer, R.R. Shah, A. Shah, D. Ling, J. Growe, M. Pink, E. Rohde, K.M. Wood, W.E. Salomon, W.F. Harrington, C. Dombrowski, W.R. Strapps, Y. Chang, D.V. Morrissey, A single administration of CRISPR/Cas9 lipid nanoparticles achieves robust and persistent *in vivo* genome editing, *Cell Rep.* 22 (2018) 2227–2235, <http://dx.doi.org/10.1016/j.celrep.2018.02.014>.
- [105] C. Jiang, M. Mei, B. Li, X. Zhu, W. Zu, Y. Tian, Q. Wang, Y. Guo, Y. Dong, X. Tan, A non-viral CRISPR/Cas9 delivery system for therapeutically targeting HBV DNA and pcsk9 *in vivo*, *Cell Res.* 27 (2017) 440–443, <http://dx.doi.org/10.1038/cr.2017.16>.
- [106] J.B. Miller, S. Zhang, P. Kos, H. Xiong, K. Zhou, S.S. Perelman, H. Zhu, D.J. Siegwart, Non-viral CRISPR/Cas gene editing *in vitro* and *in vivo* enabled by synthetic nanoparticle co-delivery of Cas9 mRNA and sgRNA, *Angew. Chem. Int. Ed.* 56 (2017) 1059–1063, <http://dx.doi.org/10.1002/anie.201610209>.
- [107] K. Lee, M. Conboy, H.M. Park, F. Jiang, H.J. Kim, M.A. Dewitt, V.A. Mackley, K. Chang, A. Rao, C. Skinner, T. Shohba, M. Mehdiipour, H. Liu, W.C. Huang, F. Lan, N.L. Bray, S. Li, J.E. Corn, K. Kataoka, J.A. Doudna, I. Conboy, N. Murthy, Nanoparticle delivery of Cas9 ribonucleoprotein and donor DNA *in vivo* induces homology-directed DNA repair, *Nat. Biomed. Eng.* 1 (2017) 889–901, <http://dx.doi.org/10.1038/s41551-017-0137-2>.
- [108] P. Barata, A.K. Sood, D.S. Hong, RNA-targeted therapeutics in cancer clinical trials: current status and future directions, *Cancer Treat. Rev.* 50 (2016) 35–47, <http://dx.doi.org/10.1016/j.ctrv.2016.08.004>.
- [109] S. Chen, N.E. Sanjana, K. Zheng, O. Shalem, K. Lee, X. Shi, D.A. Scott, J. Song, J.Q. Pan, R. Weissleder, H. Lee, F. Zhang, P.A. Sharp, Genome-wide CRISPR screen in a mouse model of tumor growth and metastasis, *Cell* 160 (2015) 1246–1260, <http://dx.doi.org/10.1016/j.cell.2015.02.038>.
- [110] C.Q. Song, Y. Li, H. Mou, J. Moore, A. Park, Y. Pomyen, S. Hough, Z. Kennedy, A. Fischer, H. Yin, D.G. Anderson, D. Conte, L. Zender, X.W. Wang, S. Thorgerirsson, Z. Weng, W. Xue, Genome-wide CRISPR screen identifies regulators of mitogen-activated protein kinase as suppressors of liver tumors in mice, *Gastroenterology* 152 (2017) 1161–1173, <http://dx.doi.org/10.1053/j.gastro.2016.12.002>.
- [111] J. Roper, T. Tammela, N.M. Cetinbas, A. Akkad, A. Roghanian, S. Rickett, M. Almeqdadi, K. Wu, M.A. Oberli, F. Sánchez-Rivera, Y.K. Park, X. Liang, G. Eng, M.S. Taylor, R. Azimi, D. Kedrin, R. Neupane, S. Beyaz, E.T. Sicinska, Y. Suarez, J. Yoo, L. Chen, L. Zukerberg, P. Katajisto, V. Deshpande, A.J. Bass, P.N. Tsichlis, J. Lees, R. Langer, R.O. Hynes, J. Chen, A. Bhutkar, T. Jacks, Ö.H. Yilmaz, In vivo genome editing and organoid transplantation models of colorectal cancer and metastasis, *Nat. Biotechnol.* 35 (2017) 569–576, <http://dx.doi.org/10.1038/nbt.3836>.
- [112] J. Weber, R. Öllinger, M. Friedrich, U. Ehmer, M. Barenboim, K. Steiger, I. Heid, S. Mueller, R. Maresch, T. Engleitner, N. Gross, U. Geumann, B. Fu, A. Segler, D. Yuan, S. Lange, A. Strong, J. de la Rosa, I. Esposito, P. Liu, J. Cadilhanos, G.S. Vassiliou, R.M. Schmid, G. Schneider, K. Unger, F. Yang, R. Braren, M. Heikenwalder, I. Varela, D. Saur, A. Bradley, R. Rad, CRISPR/Cas9 somatic multiplex-mutagenesis for high-throughput functional cancer genomics in mice, *Proc. Natl. Acad. Sci.* 112 (2015) 13982–13987, <http://dx.doi.org/10.1073/pnas.1512392112>.
- [113] R.J. Platt, S. Chen, Y. Zhou, M.J. Yim, L. Swiech, H.R. Kempton, J.E. Dahlman, O. Parnas, T.M. Eisenhaure, M. Jovanovic, D.B. Graham, S. Jhunjhunwala, M. Heidenreich, R.J. Xavier, R. Langer, D.G. Anderson, N. Hacohen, A. Regev, G. Feng, P.A. Sharp, F. Zhang, CRISPR-Cas9 knockout mice for genome editing and cancer modeling, *Cell* 159 (2014) 440–455, <http://dx.doi.org/10.1016/j.cell.2014.09.014>.
- [114] R.D. Chow, C.D. Guzman, G. Wang, F. Schmidt, M.W. Youngblood, L. Ye, Y. Errami, M.B. Dong, M.A. Martinez, S. Zhang, P. Renauer, K. Bilguvar, M. Gunel, P.A. Sharp, F. Zhang, R.J. Platt, S. Chen, AAV-mediated direct *in vivo* CRISPR screen identifies functional suppressors in glioblastoma, *Nat. Neurosci.* 20 (2017) 1329–1341, <http://dx.doi.org/10.1038/nn.4620>.
- [115] T. Wirth, N. Parker, S. Ylä-Hertuala, History of gene therapy, *Gene* 525 (2013) 162–169, <http://dx.doi.org/10.1016/j.gene.2013.03.137>.
- [116] T. Hirsch, T. Rothoeft, N. Teig, J.W. Bauer, G. Pellegrini, L. De Rosa, D. Scaglione, J. Reichelt, A. Klausenberger, D. Kneisz, O. Romano, A. Secone Seconetti, R. Contini, E. Enzo, I. Jurman, S. Carulli, F. Jacobsen, T. Luecke, M. Lehnhardt, M. Fischer, M. Kueckelhaus, D. Quaglino, M. Morgante, S. Bicciato, S. Bondanza, M. De Luca, Regeneration of the entire human epidermis using transgenic stem cells, *Nature* 551 (2017) 327–332, <http://dx.doi.org/10.1038/nature24487>.
- [117] J.R. Mendell, S. Al-Zaidy, R. Shell, W.D. Arnold, L.R. Rodino-Klapac, T.W. Prior,

- L. Lowes, L. Alfano, K. Berry, K. Church, J.T. Kissel, S. Nagendran, J. L'Italien, D.M. Sproule, C. Wells, J.A. Cardenas, M.D. Heitzer, A. Kaspar, S. Corcoran, L. Braun, S. Likhite, C. Miranda, K. Meyer, K.D. Foust, A.H.M. Burghes, B.K. Kaspar, Single-dose gene-replacement therapy for spinal muscular atrophy, *N. Engl. J. Med.* 377 (2017) 1713–1722, <http://dx.doi.org/10.1056/NEJMoa1706198>.
- [118] S. Rangarajan, L. Walsh, W. Lester, D. Perry, B. Madan, M. Laffan, H. Yu, C. Vettermann, G.F. Pierce, W.Y. Wong, K.J. Pasi, AAV5–Factor VIII gene transfer in severe hemophilia A, *N. Engl. J. Med.* 377 (2017) 2519–2530, <http://dx.doi.org/10.1056/NEJMoa1708483>.
- [119] S. Russell, J. Bennett, J.A. Wellman, D.C. Chung, Z.-F. Yu, A. Tillman, J. Wittes, J. Pappas, O. Elci, S. McCague, D. Cross, K.A. Marshall, J. Walshire, T.L. Kehoe, H. Reichert, M. Davis, L. Raffini, L.A. George, F.P. Hudson, L. Dingfield, X. Zhu, J.A. Haller, E.H. Sohn, V.B. Mahajan, W. Pfeifer, M. Weckmann, C. Johnson, D. Gewaily, A. Drack, E. Stone, K. Wachtel, F. Simonelli, B.P. Leroy, J.F. Wright, K.A. High, A.M. Maguire, Efficacy and safety of voretigene neparovec (AAV2-hRPE65v2) in patients with RPE65-mediated inherited retinal dystrophy: a randomised, controlled, open-label, phase 3 trial, *Lancet* 390 (2017) 849–860, [http://dx.doi.org/10.1016/S0140-6736\(17\)31868-8](http://dx.doi.org/10.1016/S0140-6736(17)31868-8).
- [120] P. Tebas, D. Stein, W.W. Tang, I. Frank, S.Q. Wang, G. Lee, S.K. Spratt, R.T. Strosky, M.A. Giedlin, G. Nichol, M.C. Holmes, P.D. Gregory, D.G. Ando, M. Kalos, R.G. Collman, G. Binder-Scholl, G. Plesa, W.-T. Hwang, B.L. Levine, C.H. June, Gene editing of CCR5 in autologous CD4 T cells of persons infected with HIV, *N. Engl. J. Med.* 370 (2014) 901–910, <http://dx.doi.org/10.1056/nm.1300662>.
- [121] T.I. Cornu, C. Mussolini, T. Cathomen, Refining strategies to translate genome editing to the clinic, *Nat. Med.* 23 (2017) 415–423, <http://dx.doi.org/10.1038/nm.4313>.
- [122] D. Cyranoski, CRISPR gene-editing tested in a person for the first time, *Nature* 539 (2016) 479, <http://dx.doi.org/10.1038/nature.2016.20988>.
- [123] Y. Iwai, M. Ishida, Y. Tanaka, T. Okazaki, T. Honjo, N. Minato, Involvement of PD-L1 on tumor cells in the escape from host immune system and tumor immunotherapy by PD-L1 blockade, *Proc. Natl. Acad. Sci.* 99 (2002) 12293–12297, <http://dx.doi.org/10.1073/pnas.192461099>.
- [124] M. Reck, D. Rodriguez-Abreu, A.G. Robinson, R. Hui, T. Csörsz, A. Fulop, M. Gottfried, N. Peled, A. Tafreshi, S. Cuffe, M. O'Brien, S. Rao, K. Hotta, M.A. Leiby, G.M. Lubiniecki, Y. Shentu, R. Rangwala, J.R. Brahmer, Pembrolizumab versus chemotherapy for PD-L1-positive non-small-cell lung cancer, *N. Engl. J. Med.* 375 (2016) 1823–1833, <http://dx.doi.org/10.1056/NEJMoa1606774>.
- [125] J. Eyquem, J. Mansilla-Soto, T. Giavridis, S.J.C. van der Stegen, M. Hamieh, K.M. Cunanan, A. Odak, M. Gönen, M. Sadelain, Targeting a CAR to the TRAC locus with CRISPR/Cas9 enhances tumour rejection, *Nature* 543 (2017) 113–117, <http://dx.doi.org/10.1038/nature21405>.
- [126] F. Heigwer, G. Kerr, M. Boutros, E-CRISP: fast CRISPR target site identification, *Nat. Methods* 11 (2014) 122–123, <http://dx.doi.org/10.1038/nmeth.2812>.
- [127] P.D. Hsu, D.A. Scott, J.A. Weinstein, F.A. Ran, S. Konermann, V. Agarwala, Y. Li, E.J. Fine, X. Wu, O. Shalem, T.J. Cradick, L.A. Marraffini, G. Bao, F. Zhang, DNA targeting specificity of RNA-guided Cas9 nucleases, *Nat. Biotechnol.* 31 (2013) 827–832, <http://dx.doi.org/10.1038/nbt.2647>.
- [128] K. Labun, T.G. Montague, J.A. Gagnon, S.B. Thyme, E. Valen, CHOPCHOP v2: a web tool for the next generation of CRISPR genome engineering, *Nucleic Acids Res.* 44 (2016) W272–W276, <http://dx.doi.org/10.1093/nar/gkw398>.
- [129] C.R. MacPherson, A. Scherf, Flexible guide-RNA design for CRISPR applications using protospacer workbench, *Nat. Biotechnol.* 33 (2015) 805–806, <http://dx.doi.org/10.1038/nbt.3291>.
- [130] M.A. Moreno-Mateos, C.E. Vejnar, J.-D. Beaudoin, J.P. Fernandez, E.K. Mis, M.K. Khokha, A.J. Giraldez, CRISPRscan: designing highly efficient sgRNAs for CRISPR-Cas9 targeting in vivo, *Nat. Methods* 12 (2015) 982–988, <http://dx.doi.org/10.1038/nmeth.3543>.
- [131] R. Chari, P. Mali, M. Moosburner, G.M. Church, Unraveling CRISPR-Cas9 genome engineering parameters via a library-on-library approach, *Nat. Methods* 12 (2015) 823–826, <http://dx.doi.org/10.1038/nmeth.3473>.
- [132] J. Winter, M. Breinig, F. Heigwer, D. Brügemann, S. Leible, O. Pelz, T. Zhan, M. Boutros, caRpools: an R package for exploratory data analysis and documentation of pooled CRISPR/Cas9 screens, *Bioinformatics* 32 (2016) 632–634, <http://dx.doi.org/10.1093/bioinformatics/btv617>.
- [133] W. Li, J. Köster, H. Xu, C.-H. Chen, T. Xiao, J.S. Liu, M. Brown, X.S. Liu, Quality control, modeling, and visualization of CRISPR screens with MAGeCK-VISPR, *Genome Biol.* 16 (2015) 281, <http://dx.doi.org/10.1186/s13059-015-0843-6>.
- [134] J. Yu, J. Silva, A. Califano, ScreenBEAM: a novel meta-analysis algorithm for functional genomics screens via Bayesian hierarchical modeling, *Bioinformatics* 32 (2016) 260–267, <http://dx.doi.org/10.1093/bioinformatics/btv556>.
- [135] J. Winter, M. Schwering, O. Pelz, B. Rauscher, T. Zhan, F. Heigwer, M. Boutros, CRISPRAnalyzeR: Interactive analysis, annotation and documentation of pooled CRISPR screens, *bioRxiv* (2017) 109967, <http://dx.doi.org/10.1101/109967>.